POLITECNICO DI TORINO

Master's Degree in Biomedical Engineering

Master's Degree Thesis

Investigation of Silica, Polypropylene and Titanium surfaces before and after fibrinogen adsorption

Supervisor
Prof. Silvia Spriano

Candidate
Alessia Caramiello
s290971

Co-supervisors
Dr. Sara Ferraris
Dr. Camilla Reggio

ACADEMIC YEAR 2022-2023

CONTENTS

LIST OF FIGURES

LIST OF TABLES

LIST OF ABBREVIATIONS

FB	Fibrinogen
FB_p	Fibrinogen powder
FB_p_deg	Degraded fibrinogen powder
SiO_2	Silica
SiO_2_FB	Silica with fibrinogen
SiO_2_FB_w	Wet silica with fibrinogen
PP	Polypropylene
PP_FB	Polypropylene with fibrinogen
PP_FB_w	Wet polypropylene with fibrinogen
Ti64	Ti6Al4V alloy
Ti64_FB	Ti6Al4V alloy with fibrinogen
Ti64_FB_w	Wet Ti6Al4V alloy with fibrinogen
CT	Chemical treated Ti6Al4V alloy
CT_FB	Chemical treated Ti6Al4V alloy with fibrinogen
CT_FB_w	Wet chemical treated Ti6Al4V alloy with fibrinogen
OH	Hydroxyl group
FpA	Fibrinopeptides A
FpB	Fibrinopeptides B
Asn	Asparagine
Ser	Serine
Thr	Threonine
NXS	Asn-X-Ser sequence
NXT	Asn-X-Thr sequence
VTE	Venus Thromboembolism
Arg	Arginine
Gly	Glycine
Pro	Proline
GPR	Gly-Pro-Arg sequence

His	Histidine
GHRP	Gly-His-Arg-Pro
FBR	Foreign Body Reaction
GF	Growth Factor
PMN	PolyMorphoNuclear
ROS	Reactive Oxygen Species
FBGCs	Foreign Body Giant Cells
BMP	Bone Morphogenic Proteins
SDS	Sodium Dodecyl Sulfate
FTIR	Fourier-Transform InfraRed
ATR	Attenuated Total Reflection
AFM	Atomic Force Microscopy
H_2O	Water
Ca^{2+}	Calcium ion
QCM-D	Quartz Crystal Microbalance with Dissipation Monitoring
rms	Root Mean Square
EtOh	Ethanol
HF	Hydrofluoric acid
H_2O_2	Hydrogen peroxide
NaCl	Sodium chloride
FBS	Fetal Bovine Serum
EDL	Electrochemical Double Layer
IEP	IsoElectric Point
KCl	Potassium chloride
NaOH	Sodium hydroxide
HCl	Hydrochloric acid
SEM	Scanning Electron Microscopy
EDS	Energy-Dispersive X-Ray Spectroscopy
FESEM	Field Emission Scanning Electron Microscopy

IR	InfraRed
SiOH	Silanol group
C	Carbon
O	Oxygen
Si	Silicon
Na	Sodium
Cl	Chlorine
CH_3	Methyl group
CH_2	Methylene group

ABSTRACT

Fibrinogen (FB) is a protein that plays a crucial role in lots of processes in the organism, in particular for what concerns the interaction between implants and tissues, through the formation of a substratum which is essential for adhesion and aggregation of cells or platelets (clotting). This process may lead to the full integration of the implant or to chronic inflammation which determines the subsequent implant failure.

During biomaterial implantation, several steps occur including, first of all, protein adsorption which strongly depends on surface features such as wettability, charge, topography and roughness. Proteins (such as fibrinogen) may assume various orientations and may adsorb in variable amount and, as a consequence, may undergo different structure variations, eventually denaturing, i.e. in case of hydrophobic surfaces or hydrophilic ones with a high density of charged functional groups.

For this reason, fibrinogen adsorption is studied in this thesis on two model surfaces with different wettability that are silica (SiO_2) as a model of hydrophilic surfaces and polypropylene (PP) as a model of hydrophobic ones, both biocompatible and usable in biomedical applications. They are also compared to a Titanium alloy (Ti6Al4V, defined as Ti64) and to a chemical-treated Titanium alloy (CT), characterized by a complex surface (multiscale surface topography with a nanotexture overlapped to a micro-roughness), a high density of acidic hydroxyl (OH) groups, and a bioactive behavior.

All samples were properly characterized by several techniques and tested under different conditions, with and without fibrinogen, to identify their surface behavior and features, both qualitatively (i.e. through imaging techniques) and quantitatively, characterizing the amount of the adsorbed protein, its conformation, and type of bonding with the surface, in view to predict and understand the material interaction.

The final purpose is to design cutting-edge biomaterials, extending their use in the biomedical field.

INTRODUCTION

During the last decades, the use of new implantable materials in biomedical field has sprung up and become more and more popular in order to improve the healing step and the subsequent osseointegration process of the implant.

The interaction between the biomaterial and the host organism is based on a very complex sequence of steps which includes, first of all, the adsorption of proteins of biological fluids such as blood on the materials' surface.

Since one of the main proteins involved in this process is the fibrinogen, this thesis work aims to study the interaction between this protein and different types of materials, investigating in particular the materials' surface properties before and after the fibrinogen adsorption.

Silica and polypropylene are used as models of hydrophilic and hydrophobic surfaces respectively: these materials are properly characterized in order to benefit from the obtained results, extending them to other materials of clinical interest such as Ti6Al4V alloy, chemically treated or not.

The first chapter is about fibrinogen, in particular its biochemistry and its role in the coagulation process up to the formation of fibrin; the final part of this chapter is reserved to the aspect of tissue integration of biomaterials in general, with a special focus on osseointegration.

In the second chapter the theme of the interaction between fibrinogen and materials is addressed, describing the fibrinogen adsorption process and the influence of material surface properties (wettability, roughness-topography and surface charge) on it.

The third chapter contains the experimental part: first of all, the samples preparation and the fibrinogen adsorption process are described, then all the surface characterization techniques that have been applied are reported (SEM/EDS, FESEM, FTIR, profilometry, confocal microscopy, contact angle and zeta potential).

The fourth chapter, after a brief explanation of the features of the used materials, aims to show all the data that have been obtained during the processes and the measurements, with the discussion of all the results.

Conclusions of the work are in the fifth chapter, together with an analysis of the possible next steps and further studies about the problem taken into consideration.

1 FIBRINOGEN

1.1 Biochemistry of fibrinogen

1.1.1 Fibrinogen biosynthesis and structure

Fibrinogen, also known as "coagulation factor I" is a soluble macromolecule that plays a crucial role in lots of processes in the organism such as hemostasis, wound healing, inflammation and angiogenesis. In fact, it is predominantly present in the plasma, even though it is also in platelets, lymph and interstitial fluid [1], [2].

Fibrinogen is a 340-kDa homodimeric glycoprotein which is synthesized in the endoplasmic reticulum by liver's parenchymal cells thanks to molecular chaperones that act as binding agents [3]. Subsequently it is subjected to quality control mechanisms in order to distinguish assembled fibrinogen forms to unassembled ones that are degraded intracellularly [1]. Finally, assembled fibrinogen is secreted and it circulates in plasma at concentrations of 2-5 mg/ml in healthy individuals; this value can further increase in case of acute inflammation, during which plasma fibrinogen levels can exceed 7 mg/ml [4]. This process follows the up-regulation of the acute phase proteins, e.g. the fibrinogen itself during damages to the body such as injuries or inflammations [1].

The fibrinogen molecule consists of 2Aα, 2Bβ and 2γ polypeptide chains, whose primary structure is specified by three closely linked genes (FGA, FGB and FGG respectively) clustered on human chromosome 4, linked by 29 disulfide bridges to make two symmetrical half-molecules [1]. In particular the synthesis process can be seen as divided into three steps: first of all, Aα-γ and Bβ-γ heterodimers are assembled starting from the single chains; in the second step these complexes interact with each other to form Aα/Bβ/γ half-molecules that finally form hexameric complexes $(Aα/Bβ/γ)_2$ in the third step [4].

Fibrinogen can also undergo different post-translational modifications such as phosphorylation, glycosylation, nitration and oxidation that affect its biological function. These processes have a significant impact on the physiology and pathophysiology of blood coagulation, the course of fibrinolysis and the blood clot structure [2].

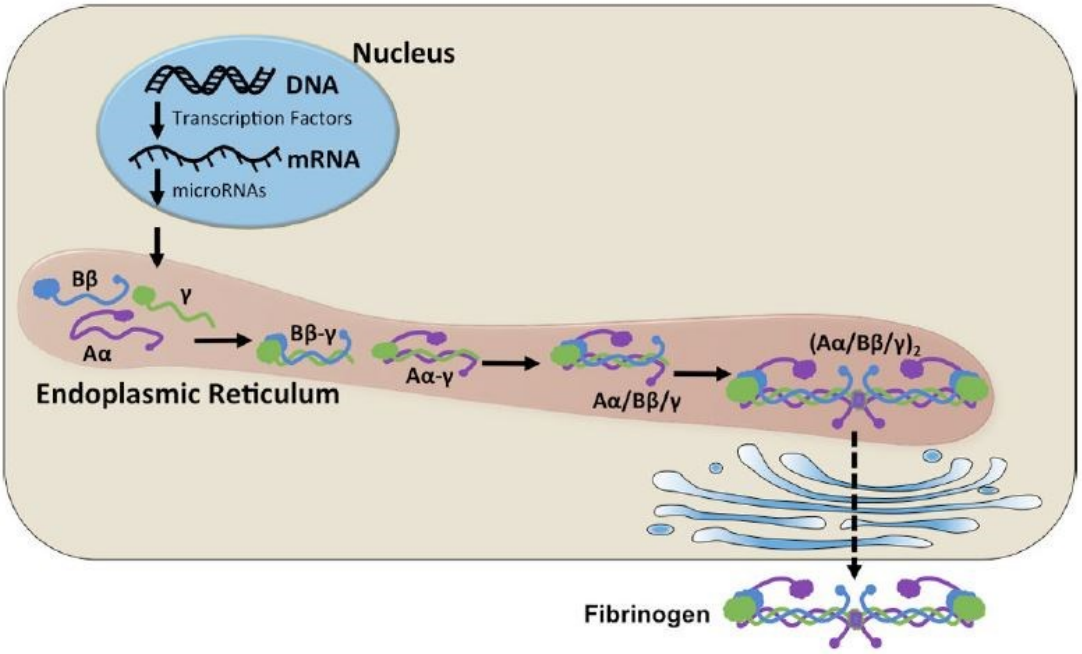

Figure 1: Fibrinogen synthesis [4]

Every single molecule has an elongated rod shape 45 nm in length and ~2-5 nm in diameter; it presents a central "E region" and two globular thicker "D regions" in the extremities [1], [4], [5]. In the globular part of the E region, called *"central nodule"*, the N-termini of the six fibrinogen chains are concentrated (γ chains form an asymmetric *"γN- domain"*, while Aα and Bβ chains form a *"funnel-shaped domain"*), plus these chains extend outward in a coiled-coil arrangement, generating two *"coiled-coil-E domains"* thanks to C-terminal parts of the Aα, Bβ and γ chains. In particular, the N-terminal ends of the Aα and Bβ chains is composed by small fibrinopeptides A and B known as "FpA" and "FpB" [1]. However, in D regions the N-termini of all the chains form a *"coiled-coil-D domain"* on each side comprising a triple α-helical, plus there are two globular zones known as βC and γC that are the terminal parts of the Bβ and γ chains respectively where the chains' C-termini are located (they form *"β-nodule"* and *"γ-nodule"*). Lastly, the Aα chains, that are the longest ones, organize themselves at the end of the coiled-coil region, extending into two highly-flexible series of repeats named *"αC-connectors"* followed by two globular and not very stable *"αC-domains"* [1], [4], [5].

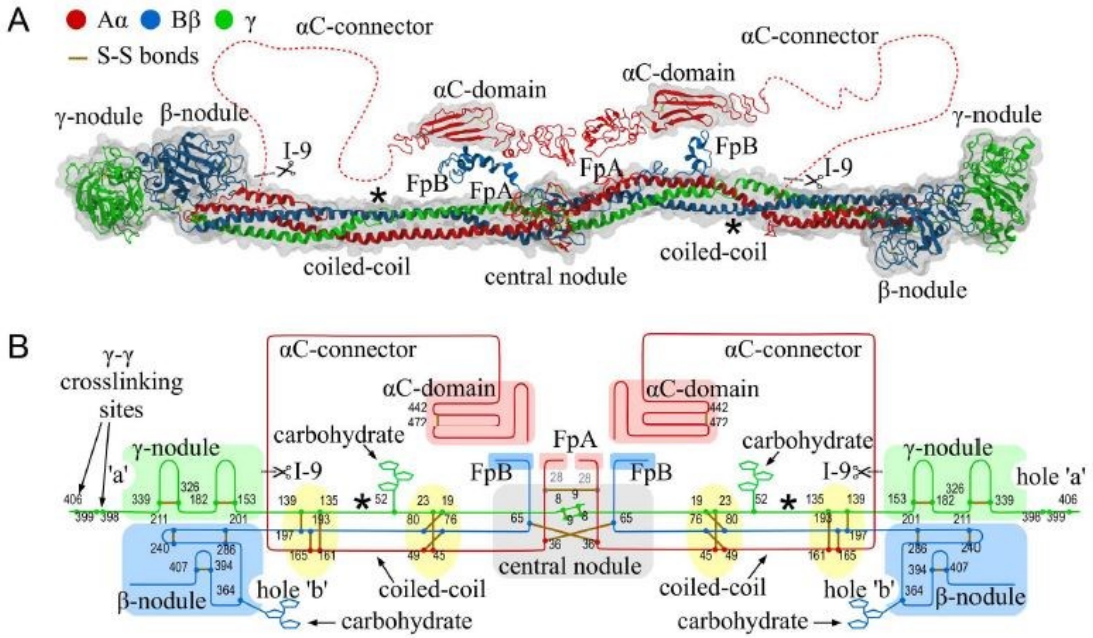

Figure 2: (A) Fibrinogen structure; (B) Schematic diagram of the polypeptide chains of fibrinogen [70]

Directly related to the structure there is a heterogeneous charge distribution in fibrinogen molecule which is really difficult to calculate, depending both on pH and ionic strength: in the central area a negative charge is predominantly located at physiological pH (even though there is a great dependence on pH itself), whereas the end part of the Aα chains is positively charged up to pH = 11 [6], [7].

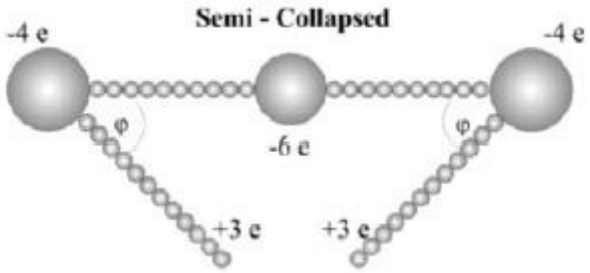

Figure 3: Typical charge distribution in fibrinogen in physiological conditions [7]

1.1.2 Metabolism of fibrinogen

The study of the metabolism of fibrinogen is based on the evaluation of its half-life which, in normal condition, is about 3-5 days. Currently, physiological catabolic pathway of

fibrinogen is unknown, even though it is recognized that 2-3% of fibrinogen loss in healthy individuals is due to coagulation and fibrinolysis processes [1].

Intravascular fibrin formation (during blood coagulation process) and degradation of fibrinogen by plasmin (fibrinolysis) have thus been proposed as two pathways of fibrinogen catabolism: however, in both cases, in presence of heparin (inhibitor of blood coagulation) and of tranexamic acid (inhibitor of fibrinolysis) respectively, significant variations of half-life have not been observed [1].

During an inflammation process, specific intracellular signaling pathways in hepatocytes are triggered and different transcription factors allow for modulation of gene expression because of the activity of interleukin-6 and various pro-inflammatory mediators that, as mentioned above, up-regulate the fibrinogen [1].

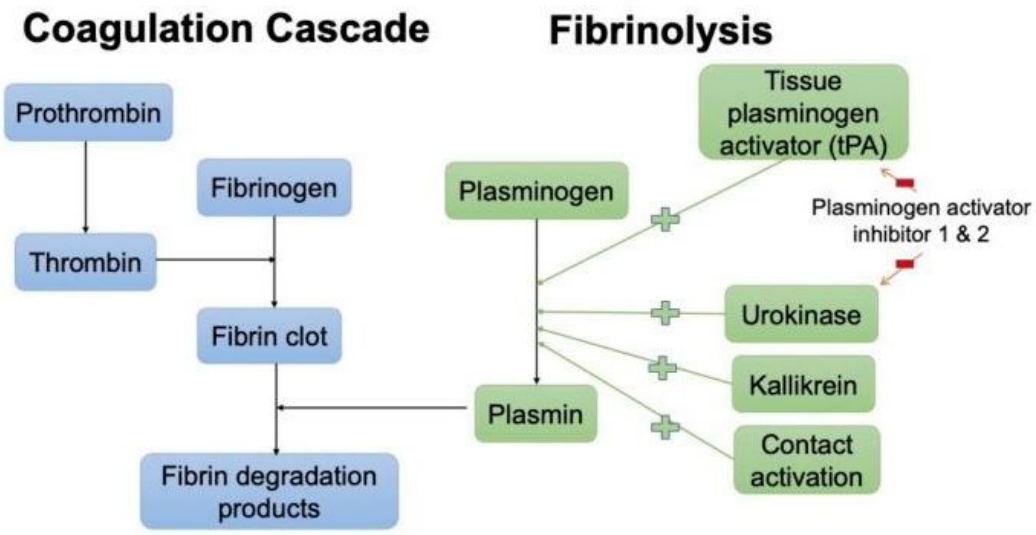

Figure 4: Simplified scheme of coagulation and fibrinolysis pathways [71]

Despite scientific studies have shown two different types of fibrinogen, referred to as "intracellular fibrinogen" which is stored in platelet α-granules and common "plasma fibrinogen", it is unknown whether there are structural and functional differences between them. It is noteworthy that patients with low levels of plasma fibrinogen, also present low level of intracellular fibrinogen [1].

Fibrinogen can be also synthesized in some extra-hepatic tissue both in physiological and pathological conditions as happens in lung epithelium (another example is about

epithelial cells from intestine). Although, the role of fibrinogen derived from extra-hepatic tissues is not yet known [1].

1.1.3 Features of fibrinogen

Thanks to a bending process of the coiled-coils around a specific central hinge point in a non-helical portion of the γ chain, fibrinogen presents an interesting conformational flexibility. According to recent research, coiled-coil region's functional role is closely related to the tensile deformation of fibrin fibers that are able to partially break up and undergo a spring-like reversible extension-contraction right after, in order to facilitate the accommodation and the propagation of the tensile stress along the fiber axis; α-helices can also convert into β-sheets following a severe tensile or compressive deformation [1].

Another important feature is about the presence of different types of binding sites for calcium ions, that contribute towards some main fibrinogen functions such as fibrin polymerization during which Ca^{2+}-binding allows the improvement of the lateral aggregation in order to form thicker fibers. For this reason, grave functional consequences could be observed in case of mutations affecting Ca^{2+}-binding sites [1].

In high-affinity binding sites the dissociation constant for calcium ions is sufficient to allow the full occupation in fibrinogen of these sites at physiological Ca^{2+} concentrations: this aspect can be observed in γ1 e β1 sites, located in γ chains and β-nodules respectively. In particular, the bond between calcium ions and γ chains is able to protect the γ chains themselves from enzymatic degradation. At the same time, there are two other Ca^{2+}-binding sites with much lower affinities called γ2 e β2: γ2 sites derive from a molecular rearrangement induced by crystal packing, considering that impairments of these sites just cause moderate effects on the functional properties and the crystal structure of the fibrinogen; β2 sites, instead, have a crucial role in the lateral aggregation of protofibrils and they probably control the accessibility of the tissue plasminogen activator t-PA-binding site in fibrinogen. Other low affinity Ca^{2+}-binding sites are associated with the sialic acid residues on the carbohydrate chains [1].

The last important feature is about the presence of carbohydrate attachment sites that present the typical NXS (Asn-X-Ser) or NXT (Asn-X-Thr) sequences of N-glycosylation: two of them are connected to the β-nodule, while the remaining two are connected to the coiled-coil. About the Aα chains, although the presence of two NXS sequences, any type of carbohydrate is absent. Again, the presence of carbohydrate on fibrinogen strongly influences the process of fibrin polymerization and the clot structure. In fact, the formation of fibrin networks containing thinner fibers with a higher density of branch points can occur as a consequence of different types of livers diseases (e.g. cirrhosis), that induce the increase of the levels of sialyation of the carbohydrate in the fibrinogen itself. In addition, clot structure can change as a result of a complete removal of carbohydrate, with the formation of very thick fibers. These aspects could be seen as a demonstration of the fact that both the charge and the mass of carbohydrate are decisive in the modulation of the extent of lateral aggregation [1].

1.1.4 Variations and modulation of fibrinogen structure and properties

Plasma concentrations of fibrinogen as well as its biochemical properties may be influenced by a number of different molecular modifications, including gene polymorphisms, alternative splicing and post-translational modifications [2]. According to recent studies, healthy individual could present more than a million non-identical forms of fibrinogen following the different combinations of modified or inherently polymorphic sites [1]. Despite this, individuals with increased cardiovascular risk have shown various fibrinogen modifications in plasma clots [2].

About genetic mutations, they are associated with abnormal fibrin clot formation and bleeding and/or thrombosis. In this context, the most abundant fibrinogen variant is γ' fibrinogen which provides about 8-15% of total fibrinogen in healthy individuals [4]: it is made up of approximately 90% heterodimers containing one γ' chain and one γA chain, while the remaining 10% contains two γ' chains; γ' chains seem to play different roles in hemostasis. One of the main features of γ' fibrinogen is about its impact on the clot

architecture that appears mechanically stiffer and much more resistant to fibrinolysis process [2].

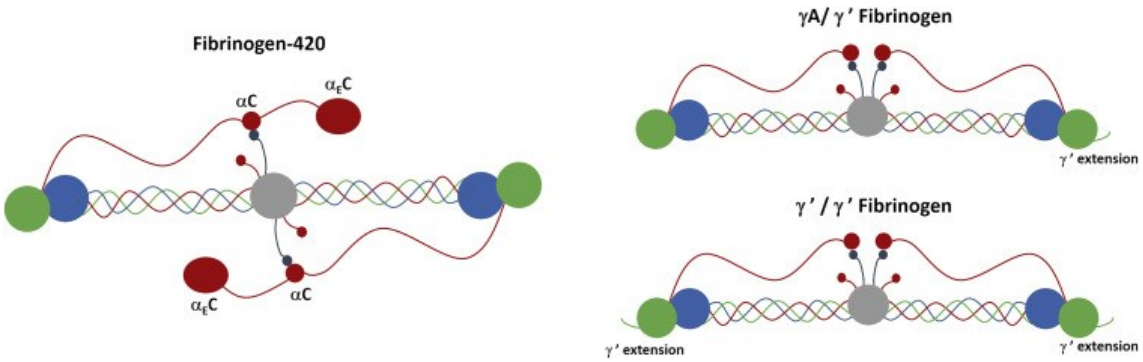

Figure 5: Comparison between the structures of normal fibrinogen and γ' fibrinogen [72]

A lot of different epidemiologic studies demonstrate that altered arterial and venous thrombosis risk can be related specifically to the level of circulating γA/γ' fibrinogen. While elevated levels of γA/γ' fibrinogen cause an increased incidence of coronary artery disease, myocardial infarction and ischemic stroke, reduced values of the same ratio are connected to an increased risk of VTE (Venous Thromboembolism) and thrombotic microangiopathy. These evidences emphasize both the tendency to promote arterial thrombosis and the ability to protect against venous thrombosis of γA/γ' fibrinogen [4].

On the other side, post-translational modifications, that affect the fibrinogen biological function acting on the rate of fibrin polymerization, the blood clot structure, the course of fibrinolysis and the physiology and pathophysiology of blood coagulation, are more common [2], [4]. This is probably due to the high concentration of fibrinogen in circulation, which can be easily targeted by enzymes, heading for a structure and function change [4]. The C-terminal portion of the Aα chain is more susceptible to the intracellular and extracellular proteolytic enzyme action than Bβ and γ chains, in which the digestion occurs only at specific sites [1].

The post-translational modifications consist of multiple biochemical reactions that could be associated with both physiological and pathological conditions, such as inflammation or ischemia. Some examples of these types of modifications are: nitration (thanks to neutrophils and monocytes that generate nitrating metabolic intermediates), oxidation (proteins are a common target for oxidative processes), homocysteinylation, glycation,

etc. These modified forms are involved in functional and structural variations of the properties of fibrinogen [1], [4].

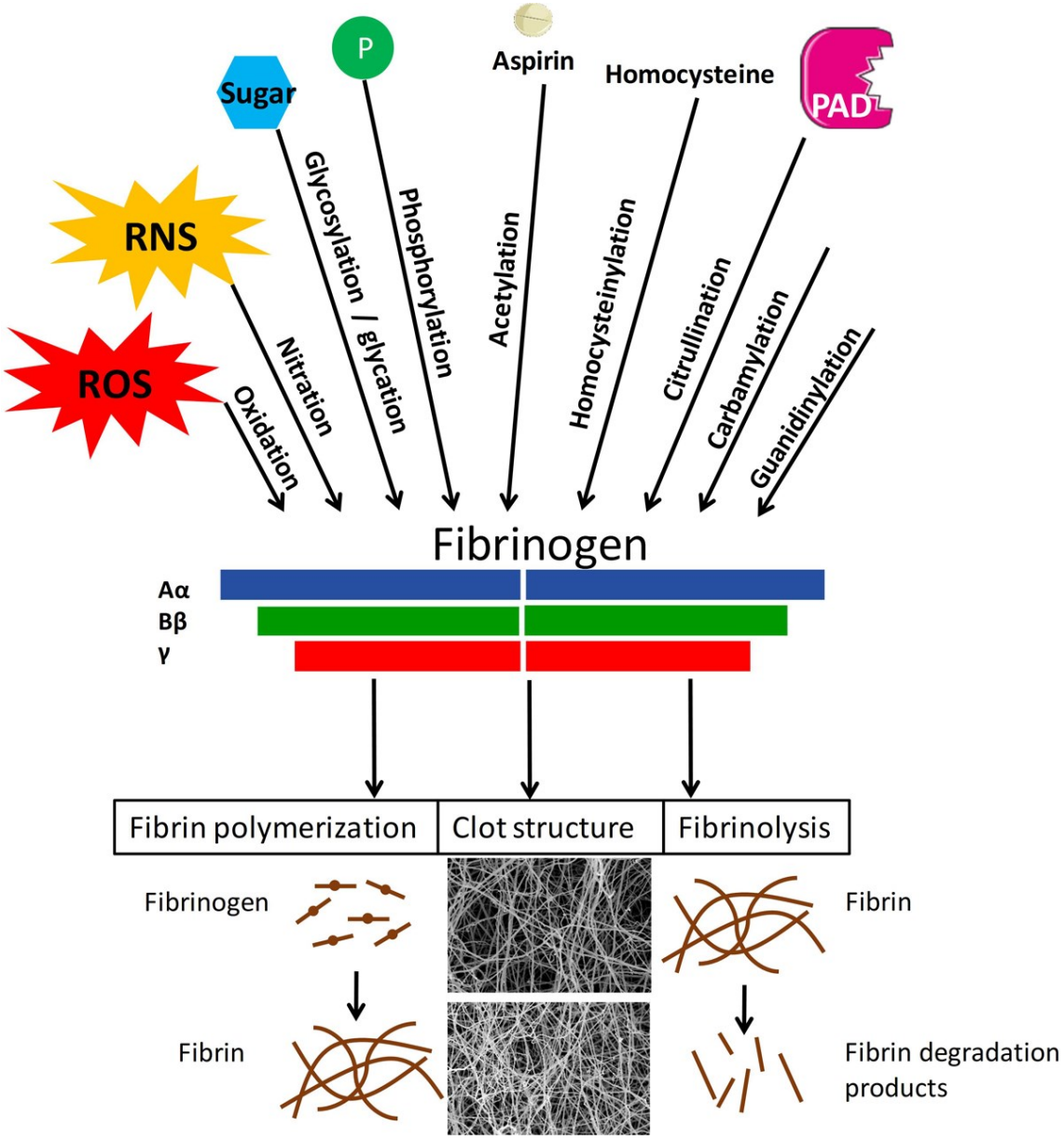

Figure 6 : Examples of post translational modifications of fibrinogen and their consequences [73]

Apart from the kind of modification, the study of variations of fibrinogen is still in a research phase, though it remains unclear whether these clot abnormalities are only a biomarker for a pathophysiologic mechanism, so that they could be a consequence of the pathology, or whether they represent the cause for the disease etiology [4].

1.2 Role of fibrinogen in the coagulation

1.2.1 Blood coagulation: introduction

"Coagulation", also known as "clotting", is the process by which blood passes from a liquid state to a gel one, forming a blood clot, in order to stop bleeding. The generation of a mechanically stable clot is essential to ensure the prevention of blood loss ("hemostasis") as well as to promote wound healing. During the coagulation, despite its characteristics of solubility in normal conditions, fibrinogen is able to convert into an insoluble entity: in fact, starting from a vessel wall injury, activated blood cells or a foreign surface, a cascade of enzymatic reactions is activated and fibrinogen turns into insoluble fibrin until platelets are activated and adhere at the site of vasculature injury [8]. At the end of the clotting, different types of enzymatic reactions allow the fibrin clot proteolytic dissolution in a process called "fibrinolysis", in order to restore the impaired blood flow: the main enzyme involved is plasmin, a serine protease which derives from plasminogen, its inactive precursor, after that plasminogen itself adheres to the fibrin clot. Finally, following the clot dissolution, soluble fibrin digestion products are released into the circulating blood [1], [9].

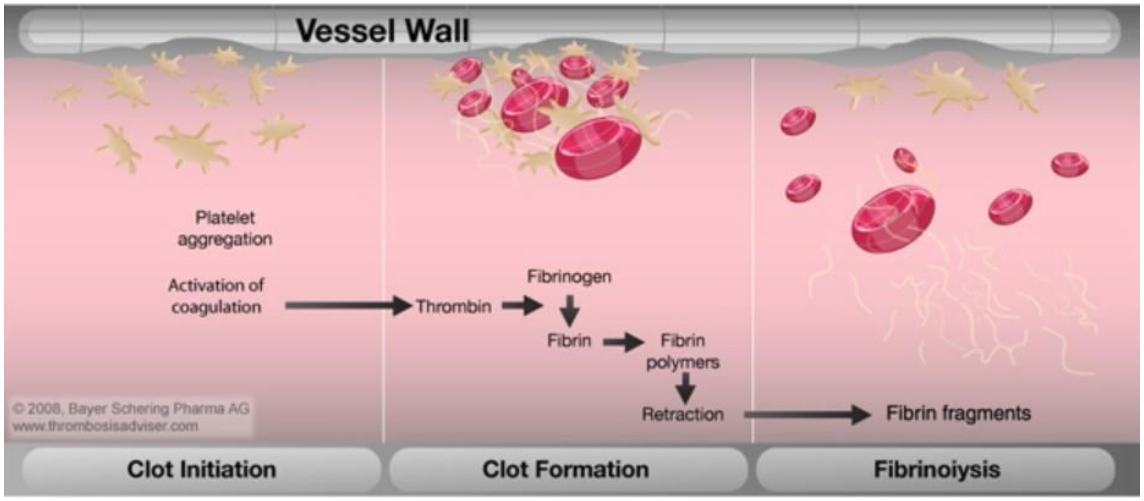

Figure 7: Steps of clotting process [74]

Moreover, fibrinogen plays a crucial role in the initial phase of the hemostasis, known as "primary hemostasis", during which it acts as a connection point for the activated platelets thanks to its affinity with the integrin αIIbβ3, the major adhesive receptor on platelets themselves [1]. This process, that is precisely called "clot contraction" or "retraction", strongly depends on both the concentrations of platelets and fibrinogen [4].

In physiological condition, fibrinolysis and clotting are perfectly balanced: the prevalence of one of these processes could lead to severe consequences such as excessive bleeding or thrombosis in the two cases respectively. Specifically thrombosis, which consists in the formation of a thrombus, i.e. a clot that partially blocks the blood flow through a vessel, is the main cause of several pathological conditions as myocardial infarction, ischemic stroke and other cardiovascular diseases [1].

A lot of parameters such as the concentrations of protocoagulants, anticoagulants, fibrin(ogen)-binding proteins, molecules and metal ions ant the contributions of blood and vascular cells, cell-derived microvesicles and presence of blood flow could influence the clot properties in terms of formation, structure and stability [4].

1.2.2 Coagulation process

The process of conversion from fibrinogen to fibrin occurs in two major steps: enzymatic and non-enzymatic. In the enzymatic step a fibrin monomer is formed thanks to the action of the thrombin, normally present in the blood, which catalyzes the cleavage of the fibrinopeptides of fibrinogen producing fibrin monomers: through the activation of its zymogen, called “prothrombin”, thrombin is able to implement a serine protease process thanks to its high specificity. During the non-enzymatic step, starting from a process of spontaneous self-assembly, the obtained monomeric fibrin is able to produce fibrin oligomers, which can get longer until they create two-stranded protofibrils. These protofibrils, thanks to both lateral and longitudinal aggregation process, lead to the formation of fibers that yield a three-dimensional gelled network, that is the clot. Finally, there is the production of a mechanically and chemically more stable mature fibrin clot thanks to the action of Factor XIIIa, a plasma transglutaminase, that performs a covalent crosslinking in order to stabilize the fibrin polymer [1], [10].

Fibrin formation and structure are strongly influenced by the levels of thrombin concentration: while an elevated concentration of thrombin may produce fibrinolysis resistant clots thanks to the generation of a dense network of highly-branched fibrin fibers, the clots derived from low levels of this enzyme are more vulnerable to fibrinolysis because of the formation of coarse networks of unbranched fibrin fibers [4], [9].

According to different studies, it is possible to affirm that fibrin structure is really determinant of hemostasis and thrombosis: fibers generated by high concentration of thrombin are thinner, more compact and have smaller pores, so that they can be correlated to an increased thrombotic risk; on the other side, clots derived from lower concentration of the enzyme show thicker and less compact fibers and larger pores, with an increase of bleeding risk. It is also appropriate to underline that, in the case of fully hydrated clots, the increase of the thrombin concentration causes an important decrease of the average protofibril content per fiber, but a bland decrease of fiber size, leading to a generally less compact fiber. For this reason, it is possible to assert that the generation of thinner fibers can be related to a process of fiber compaction or shrinkage that occurs during dehydration [4], [9].

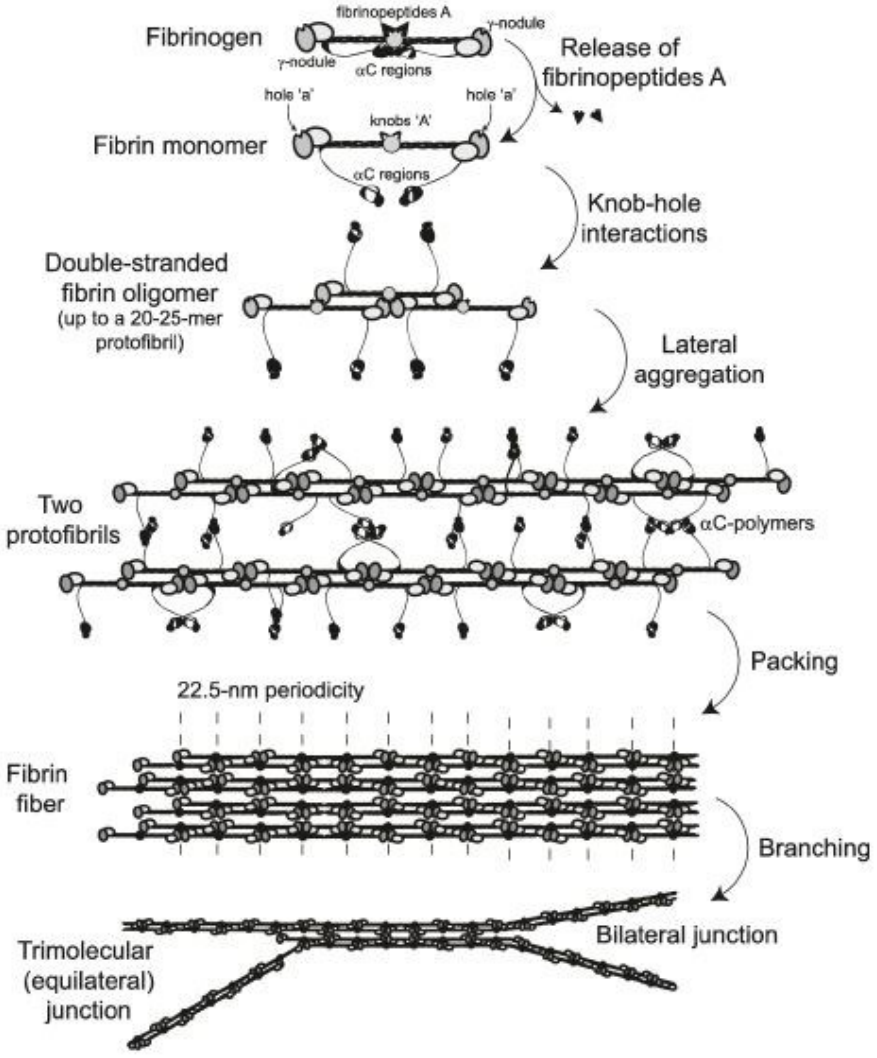

Figure 8 : Schematic diagram of fibrin polymerization [1]

By analyzing all the steps, firstly there is the cleavage of FpA (residues 1-16, AαArg16-Gly17 peptide bond) and, more slowly, of FpB (residues 1-14, BβArg14-Gly15 bond) of Aα and Bβ chains respectively by the action of the thrombin, with the reaching of the maximum value of the rate of release of FpBs when polymerization is almost complete: in fact, thrombin action allows to the exposure of new polymerization sites that in normal fibrinogen are masked. After the release of fibrinopeptides, this cleavage process leads to the exposure of new N-terminal sequences: Aα without the FpA and Bβ chains without the FpB are called "*knobs A*" and "*knobs B*" respectively [1], [10]. The conversion of fibrinogen into fibrin monomer can be described as $(A\alpha\ B\beta\ \gamma)_2 \rightarrow (\alpha\ \beta\ \gamma)_2 + 2FpA + 2FpB$ [1].

About the cleavage of FpBs in surface-attached fibrinogen, it is faster than FpAs', in function of fibrinogen surface density and orientation, as a demonstration of the different ability of thrombin to access and cleave FpAs and FpBs depending on the fibrinogen conformation. In fact, the accessibility of the N-terminal portions of the Aα chains containing FpA to the active site of thrombin is higher and this difference with the case of FpA is based on the spatial restrictions of the binding of thrombin to fibrinogen. Eventual mutations in thrombin cleavage sites at positions AαArg16 or BβArg14 may cause the formation of impaired fibrin, because of the impediment to the FpA or FpB release respectively [1].

An important step to induce fibrin polymerization is the formation of the "*A-a interaction*", a strong, highly specific and stable intermolecular association between knobs A, i.e. new N-terminal sequences Gly-Pro-Arg (GPR) and the so called "*holes*" (or *pockets*) *a*" that are always open in the γ-nodules and that are strongly complementary to the knobs A themselves [1], [10]. These interactions are able to hold two fibrin monomer molecules together, previously obtained from the cleavage of FpA, that interact in order to form a half-staggered dimer. A third fibrin molecule is added and it forms an end-to end connection where the two adjacent molecules touch each other, while a D:D interface that comprises the junction between monomers in each of two strands in fibrin oligomers is formed starting from the interaction between the lateral D regions of two molecules. So, thanks to the longitudinal addition of fibrin monomers, longer two-stranded fibrin oligomers of varying length are formed; furthermore, two strands of fibrin oligomers can

laterally interact thanks to the central E region of one fibrin molecule and two lateral D regions of two other molecules. Interactions at the D:E and D:D interfaces, together with A-a interactions, allow to maintain the D-E-D complex. As the process continues, the longitudinal addition of the fibrin monomers to the oligomers leads to the formation of two-stranded protofibrils: they are about ~20-25 monomers long (0.5-0.6 μm) and they are able to self-interact, aggregating laterally [1], [10].

In a similar way, after the cleavage and the release of FpB, the β chain acquires a new N-terminal sequence Gly-His-Arg-Pro (GHRP), which is the working part of knob B that forms the "*B-b interaction*", binding to hole b [10].

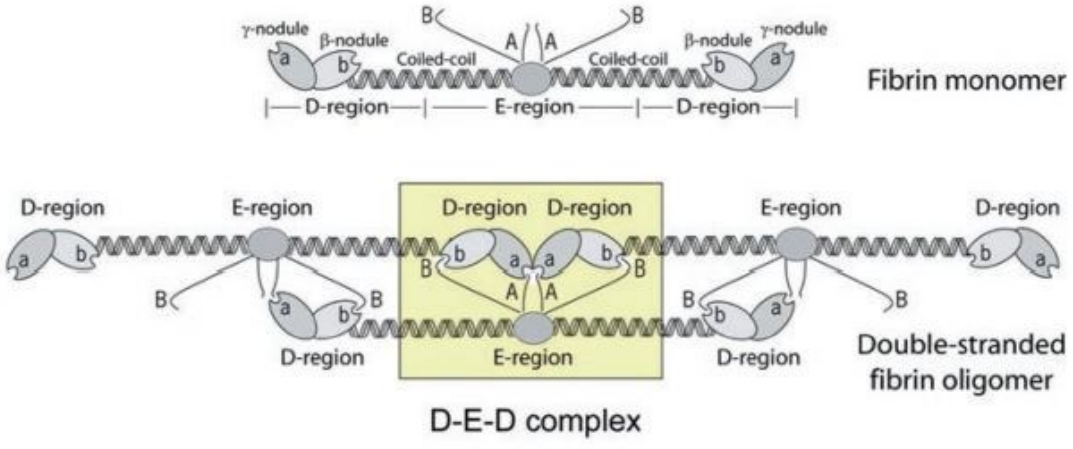

Figure 9: Schematic diagram of knob hole interactions with the formation of D E D complex [1]

The lateral aggregation of protofibrils only happens after the reaching of a certain threshold length, implying that the bonds mediating the interactions between protofibrils themselves are weak. This process, independently of the release of FpB, makes it possible to form more or less thick fibers, leading to the generation of a fibrin molecule, although it is mostly still unknown in terms of mechanisms, structural motifs and driving forces involved. The fibrin fibers are neatly packaged and organized with a high regularity both in lateral and longitudinal direction and they are characterized by a 22.5-nm periodicity corresponding to half the length of the fibrin molecule. This periodicity is ensured by a stretching of the protofibrils that are newly added to the outside of a fiber as soon as their path length increases. The lateral aggregation continues until the protofibril stretching energy become higher than the energy of bonding: this aspect can be tuned thanks to a thermodynamic mechanism which monitors the diameters of fibers. There are different

structures that probably participate in inter-protofibril lateral aggregation, including "*knobs B*" and "*holes b*" [1].

αC regions also have an important role during fibrin polymerization: they cause an increase of lateral aggregation, while not being necessary. Compared to a case of full-length fibrinogen, an eventual lack of the αC regions determines the formation of clots with thinner fibers and a higher density of branch points. In fact, in general, a decrease of the number of lateral aggregations leads to thinner fibers and more branch points in the final fibrin molecule; by contrast, as the number of lateral aggregations increases, thicker fibers and fewer branch points are formed [1].

The αC regions contribute is related to their capability of self-interacting both within and between protofibrils thanks to their flexibility and protrusions. These regions are able to trigger an αC-αC polymerization based on two different mechanisms: one of them, that is a self-association of the αC-domains, takes place at the level of N-terminal subdomains by β-hairpin swapping, while the second one is about the interaction of the C-terminal subdomain with the αC-connector. Thanks to these types of interaction there is the formation of αC polymers, accompanied by a reinforcement played by an additional crosslinking under the action of Factor XIIIa [1].

The generation of the final space-filling 3D network occurs after the thickening by lateral aggregation and the growth in length of the fibrin fibers which, during this period, also branch. The branch points are formed thanks to two different molecular mechanisms known as "*bilateral junction*" and "*trimolecular* (or *equilateral*) *junction*". If the new fiber is originated by two separate protofibrils obtained by a divergence as a consequence of an incomplete lateral aggregation of two protofibrils, the branchpoint is a "bilateral junction". On the other side, it is possible to talk about "trimolecular junction" if there is an independent growth of the monomeric molecule and the protofibril to which it is bound, in order to form two strands each: this is allowed by the fact that a fibrin monomer attaches to the end of a protofibrils via only one A-a interaction (or one γ-nodule) [1].

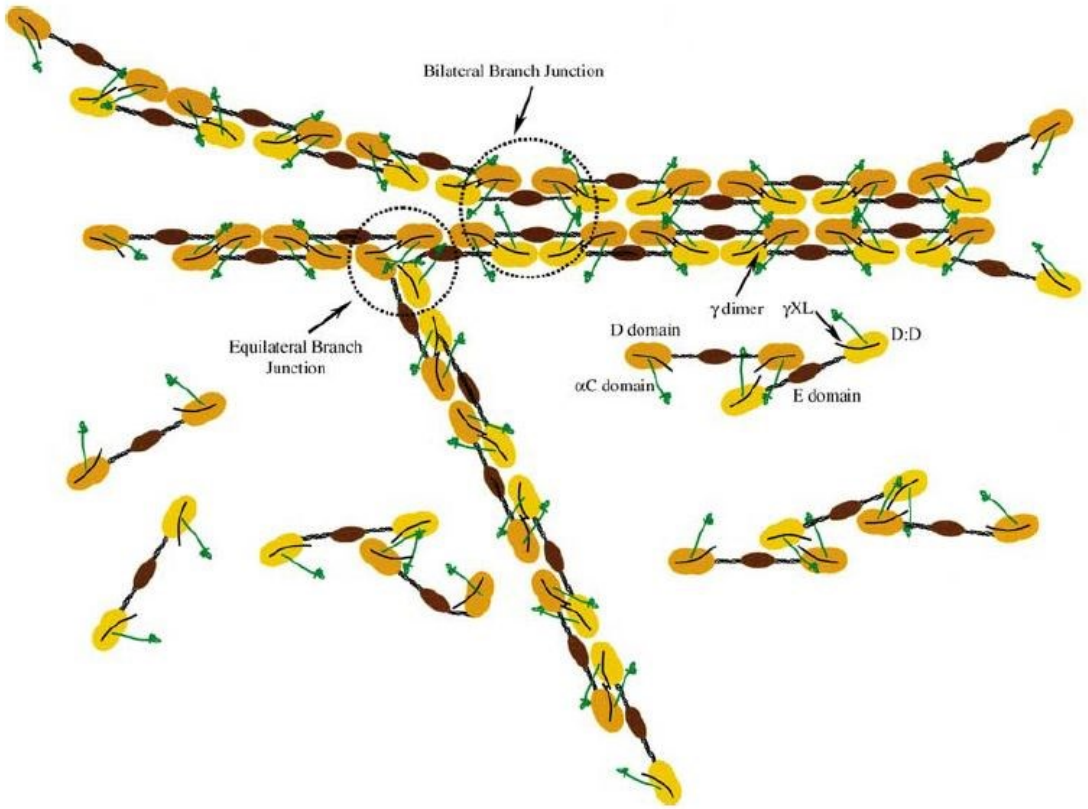

Figure 10: Schematization of bilateral and equilateral junctions [75]

However, different studies demonstrate that the type of initial branchpoint does not influence much the final network structure, given that most of branch points in clots are made of the joining of three fibers of about the same diameters together [1].

At the time that 15-20% of conversion of the fibrinogen to fibrin has occurred, the process of gelation starts so that definitive fibrin clot can be generated thanks to the transition from sol to gel upon the formation of a 3D filamentous network: it is clear that the network is not yet stable and fully branched at the reaching of the gelation point. As a consequence of this aspect, new fibers and branch points continue to form in the gel. Different types of variable parameters such as the fiber diameter, density and length, number of branch points and the size of pores can be used as a method to characterize and describe the structure of fibrin networks: the extreme heterogeneity of these parameters can be related to the kinetics of fibrin polymerization [1].

The gelation point, which could be determined as blood/plasma clotting time, represents a critical moment of the coagulation process, so much so that it may be used as a test to reveal coagulation disorders in many clinical assays [1].

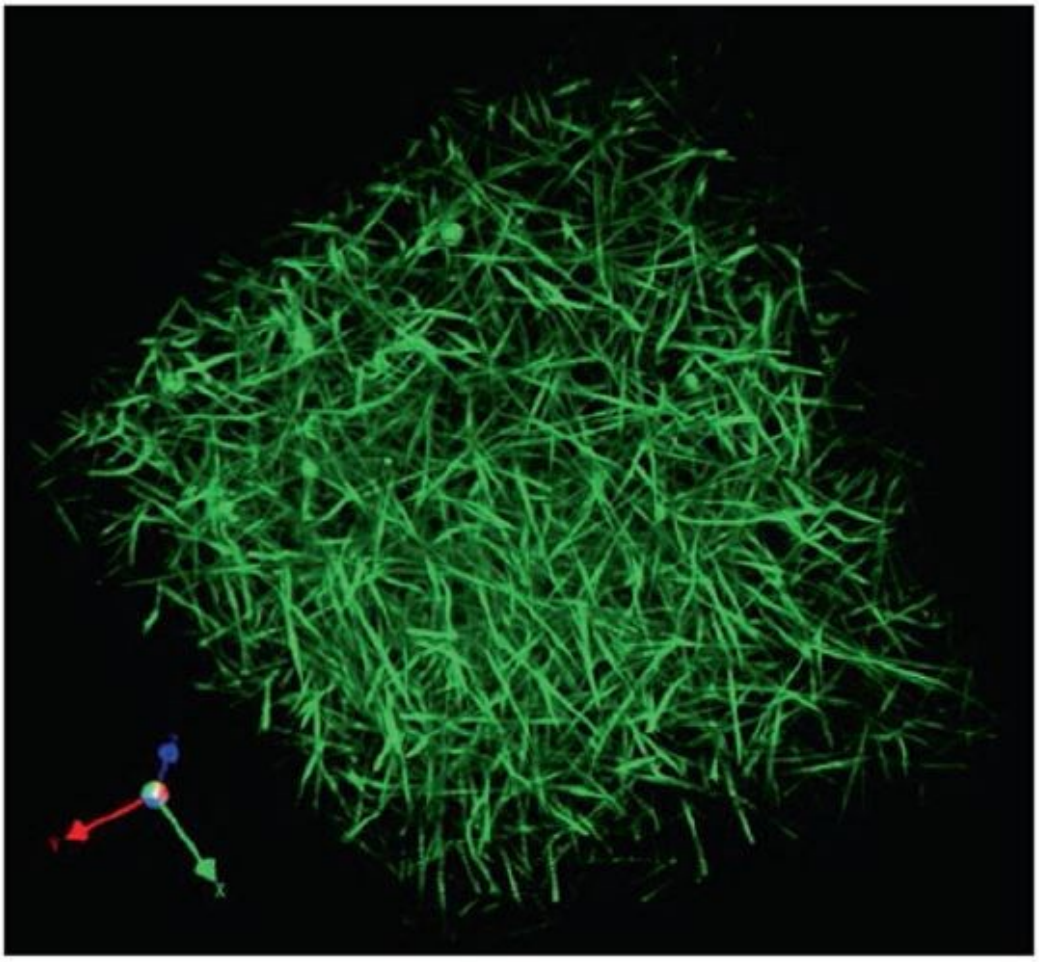

Figure 11: 3D reconstruction of the fibrin clot network of a hydrated fibrin gel obtained using fluorescent confocal microscopy. The labeling is made using Alexa 488 [1]

Finally, there is the covalent crosslinking in order to stabilize the clot against proteolytic and mechanical damages, as before this process fibrin polymerization is still reversible. The crosslinking happens thanks to Factor XIIIa, a plasma transglutaminase derived from the activation of Factor XIII zymogen through the work of thrombin in the presence of Ca^{2+}. The crosslinking point derives from longitudinally orientated covalent isopeptide ε-(γ-glutamyl)-lysyl bonds between two end-to-end interacting molecules in correspondence with a specific crosslinking site that is comprised into amino acid residues in the C-terminal ends of the γ chains of fibrinogen [1].

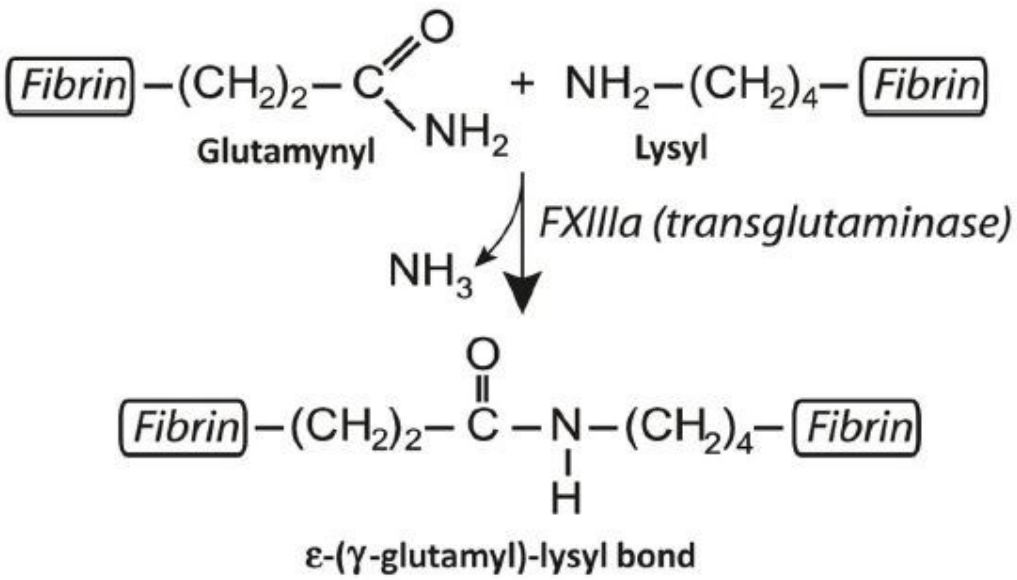

Figure 12: Crosslinking process of fibrin and formation of ε --(γ glutamyl) lysyl bonds catalyzed by Factor XIIIa [1]

As an alternative, it is possible that the same isopeptide bonds are more slowly catalyzed between the αC regions with the aim of stabilizing long αC polymers. The third example of crosslinking involves the formation of α-γ-heterodimers among α and γ chains [1].

Thanks to the crosslinking within and between protofibrils, a more stable, mechanically strong and resistant to fibrinolysis clot is obtained: in fact, the polymerization becomes irreversible. The only way to dissolve the crosslinked fibrin is through the reduction of disulphide bonds that hold polypeptide chains together or by chemical or enzymatic hydrolysis of peptide bonds [1].

It is important to emphasize that formation, structure and properties of the fibrin network may be influenced by the blood flow: considering that in normal human plasma there is a fibrinogen concentration of 3 g/l, the majority of the clot mass will be made up by liquid (99.7%), while the remaining part (0.3%) will be protein. In presence of flow conditions, the amount of fibrinogen increases, so that the fibers of the clot will be denser, thicker, and more packed, with some of them orientated along the direction of the flow itself: these changes can also influence the susceptibility of the clot, which is stiffer and less malleable, to the enzymatic lysis, so that it requires longer degradation time [1], [11]. On the contrary, fibrin clots which derive from lower fibrinogen concentration, are

characterized by a looser structure [11]. Finally, it has been demonstrated that the shear forces of blood flow increase the risk of the detachment of a piece of clot that could be transported by the blood stream into another vessel, blocking it: it is referred to as “embolization” [1].

Regardless of this, both in vivo and in vitro there are a lot of parameters which could affect fibrin features and behavior such as ionic strength, pH, endogenous and exogenous substances e.g. lipids, proteins, nucleic acids and all the physiological and pathological natural and artificial compounds that are present in the organism [1].

1.2.3 Fibrin characteristics

About biological properties of the fibrin, it is crucial in preventing blood loss, but also acts as a temporary scaffold during tissue healing and remodeling after an injury, supporting the tissue itself; in addition, fibrin can bind to different proteins and growth factors in a specific way so that it can actively generate specific receptor-mediated interactions with cells or it can be released in the site of the damage to facilitate wound healing [9].

About mechanical aspects, thanks to its both elastic and viscous properties, fibrin can be defined as a viscoelastic polymer: viscoelasticity can be described as the mechanical response in function of the rate and duration of loading [1], [9]. While the reversible mechanical deformation can be used in order to define the elasticity or, equivalently, the stiffness, a slow irreversible deformation induced by force and known as “creep” can describe the viscosity or, equivalently, the plasticity. At the same time both elastic and viscous response can be characterized starting from “shear storage modulus” (G’) and “shear loss modulus” (G’’) respectively: G’ is defined as the part of shear stress that is in phase with strain, while G’’ is related to a lag condition between shear and stress. These parameters as a whole can describe the clot response to the forces that are applied on it [1].

Fibrin behavior can be described thanks to a stress-strain curve, that reports an applied stress, defined as a ratio between force and area, against the degree of induced

deformation, that is the strain [1]. The studies that have been carried out on fibrin show that it undergoes a particular non-linearity phenomenon known as “strain hardening” or “strain stiffening”, typical of biological gel-like structures: at lower strains, there is a direct proportionality between stress and strain, with a constant elastic modulus (that is reflected in a constant curve slope), whereas at larger strains there is a huge increase of the stiffness (elastic modulus) following the breaking of the linearity, that graphically manifests itself through the dizzying rise of the slope of the curve [1], [9].

The stress-strain curve of the fibrin comprises three different regions: the first part describes the linear viscoelastic response to compression that occurs when most fibers are straight and degrees of compression are low, the second zone underlines an elastoplastic plateau that is representative of the collapse of a high quantity of fibers, finally, the third zone, is related to a nonlinear response, following the bending of fibers after buckling and inter-fiber contact, that occur at the same time as the network densification, for higher degrees of compression [9], [12].

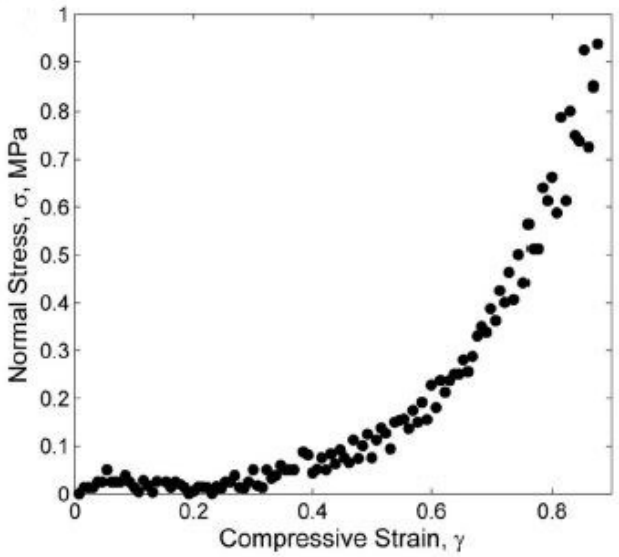

Figure 13: Example of the trend of the stress strain curve for fibrin clots [12]

It also has been observed that the deformation of the fibrin matrix is nonuniform, so that an eventual downward force applied on the top surface may tend to compress the top layers earlier and stronger than the lower parts [9].

So, in light of this, it is possible to affirm that, as no major changes take place in fibrin structure during creep experiments, it can be defined as an “experienced structure” [9].

The extreme extensibility observed and quantified in most of the research studies highlights stabilized plasma clots fibrin fibers' capability of stretching to over three times their relaxed length before breaking under stress blood. Obviously, the stretching process leads to an increase of the stiffness of the fibers themselves and, consequently, to a distribution of the strain load to the less strained fibers, with the reduction of the strain concentrations. It is important to notice that non-linear behavior can be observed in case of compressive deformations, as well as shear and tension [1].

Viscoelastic properties turn out to be more accelerated in pathological conditions as pulmonary embolism unlike healthy subjects; also clots seem to be stiffer in patients who have had heart attack at an early age [1].

Since platelets sense the stiffness of the underlying fibrin substrate, platelets activation, adhesion and spreading may increase following the rise of the hardness of the substrate itself [1].

1.3 Tissue integration of biomaterials

1.3.1 Biomaterials: introduction

A biomaterial, which is defined as any matter, surface or construct that interacts with biological systems, can be derived in nature or be synthesized via bioengineering approaches [13]. Coming into contact with the organism, the biomaterial must have some important physical and chemical features, be inert and evoke a limited immunological response from the host as it has to integrate with the tissue: the biological interactions with the host depend in particular on the layer of serum proteins adsorbed nonspecifically on the material surface [14], [15]. This aspect is related both on surface chemistry and topography and can be improved thanks to different types of surface modifications, even because the adsorption is not always specific and the proteins themselves may be denatured or displaced [15].

The main idea is to design new biomaterials in function of the information, obtained by definite analysis, about the structure and the functions of the extracellular materials, that represent the basis of self-organizing capacity of the cells to generate a tissue: in fact, cells are able to perceive, interact and ingest the material, in function of both chemical and mechanical (through mechanosensing) features of the biomaterial [15]. The biomaterial design must ensure an appropriate integration and a good performance [14].

The performance of the biomaterial could be also affected by external and environmental parameters such as temperature, ion flows and electromagnetic fields or signals in general, beyond that its mechanical properties and size [15].

Biomaterial needs to interact with the host immune system, triggering two important processes known as “foreign body reaction” (FBR) and inflammation, so that a full integration can occur: in particular, only recently, it has been conceived that inflammation response is essential in order to reach optimal tissue repair and regeneration [14]. A good host engagement depends on the extent of the disturbance of the host homeostasis, in that FBR can cause a detrimental or beneficial response [14].

1.3.2 Inflammation and foreign body reaction

The implantation of the biomaterial instantly determines the adsorption of proteins, lipids and sugars from blood on its surface, with the subsequent recruitment of innate immune cells: depending on material composition, topography, roughness and chemistry, there will be a different immune response [14].

After the biomaterial implantation a sequence of processes is triggered: the events are injury, blood-material interaction, matrix formation, acute and chronic inflammation, development of a granular tissue, foreign body reaction and development of a fibrous capsule which envelops and isolates the biomaterial, over a period of weeks to months [14], [16].

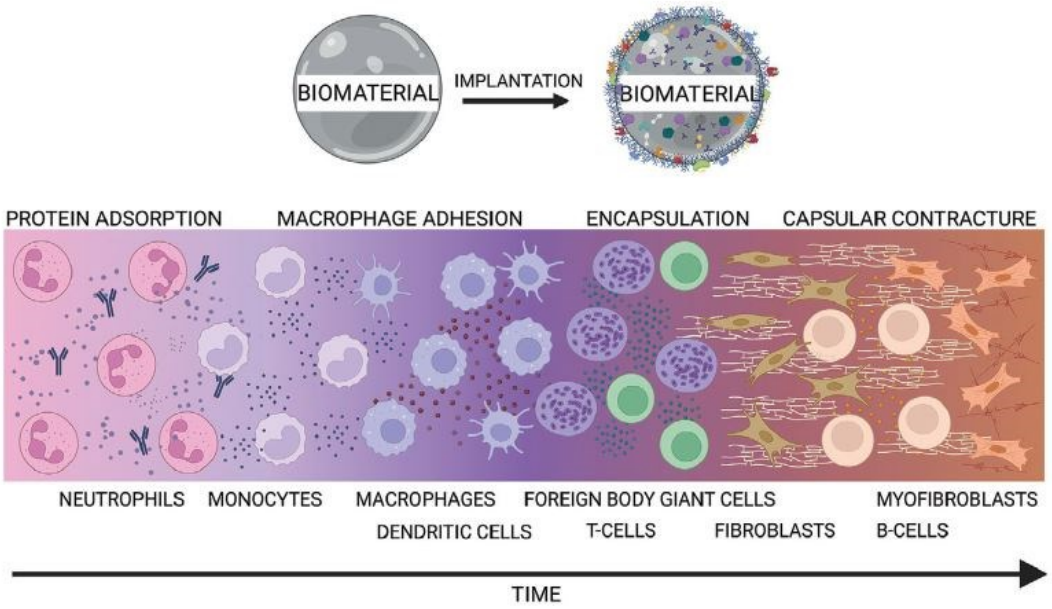

Figure 14: Schematic representation of FBR to biomaterials [14]

It is important to underline that the ideal outcome should include a rapid resolution of the healing process, with the reaching of a steady state and the subsequent complete integration of the implant with the biological environment without the formation of the fibrous capsule. Nevertheless, one of the most frequent complications of an implantation is the formation of the fibrous capsule itself, especially in case of extensive damage which cannot heal properly e.g. after a chronic inflammation [17].

About the entire process, first of all, the presence of an injury to the vascularized zone of the tissue causes an inflammatory response so that the damaged area can be isolated and

the tissue can heal: as this process determines different variations in vascular flow and permeability, a greater quantity of fluids and proteins can get to the site of the injury thanks to an increase of the blood flow [14].

The ensuing protein adsorption on the biomaterial surface, which concerns the first seconds from the implantation, allows to create in a very dynamic way a blood-based transient provisional matrix on and around the biomaterial that facilitates wound healing and FBR processes thanks to structural, biochemical and cellular components supply [14], [16], [18]. During this process fibrinogen is essential to control macrophage fusion and the subsequent fibrous capsule formation also because the provisional matrix is rich in mitogen, chemoattractants, cytokines, growth factors (GF) and other bioactive agents that modulate macrophage activity through the action of specific activating or inhibiting substances, as well as the proliferation and activation of other cell populations in inflammatory and wound healing response. As fibrinogen provides a substratum for platelet adhesion and stimulates platelet aggregation, at this stage also thrombus formation begins to happen following the activation of the whole coagulation system, the complement system, fibrinolysis, the kinin-generating system and platelets [11], [14], [18]. Finally, the adsorption or immobilization of fibrinogen on the surface is also essential to prevent the additional adsorption of other serum proteins [11].

With the passing of the time, the proteins undergo the so called "*Vroman effect*", under which there is a continuous alternation between adsorption and desorption of the proteins themselves, because smaller proteins are progressively replaced by larger ones [16].

After the process of protein adsorption, within minutes of implantation, the acute inflammation occurs, with a degree that depends on the injury level in the implantation procedure, the involved tissue or organ and the extent of provisional matrix formation [16], [18]. The main role of this stage is played by neutrophils, that are polymorphonuclear leukocytes (PMNs): they remain into the tissue for up to three days so that they can remove debris through the phagocytic process; nevertheless, acute inflammatory responses to implanted biomaterials are also mediated by cell degranulation that leads to histamine release and, above all, fibrinogen adsorption [14], [18]. Acute inflammation generally resolves in very short time, less than one week [18].

Once acute inflammation concludes, chronic inflammation begins: it is characterized by a lower uniformity from a histological point of view, with the presence of mononuclear cells, such as monocytes and lymphocytes other than plasma cells, at the level of the implant site and it is aimed to encapsulate the implant in a fibrous tissue [16], [18]. Depending on the processes of recruitment of monocytes and their differentiation into macrophages, recruitment of more cells, degradation of the biomaterial and beginning of the healing process may differently occur: within two days of implantation the population of macrophages completely replaces the initial neutrophils [14], [16].

As macrophages are not able to phagocytose the implant because of its dimensions, they tend to secrete some factors as degrading enzymes and reactive oxygen species (ROS) in order to break down the foreign body and try to phagocytose its smaller fragments [16] Furthermore, the inflammatory response could be aggravated by the recruitment of neutrophils and fibroblasts led by proinflammatory macrophages or, in addition, blood vessel formation may occur after the recruitment of fibroblasts that secrete vascular endothelial growth factors [14]. Also in this case the duration is short, about two weeks and, especially for biocompatible materials, it remains confined to the implant site: in fact, the eventual persistence of an inflammatory state is symptomatic of the presence of an infection [18].

After acute and chronic inflammation there is the formation of the granulation tissue: it is the precursor to fibrous capsule and is characterized by the presence of macrophages, the infiltration of fibroblasts and neovascularization in the new healing tissue. Granulation tissue allows the separation between the implant and the cellular components of the foreign body reaction: it derives from the fusion of the macrophages into bigger entities called "*foreign body giant cells*" (FBGCs) and the action of properly recruited fibroblasts [14]. This leads to the formation of the FBR capsule which is accompanied by the extension of new blood vessels into the new tissue compartment in order to supply it with nutrients; moreover, the capsule becomes thicker until the complete isolation of the implant from the surrounding tissue is guaranteed [16].

As the FBR cannot be entirely avoided, it is important to accommodate some degree of FBR itself, trying to minimize its severity and to leverage host immunology beyond FBR in order to allow the full tissue integration [14], [16].

1.3.3 Osseointegration

As opposed to the formation of a fibrous tissue at the bone-implant surface, a process known as "*osseointegration*" can occur, in order to establish a full integration of the tissue with the biomaterial after the implantation itself through a direct and stable anchorage of the implant thanks to the formation of new bone around it. According to a modern biomechanical definition, osseointegration can be seen as "*a process whereby clinically asymptomatic rigid fixation of alloplastic materials is achieved, and maintained, in bone during functional loading*". Osseointegration cannot be considered as an independent process, but it depends on two phenomena which precede it, called "*osteoinduction*" and "*osteoconduction*" respectively, even though it requires that the bone anchorage is maintained over time, so that it is referred to as "secondary stability" [19], [20].

Osteoinduction can be observed in all the bone healing processes: it starts immediately after the injury and is defined as a step which induces osteogenesis thanks to the recruitment of undifferentiated mesenchymal cells of the bone tissue in order to form osteoprogenitor cells and their subsequent differentiation into preosteoblasts after providing specific stimuli. Both physical stimuli such as stress or electrical signals and the release of "*bone morphogenic proteins*" (BMP) and other different biochemical and biophysical messengers are essential in inducing the bone formation and the repair of the tissue by sensitising different types of surviving cells. It is important to underline that the pre-existing osteoblasts contribution to the bone induction is minimal compared to that of preosteoblasts obtained by differentiation [19].

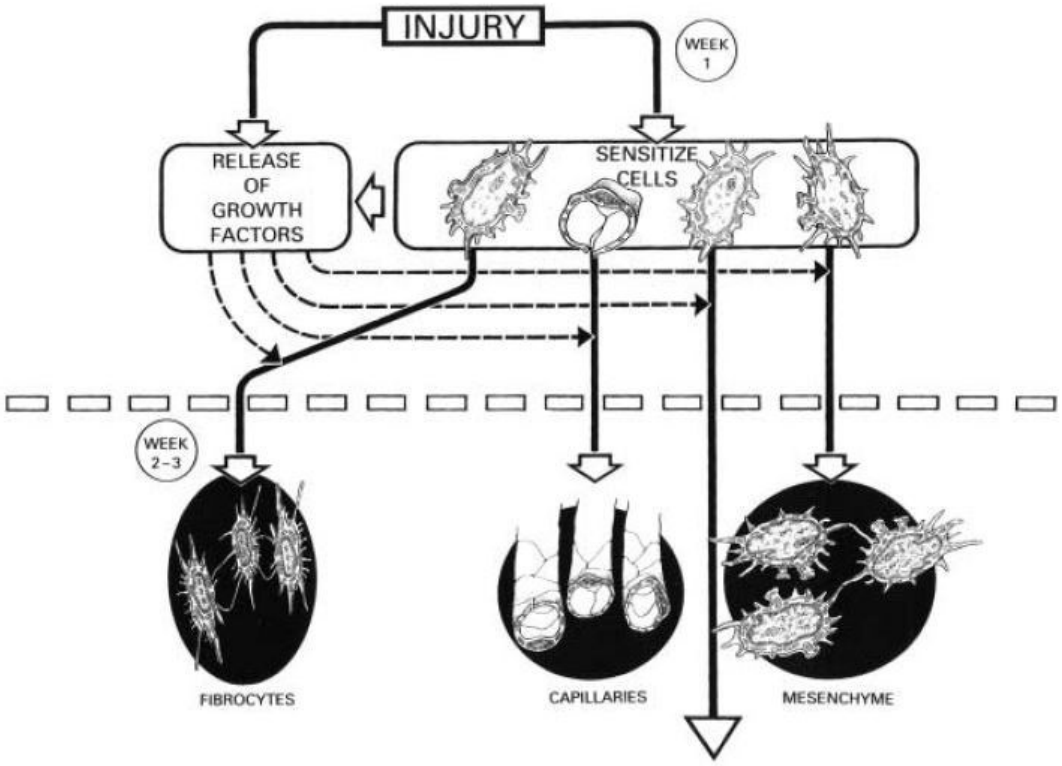

Figure 15: Schematization of the primitive healing response with stimulation of different types of cells [19]

Osteoconduction is related to the bone's capability to grow on a surface (e.g. of an implant), so that it does not easily occur on lowly biocompatible materials, in contrast it occurs on the surface or down into pores, channels or pipes of more biocompatible ones. It depends on the differentiated bone cells action and needs a proper blood supply, in fact a full vascularisation is necessary in order to guarantee a correct bone formation; furthermore it is also dependent on the biomaterial used and its reactions [19].

Finally, osseointegration occurs when the osseous tissue attaches to the material without the interposition of connective tissue. Different parameters could influence the osseointegration such as implant physical and chemical characteristics of the implant and its lack of mobility under physiological loading, bone characteristics related to its quality or its amount or the protocol used for the functional loading of the implant and its duration. The activation of osseointegration leads to different biological events which can be described as divided into three steps: first of all, the formation of woven bone allows the implant incorporation in the bone, secondly the bone mass has to adapt to the load, finally there is the total adaption of the bone structure to the load, through a "bone remodeling" process [20].

In this case progenitor cells totally differentiate into osteoblasts in order to guarantee a good intramembranous ossification with the bone gap that is gradually filled by the body of the implant itself to minimize the amount of new bone that has to refill the zone [20].

The establishment of an optimal primary implant stability represents an indispensable step for achieving a sufficient osseointegration, but different aspects must be controlled simultaneously with the aim of obtaining a successful osseointegration [20].

First of all, the geometry of implant is really important: the bone tends to grow in a preferential way on ridges, crests and edges of the implanted material surface; furthermore, in order to provide a good primary implant stability and an ideal transfer of stresses, the shape of the implant itself has to be monitored, in that it affects the surface area available. For this reason, additional surface treatments can be performed on the implant surface to obtain a biocompatible and bioactive surface, thanks to the realization of a specific microdesign [20].

The implant dimensions likewise influence the available surface area and, consequently, the osseointegration; in addition, the length of the implant must be controlled too, in order to allow a correct and proportionate transfer of forces [20].

Finally, a bone weakened by pathological conditions such as osteoporosis or unfavorable surgical conditions such as high temperatures or a great tissue damage may hinder the correct occurrence of the osseointegration process [20].

2 FIBRINOGEN-MATERIALS INTERACTIONS

2.1 Fibrinogen adsorption

2.1.1 Fibrinogen adsorption: introduction

Whenever a foreign material comes in contact with the organism, on its surface a spontaneous process of adsorption of water molecules and solvated ions occurs, followed by a protein adsorption of the surface itself [21].

One of the main risks correlated to this last aspect, regardless of whether the biomaterial is implanted for a limited time or for life is, together with the triggering of an immune response, the formation of a clot on the surface of the implantation. These clots could be dangerous in that they could foul the implanted device, causing local problems e.g. vessel occlusion or systemic problems if they break away and begin to move to other organs. This problem is accentuated by the fact that, differing from healthy endothelium, foreign surfaces are not endowed with mechanism to resist thrombosis, indeed, most of the implanted devices are able to activate different inter-connected processes that lead to protein adsorption, platelet and leukocyte adhesion, thrombin generation and complement activation [22].

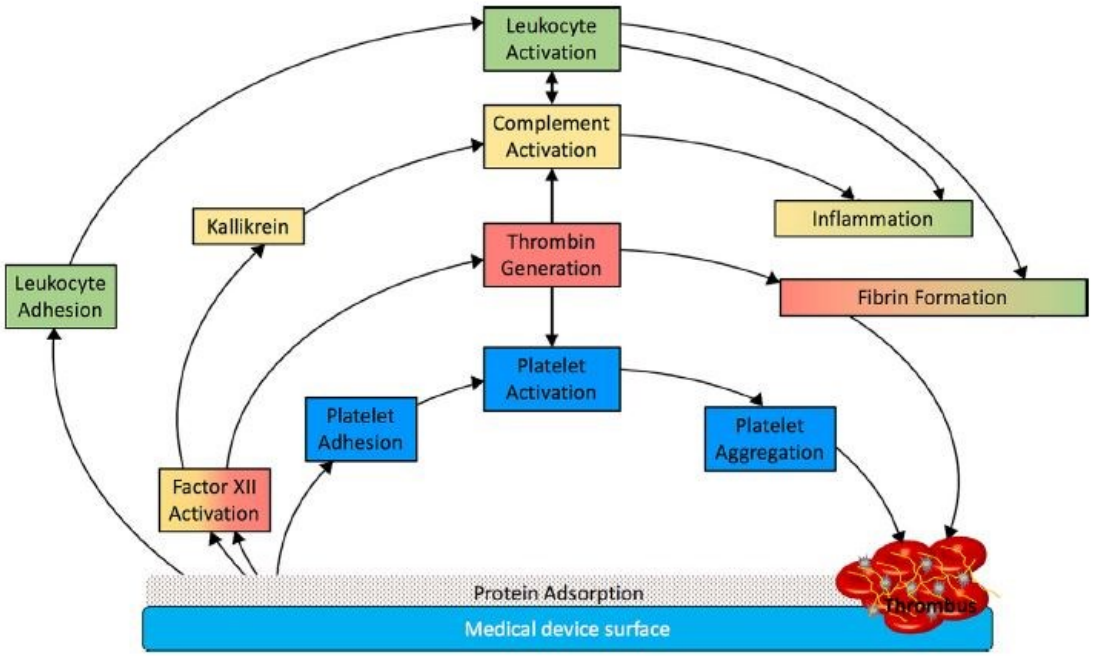

Figure 16: Main processes activated by the implantation of a medical device [22]

On the other hand, when the implanted surface interfaces with the bone, the formation of a blood clot in correspondence of the gap between host bone and implant, caused by the direct contact between the material and the blood, represents a fundamental step for the bone healing. The blood clot is able to induce bone formation, supporting both "*distance* and *contact osteogenesis*", two different types of peri-implant endosseous healing: while the first one is based on the formation of new bone around the old bone with a specific distance from the implant, the second one manifests itself as the formation of new bone directly on the implant surface [23].

The clot represents a sort of scaffold which supports osteogenic cells adhesion and migration, necessary for the bone healing: the clot is able to release various osteogenic factors which stimulate the differentiation of pre-osteoblasts into osteoblasts; at the same time the fibrin structure can influence the differentiation of mesenchymal stem cells, that have a crucial role in the bone healing too. The process is further supported by the formation of extracellular matrix at the injury sites [23].

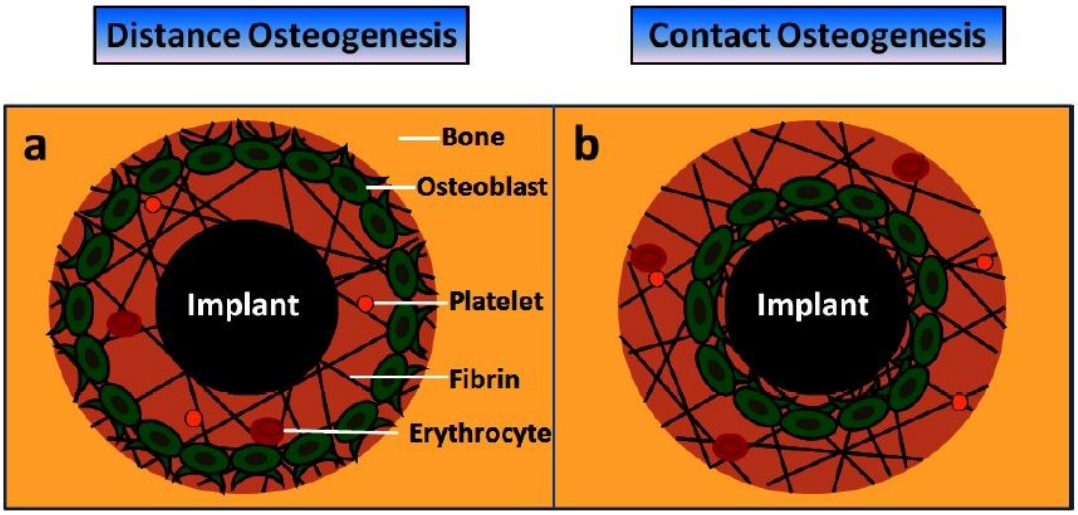

Figure 17: Difference between distance and contact osteogenesis [23]

Depending on the physicochemical properties of the surface of the biomaterial, the profile of the adsorbed layer could be different, driving in a different way the cellular interaction with the material and dynamically modulating the thrombosis on the artificial surface [22]. For this reason, the knowledge of the relationship between surface properties and protein adsorption phenomenon is fundamental in order to study the biocompatibility of

the biomaterial, strongly affected by the properties of adsorbed fibrinogen that, for this reason, is usually used as a biocompatibility indicator [21], [24].

The main plasma protein involved in blood-material interaction is fibrinogen: its surface adsorption, which is really complex and involves noncovalent interactions, electrostatic forces, hydrogen bonding and van der Waals forces, is related to different surface properties such as wettability (related to chemical composition), roughness and topography, surface charge and energy [21], [22], [24]. Differences in terms of amount, densities, conformation and orientation can be observed as a consequence of these various parameters [25]. Although the process of adsorption of fibrinogen is not yet fully known, it is probably related to the interaction between D and E domains with the material surface after the contact with the foreign material itself; after that, as explained above, the release of fibrinopeptides is guaranteed following the D and E domains conformation changes [24].

In general, regarding the protein adsorption, the protein monolayer has a thickness of about 2-10 nm with an extremely variable protein concentration that can even be 1000-fold higher than that in plasma. This adsorption, which is reversible, can be explained thanks to the Vroman effect: immediately after the fibrinogen, other adhesive proteins as fibronectin and von Willebrand factor are adsorbed on the surface of the biomaterial and cooperate with the fibrinogen itself in order to mediate the platelet adhesion [22].

Nevertheless, the major contribution to the platelet adhesion is given by fibrinogen, thanks to its great ability to bind specifically to the platelet through $\alpha_{IIb}\beta_3$ that is the most abundant integrin on the platelet surface and that is able to bind to fibrinogen both in its quiescent and active state [22].

Fibrinogen adsorption can be characterized starting from the evaluation of different types of peaks of adsorption in time, concentration or spatial domain, that are related to the Vroman effect. For what concerns the time domain, after reaching the maximum value in a short time following the contact between the material and the plasma, the displacement of the initially adsorbed fibrinogen occurs, so that a decrease is observable. About the concentration domain, considering that the adsorption is studied from various dilutions of plasma, after 1-2 hours, when steady state adsorption values are established, the peak

is exhibited at intermediate plasma dilutions, depending on the type of surface. Finally, the evaluation of the peak of fibrinogen adsorption in the spatial domain is based on the measurement of the binding at a specific distance away from the contact point of a concave lens placed on the adsorbing surface [26].

2.1.2 Postadsorptive transitions in fibrinogen

The adsorbed proteins on solid surfaces are subjected to important conformational and structural changes that can be identified as "postadsorptive transitions", mainly because of their great instability and their tendency to unfold in order to guarantee a closer bond with the adsorbing surface itself [26]. These conformational rearrangements are related to changes in the secondary structure which can be more or less similar to that of native protein and depends on the typology of surface [27], [28].

As a general principle, the two main configurations that can be observed are a "*trinodular model*" or a "*complex model*", provided that they represent a starting point which can further undergo changes. While the trinodular model includes a smaller central E nodule with two bigger D nodules, all of them with a spherical shape and linked by coiled-coil connectors, the complex model is based on heptanodular domains with βC and γC lobes, a globular αC domain deriving from the extension of the α chain starting from them and lastly a small and non-helical globular domain which create a binding site to plasmin. The different configurations can be catalogued and described on the basis of the surface features [28].

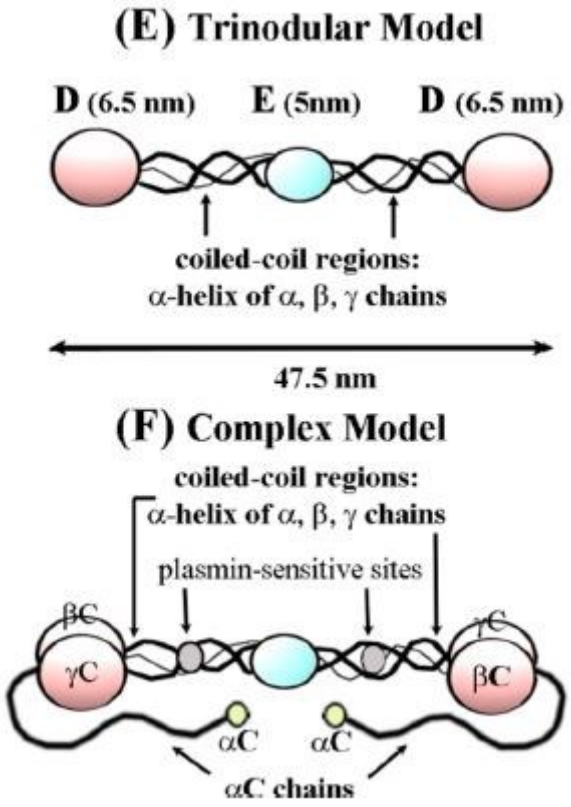

Figure 18: (E) Trinodular model; (F) Complex model [28]

An interesting example can be related to a specific type of modified surface which can lead to a disintegration of protein chains for most of the fibrinogen molecules on the surface: in this case only the two D nodules are visible, with swollen features, creating a binodal model, as a sign of a denaturation process. In more complex situations, one or both D domains can also be denatured [28].

The second example is more similar to the complex model and involves an elongated conformation with narrower and thinner domains, maybe caused by the presence of αC chains/nodules and plasmin-sensitive sites [28].

Another type of configuration presents a trinodular conformation with smaller nodules than that of a classical trinodular model and the absence of connector threads between the three parts [28].

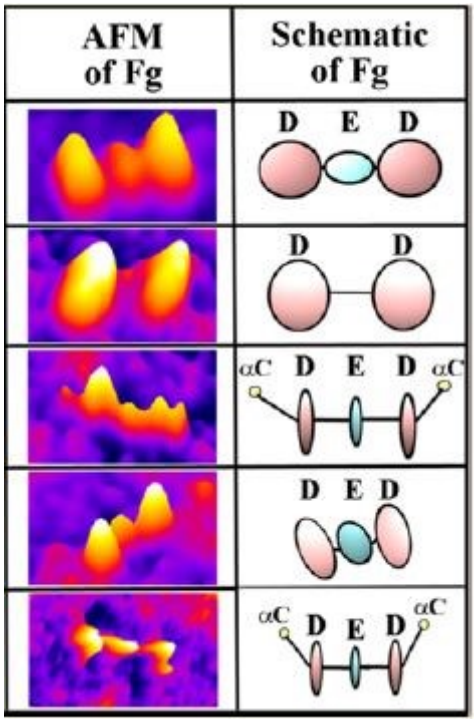

Figure 19: Different schematizations of fibrinogen structures and AFM images [28]

These changes can be characterized by both physiochemical and biological methods [26].

One of the main examples of evaluation is related to the ability of some detergents as sodium dodecyl sulfate (SDS) to remove adsorbed fibrinogen from different surfaces: the tests demonstrate that two important parameters may affect this feature. On the one hand, the immediacy of the test after the protein adsorption step seems to determine an increase of the elutability, while there is a slow decline to much lower levels of elutability itself if the test is performed after a long period of immersion of the surfaces with adsorbed proteins in specific buffer. On the other hand, the temperature is a critical parameter too: while incubation of adsorbed proteins at high temperatures is able to accelerate this decline in elutability, a deceleration is guaranteed in case of lower temperatures. This last aspect is completely in line with the known effect of temperature on the conformational stability of proteins. Another variable is related to the degree of dilution in that a more dilute protein solution presents a larger number of unoccupied surface sites for an adsorbed protein molecule so that it can form more bonds during the unfolding process

on the surface: in this case a decrease of elutability is verifiable. This aspect is representative of an unfolding process which causes a specific interaction between the protein and the surface with a resulting increase of its displacement by the detergent [26].

FTIR method, through the evaluation of spectral changes in the adsorbed proteins, confirms that proteins after adsorption are characterized by different conformational changes too: in fact, variations in infrared frequencies related to the conformation of the peptide bonds in proteins are visualized. So, it is possible to affirm that there is a good correlation with time dependent changes in the adsorbed fibrinogen. This technique acts as a support to the previous but it can also be applied directly on the surface [26].

Further studies can be done using a different type of displacing agent such as the mixture of proteins in blood plasma, which is more bland: in this case faster changes can be observed compared to SDS case as a demonstration of the fact that competing plasma proteins seem to be weaker surfactants in comparison to conventional detergents [26].

Lastly, as observed above, atomic force microscopy (AFM) can be also used in this field, in order to analyze the surface directly, obtaining high-resolution nanoscale images with conventional or electrochemical methods in a minimally invasive way [28], [29].

2.2 Relationship between fibrinogen and biomaterials

2.2.1 Influence of material surface properties on the fibrinogen adsorption

In normal conditions, correlations between surface physiochemical properties and protein adsorption can be identified; however, it is not possible to make generalization about this aspect for different types of materials families such as polymers and metal oxides. At the same time, different proteins on the same surface may behave differently during the adsorption process, depending on their physiochemical characteristics [21].

Since most of the oxides that are normally used in biomedical field exhibit good bio-corrosion resistance and mechanical properties, they are considered promising material for the development of biocompatible coatings in general, also considering their inherent capacity to promote cellular adhesion and proliferation [21].

Considering that these parameters can affect each other, an independent evaluation of all the properties will take place, in order to study the fibrinogen adsorption, a complex multistage process, on different types of surfaces [21], [25].

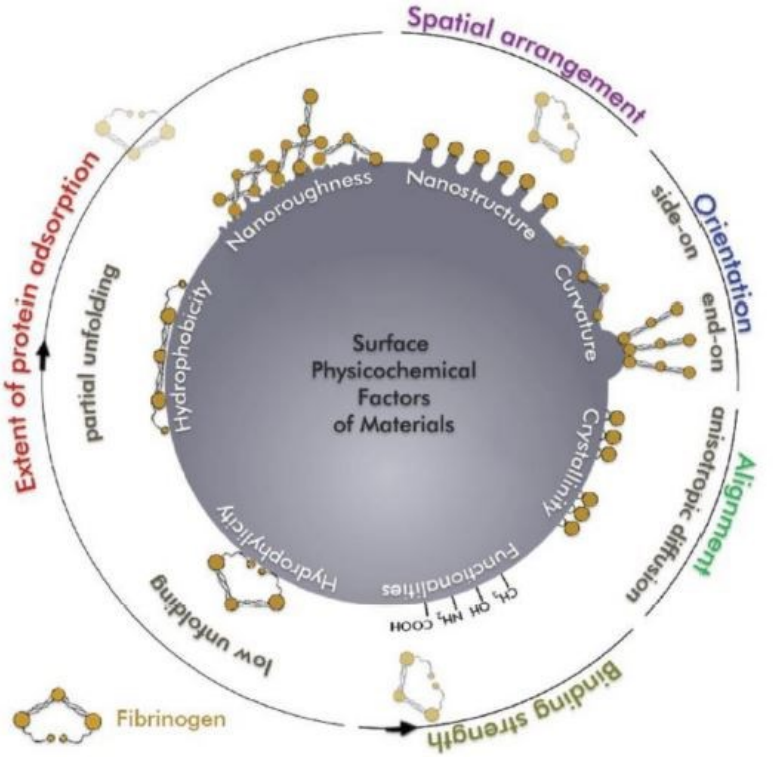

Figure 20: Effects of the physiochemical properties of material surface on different aspects of protein adsorption [76]

2.2.2 Wettability

For what concerns the wettability, lots of studies related to the impact of wettability on the characteristics of adsorbed proteins, in particular fibrinogen, have been conducted. Wettability can be evaluated by contact angle and both hydrophilic and hydrophobic samples with no significant differences in roughness can be tested [21].

Since the total surface energy $\gamma^{LW/AB}$ is due to a polar contribute γ^{AB} and a non-polar one γ^{LW}, there is a great correlation between the wettability and the surface energy itself: this is due to the fact that an increase of the contribution from the polar interactions to $\gamma^{LW/AB}$ can be reflected into a big wettability i.e. hydrophilic samples. On the other hand, the surface energy of hydrophobic samples is mainly defined by dispersive interactions, with very low contribution from the polar interactions. For this reason, the ratio $\gamma^{AB}/\gamma^{LW/AB}$ can be considered as a direct indicator of the hydrophilic/hydrophobic character of a surface: a smaller value determines a smaller polar nature of the surface with weaker interactions with polar molecule as H_2O itself [21].

Regardless of the hydrophilic/hydrophobic nature of the sample, the behavior of the fibrinogen adsorption is time-dependent: three different types of adsorption rate regimes can be distinguished. The first one, which is really fast, involves an exponential acceleration of the adsorption during the first ≈ 50 s of immersion; the second one, starting ≈ from 50 s until 400 s of immersion, is characterized by a sudden decrease of the adsorption rate; finally, about the third regime, it slowly tends to an equilibrium state thanks to a quasi-asymptotic behavior, as surface coverage increase, in that free sites for which fibrinogen competes in the process become fewer [21], [25].

In general, the protein adsorption is guaranteed by the overcoming of certain energetic barrier rather than a simple mass transfer/diffusion process: the fact that the nature and size of this barrier are constantly subjected to changes could explain the presence of different adsorption-rate regime in function of time. In particular the adsorption process is controlled by various physiochemical phenomena during the different steps such as: diffusion, hydrophobic interactions, conformational changes or denaturation of proteins etc [21]. At the end of the adsorption process on hydrophobic surfaces, a less organized secondary structure than that on hydrophilic ones can be observed: in fact, in the first

case, a huge loss of the α-helical component accompanied by an increase in the β-sheet or random structure portion can be observed [25].

A further explanation may be the formation of a multilayer during the adsorption process with a slowdown in the adsorption-rate for each subsequent deposited layer [21].

Considering that in simple terms, fibrinogen molecules can be represented as rods, there are three main configurations that adsorbed fibrinogen can assume depending on the wettability characteristics of the surface: the first one, known as "*standing-up* (or *end-on*) *configuration*" is characterized by a greater thickness d_p, the second one presents a tilt with a bland decrease of the thickness value, finally, the third configuration, that is called "*side-on configuration*" and is caused by a relaxation mechanism, is distinguished by a larger protein contact area with a consequent minimization of the surface energy [21], [30].

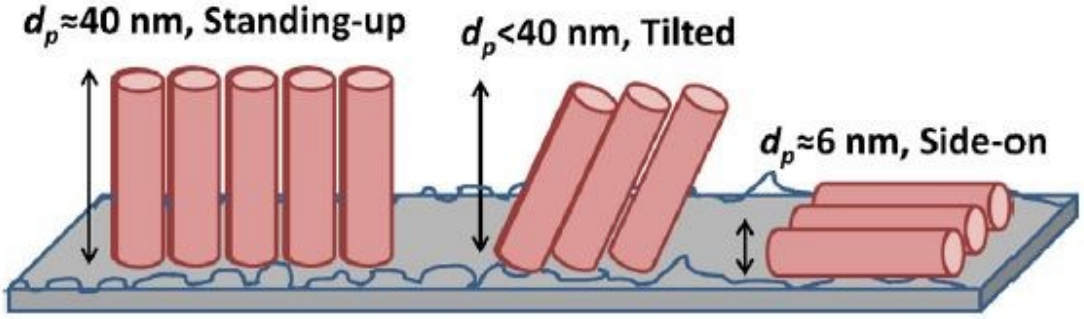

Figure 21: Three possible configurations of adsorbed fibrinogen [21]

Several aspects must be considered with reference to parameters that affect the adsorption: first of all, even on the same surface, drastic changes in the conformation of the protein can be induced, probably by a dehydration phenomenon: a study conducted after surface rinsing and air-drying could induce a variation in the conformation and, consequently, in the thickness value, as a demonstration that there are discrepancies between in situ and ex situ experiments. In particular, a drying process may cause a contraction in the d_p of a fibrinogen layer [21].

In addition, the refractive index n_p should be evaluated at the same time as the thickness, in that it is representative of the density of the deposited layer: hydrophobic surface likely leads to the formation of clusters and the denaturation of the protein as adsorption

increases, causing the generation of less compact layers; on the contrary, protein denaturation on hydrophilic surfaces is not promoted, so that denser layers can be visualized [21].

The evaluation of both thickness and refractive index is based on the fitting of the ellipsometric spectrum which is acquired in situ, thanks to a four phase optical model: the use of a transparent Cauchy function allows to parameterize the optical phase that represents the adsorbed fibrinogen layer [21].

Comparing results from different ex situ experiments, it is possible to confirm a thinner fibrinogen layer on hydrophilic surfaces than on hydrophobic ones, with different orientations of the protein. While hydrophilic surfaces hardly induce protein denaturation, so that an intact side-on configuration is more probable, with the eventual presence of tilted molecules, hydrophobic surfaces involve a more complex and multistage adsorption process: in the first instance, the initial fibrinogen molecules, having a rod-like shape, are irreversibly adsorbed in a side-on configuration, so with their long axis parallel to the surface but, at a certain point, the accessible surface area becomes too small, so that the new molecules have to be adsorbed in a standing-up configuration. This reorientation depends on an increase of the hydrophobic protein-protein interaction among the adsorbed molecules [21], [25].

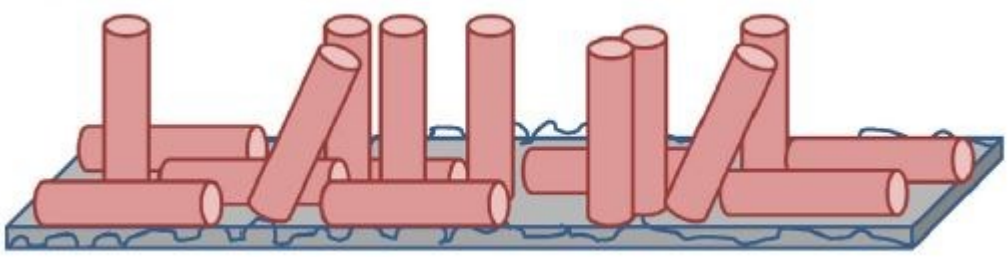

Figure 22: A layer of fibrinogen formed by different molecules adsorbed in different configurations [21]

It is important to specify that literature could report some discrepancies related to the probability of a partial reversibility of adsorption, because of the fact that binding energy in the end-on configuration results to be lower than for the side-on one [31].

Nevertheless, the unfolding process caused by denaturation upon adsorption is able to induce a reduction in height of fibrinogen molecules that have been adsorbed in a standing-up configuration [21].

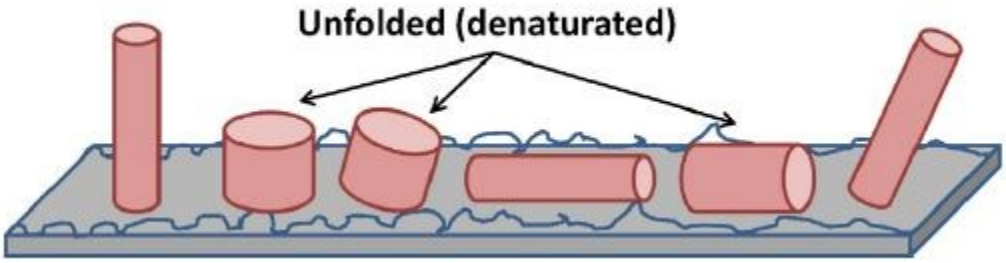

Figure 23: Fibrinogen molecules shrunk in height after the surface adsorption [21]

Another parameter that can be considered is the fibrinogen mass concentration Γ, which include both d_p and n_p, so that the strong dependency between these two last values can be eliminated: in this case, according to the faster adsorption phenomena in hydrophobic samples, a larger Γ can be esteemed, also because of the formation of protein clusters on these types of surfaces [21].

Different experimental studies, including FTIR (Fourier Transform Infrared Spectroscopy) spectroscopic images, agree that the amount of adsorbed fibrinogen is greater and stronger on hydrophobic surfaces rather than hydrophilic ones, this probably due to the fact that there is a more favorable displacement of water molecules off the surface, that promotes the molecules adsorption [21], [24].

FTIR experiments also underline that, compared to other secondary structures, alfa-helix content turns out to be dominant in the amide I band in both hydrophobic and hydrophilic surfaces, with no evident disparities between them. More consistent differences can be observed in turn and sheet contributions, although they represent a minority part of the overall secondary structure [24].

Since the ratio β-sheet/β-turn is an indicator of biocompatibility, hydrophobic samples, which present a greater contribution of turn than sheet, also because of the denaturation which can lead to lose a large degree of their helical secondary structure, exhibit low blood compatibility; on the other side, hydrophilic surfaces are more compatible with the

blood, also because of their retention of the secondary structure, which allows the coagulation and adsorption of cells [24], [25].

In addition, lower saturation values can be observed in the case of fibrinogen adsorption on hydrophobic surfaces rather than hydrophilic ones [25].

However, all these remarks may not be valid under some specific conditions. One of the most interesting research projects in this sense is about the application of surface treatments which can induce an increase of wettability, with an increase of the amount of OH groups. It has been demonstrated that a high surface hydroxylation combined with a strongly acid behavior is able to determine a strong loss of α-helices, with an increase in the content of random coils, therefore inducing a denaturation of some specific proteins (e.g. albumin), provided that a threshold in the concentration of total and acidic OH is exceeded [32].

2.2.3 Roughness and topography

The fibrinogen adsorption could be also affected, in terms of amount, conformations and orientations, by the nano-roughness of the surface, in contrast with more globular proteins such as albumin [5]. Since roughness introduces in general a great degree of disorder in the system, it is a crucial parameter to be evaluated, also because most of the adsorption aspects depend on the protein size compared to the scale of the roughness itself. In addition, roughness is able to induce a variation in the interaction potentials between the surface and the protein: the interaction can be described in different ways depending on the roughness degree of the surface itself [33].

Depending on the type of surface features, three different categories known as “patterned”, “curved” or “random” of nanoscale topography can be considered: obtaining a good quality of the data which could explain the relationship between the fibrinogen properties and the surface topography is not very simple [34].

Many of the studies that have been conducted during the last decades have shown an increased sensitivity to nanoscale roughness in case of random topography. In order to make more efficient the tests, they can be performed through the application of

topographic gradients based on sputter deposition method or nanoparticles addition on the surface [5], [34].

One of the main techniques that can be used in this field is QCM-D, through which the shift in resonance frequency and in the dissipation factor of an oscillating quartz disc can be evaluated and related to an adsorbed layer; at the same time, ellipsometry allows to obtain a surface mass density starting from the measurement of the optical thickness of the fibrinogen layer. It is important to consider that QCM-D cannot discriminate between adsorbed proteins and coupled water, so that in some cases it is not able to take account that water may physically become trapped in pores and grooves of the surface during the adsorption [35].

The most obvious result is that the surface area tends to increase when the "*rms* (*root mean square*) *roughness*" in turn increases if the indentation is larger than the protein: in general, it is possible to affirm that if the surface features are smaller than the protein (~2 nm, nearly flat surface), they will not contribute to an increase of the adsorption in that they might be not accessible to the protein. The increase of surface area is coupled to a much greater increase of the surface density [30], [33], [36]. In a similar way, by increasing surface roughness, also the fibrinogen saturation uptake increases of a much higher degree if it is related to the geometrical surface area [30], [35].

As a consequence of the increase of the surface area thanks to the increase of the roughness and thanks to the typical preferential end-on binding of a rod-like molecule, the adsorption amount itself increases, even though the available surface area rise is not as consistent as that of protein amount [5], [33], [35]. On the other hand, considering that a grater surface roughness causes a more probable denaturation of the adsorbed protein and that a denatured protein tends to occupy a larger area compared to the same protein in the native state, the saturation protein uptake that is evaluated could actually be lower [35].

Furthermore, roughness can facilitate the process of molecular reorientation during fibrinogen adsorption. It has been demonstrated that rougher surfaces tend to firstly promote the establishing of end-on orientation, then undergoing a spreading process on

the surface which is supported by D and E domains and α-helix coiled coil regions stronger interactions with surfaces [30], [35].

In general, elongated proteins such as fibrinogen itself, may primarily be bound so that they can orient their main axis along or perpendicular to the surface, until they saturate the surface, thanks to a mixture of both side-on and end-on configurations. Actually, fibrinogen tends to preferentially adsorb on rougher surfaces with an end-on configuration, in order to increase the bonds between fibrinogen molecules and the surface itself, inducing the enhancement of the surface density thanks to the mechanism of reorientation of the molecules. In the first case, considering the example of a roughness obtained by nanoparticles on the surface, since one of the D domains results to be closer to the surface, the overall angle between the whole fibrinogen molecule main body and the surface itself can be calculated as a function of the surface curvature and the angle between the D domain and the rest of fibrinogen rod [5], [30], [33], [34].

Figure 24: (b) Typical orientation of adsorbed fibrinogen on a flat surface; ((c) Typical orientation of adsorbed fibrinogen on a rough surface, in particular on a nanoparticle [5]

The evaluation of the conformational assessment through FTIR analysis can be carried out too: considering that protein infrared spectra contain peaks arising mainly from amide bond vibrations, it is possible to obtain information related to changes in secondary structure thanks to the amide I band, which is centered at ~1700-1600 cm^{-1} and closely related to C=O stretching vibrations. Different studies demonstrate that the content of α-helix structure of adsorbed fibrinogen tends to decrease following an increase in surface roughness [30].

About the secondary structure, the increase of surface roughness causes a decrease of the percentage of intramolecular β-sheet structures content, which originates from the first surface-protein interaction step, as the protein adsorption on the surface itself occurs, even though it is greater than that of free fibrinogen. This is related to the denaturation process which leads to a loss of the helical secondary structure in favor of the rise of intermolecular and intramolecular β-sheet structures, probably due to the fact that the interaction with a rougher surface seems to be stronger, determining a major protein structural perturbation [30].

Spreading results to be limited in the case of smooth surfaces, on which the end-on configuration is more probable, together with a lower loss of the helical component in the adsorbed fibrinogen [30].

It is important to underline that these considerations are related to roughness values (Ra) in a range from about ~30 nm (comparable to fibrinogen length) to ~400 nm (greater than fibrinogen length) [30].

Another topographic parameter that has to be considered is the curvature κ of the surface: a highly curved surface topography leads to a greater destabilization in side-on binding rather than end-on ones due to the need of the fibrinogen to keep the contact with the surface. The characteristic elongated conformation of fibrinogen implies that the amount of bound protein may significantly increase as a response to even a small shift in favor of end-on binding [34].

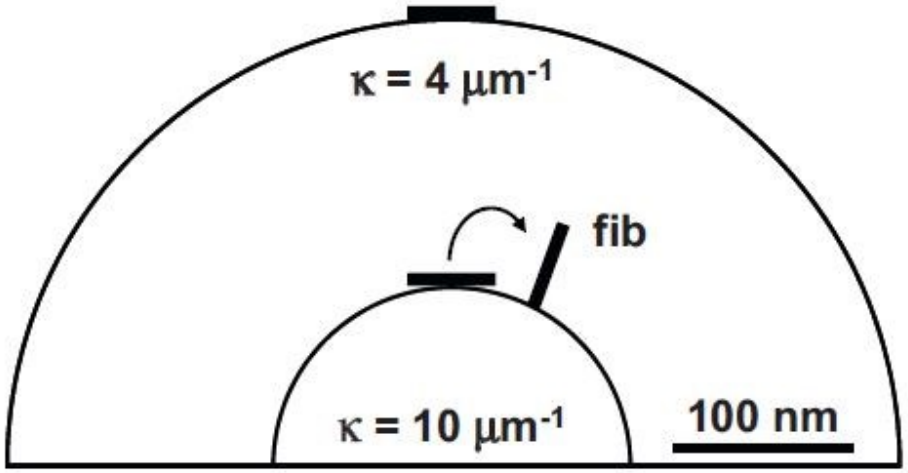

Figure 25: Schematic comparing the orientation of adsorbed fibrinogen in function of the surface curvature [34]

2.2.4 Surface charge

Recalling that, as mentioned above, fibrinogen presents a heterogeneous charge distribution, the third important parameter is the surface charge itself, which can be determined by zeta potential analysis. In some studies, the adsorption process monitoring is done through the use of radiolabeled proteins, observing the exchange between the interface and the solution: considering three different populations of fibrinogen which are rapidly exchanging, slowly exchanging and non-exchanging, there is a first evident difference between the percentage of rapidly and slowly exchanging in function of the surface charge. This is probably due to a difference in their relaxation times [6], [7], [37], [38]. In hypothesis of physiological conditions (pH = 7.4, I = 0.15 M), fibrinogen can be considered as negatively charged (negative net charge) [6], [7], [37], [38].

Assuming that the surface is positively charged and the electrostatic interactions among adsorbed molecules on the surface can be neglect, at physiological pH the fibrinogen adsorption solely depends on the side-on mechanisms, according with an increase of the maximum coverage of fibrinogen thanks to the reduction of the range of the lateral electrostatic interactions among adsorbed molecules, which leads to a higher ionic strength that is, for this reason, a crucial variable parameter. The side-on adsorption mechanism, confirmed both by theoretical and experimental tests, depends on the facing between the positively charged surface and the negatively charged fibrinogen core. At the same time, the possibility of an end-on adsorption mechanism is excluded by reason of an electrostatic repulsion between the positively terminal arms of the fibrinogen molecules and the positively charged surface [6].

This behavior can be easily observed on different types of surfaces e.g. positively charged latex particles which tend to interact with the negatively charged core of the fibrinogen [6].

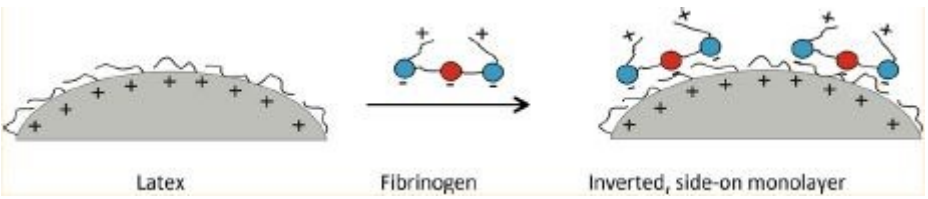

Figure 26: Schematization of fibrinogen adsorption on a positively charged surface [6]

In addition, positively charged surfaces show a great stability in fibrinogen adsorbed monolayer, which is also pretty homogeneous, without consistent orientational or irreversible conformational changes in the molecules themselves. This is due to the larger intensity of energy minimum, in turn related to the fact that positively charged arms are not involved in the binding with the surface. From a future perspective, this could be interesting in that stable fibrinogen monolayers with a specific orientation of the molecules and a great control of the coverage may be realized, in order to improve the interactions with specific other proteins [6].

In case of negatively charged surface, the interaction between fibrinogen and the surface itself, for physiological pH values, is mainly dominated by electrostatic repulsion, although the slight attractive interaction between the surface and the positively charged portion of the fibrinogen molecule: an increase of the intensity of the negative charge is reflected into a lower amount of adsorbed fibrinogen. Nevertheless, the typical electrostatic repulsion that can be observed in this situation does not represent a limitation for the protein adsorption [38].

In fact, several studies have been conducted on various types of negatively charged surfaces: although there are some differences between them, depending on the surface itself, in all situations a decrease in the rate of the first step of adsorption in function of the decrease of negative charge is observable. This means that however, the adsorption is equally favored on negatively charged surface, despite the protein is negatively charged: this is probably due to the presence of positive species such as cations (e.g. in the protein itself or in case of an electrode as a surface) which are involved in the process. This can lead to a coadsorption of cations in a proteic layer when negatively charged proteins are adsorbed on a negatively charged surface [39].

This aspect is slightly different for what concerns the second step of the adsorption process, during which there is a great dependence on the type of surface which is considered and therefore cannot be easily generalized. In fact, it is important to highlight that these considerations are extremely generalized: it has been demonstrated that the nature of the material surface has a great influence on the protein adsorption even though two samples with the same surface charge are considered [39].

Latex negatively charged particles have been studied too: differing from the case of positive charge, the maximum coverage obtained for negative latex results significantly bigger than that obtained for positive one, probably because of the specific structure that protein assumes in the second case. At the same time negatively charged surfaces induce a greater number of variations in the molecule orientation compared to positive surface, in that these last are characterized by the formation of very stable protein layers [6].

Obviously, the eventual decrease of pH would result in an increase of the positive charge, so that attraction force becomes greater than repulsion force, with a consequent increase of the adsorbed fibrinogen amount [38].

3 MATERIALS AND METHODS

3.1 Materials

The aim of the study is the comparison between two model surfaces with different wettability, silica (SiO_2) as a model of hydrophilic surfaces and polypropylene (PP) as a model of hydrophobic ones, which can be widely used in biomedical applications, especially for what concerns the implantation of biomaterials. The materials were tested under different types of conditions in order to investigate their surface behavior, characterizing them before and after fibrinogen adsorption with a view to identify their interaction with the blood.

These models can be used in order to interpretate the resulting data on surfaces of clinical interest, so that they were compared to a Titanium alloy (Ti6Al4V, defined as Ti64) and to a chemical-treated Titanium alloy (CT), characterized by a complex surface (multiscale surface topography with a nanotexture overlapped to a micro-roughness), a high density of acidic OH groups, and a bioactive behavior.

3.1.1 Silica and polypropylene samples preparation

Silica samples (SiO_2) were purchased by Heraeus HSQ300 in form of slabs: they were cut into 1 x 1 cm square samples using a diamond tipped. On the other hand, polypropylene samples (PP) were provided by DIPROMED srl in form of sheets, distinguishing between washed and unwashed sheets: the second ones were cut into 1 x 2 cm rectangular samples using a cutter.

Silica samples that had to undergo the fibrinogen adsorption process (SiO_2_FB) were marked on the back to distinguish it from the surface, while as regards the polypropylene samples used for the protein adsorption (PP_FB), they were positioned horizontally and a cut was made in the lower right corner to recognize the front.

Afterwards the samples were washed in an ultrasonic bath (Sonica ultrasonic, Soltec) in different steps: silica samples were washed with ethanol (EtOH) and ultrapure water (MilliQ), respectively once for 5 min and twice for 10 min, with rinsing step using ultrapure water between each wash; polypropylene samples were washed with ultrapure

water at 60 °C, twice for 10 min, with rinsing step using ultrapure water between each wash. The washing was different for PP samples in that EtOH could leave residues on the surface which could falsify the analyses results. In addition, some Ti6Al4V square supports that have been used to fix some of the PP samples were previously polished (P320, LaboPol-2, Struers) and washed in ultrasonic bath too: the washing program included acetone once for 5 min and ultrapure water twice for 10 min, with rinsing step using ultrapure water between each wash. For the washing, the samples were placed into Aluminum foil coated bekers to avoid contamination with the external environment.

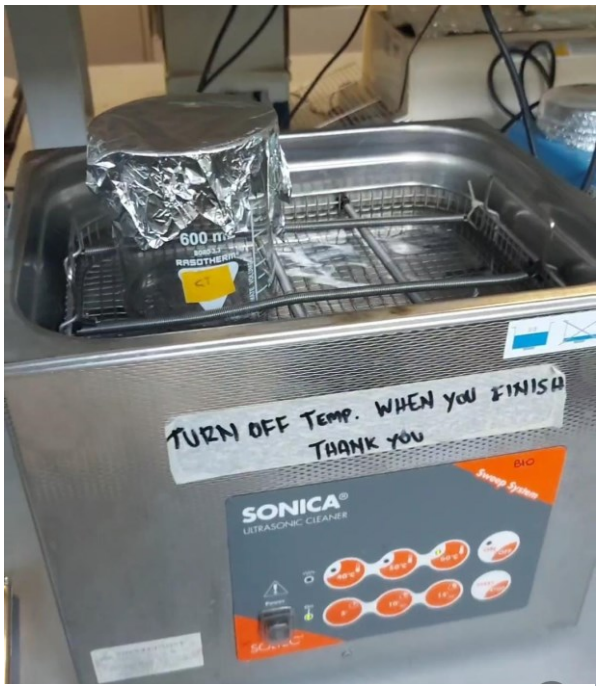

Figure 27: Samples washing process

After washing, most of the polypropylene samples were fixed with the back on Ti6Al4V square supports using double-sided tape, in order to discriminate front and back and to make the samples themselves easier to handle, not being as rigid as silica ones.

Samples were put to dry under biological hood (Faster Cytosafe-n) for 10 min: then, half of the samples were stored in 24-multiwells (separating SiO_2 and PP), while the other half were put into a 24-multiwell specifically used for the process of fibrinogen adsorption.

Since some measurements needed wet samples, a distinction between wet and dry samples was made: when wet, the samples were identified with the suffix "_w".

3.1.2 6-4 Titanium alloy samples preparation

Titanium alloy samples were Ti6Al4V disk samples, half of which subjected to fibrinogen adsorption protocol (Ti64 and Ti64_FB) and chemical treated Ti6Al4V disk samples, half of which subjected to fibrinogen adsorption protocol (CT and CT_FB), considering that fibrinogen adsorption was the last step of the study. The Ti6Al4V samples were purchased by Titanium Consulting and Trading as cylindrical bars (ASTM B348, gr5) and cut into disks of 1 cm in diameter and 0.2 cm in thickness through automatic cutting.

Two different polishing processes were considered: Ti64 samples were polished with abrasive paper in six steps (P320, P600, P800, P1000, P2500, P4000), while substrates intended for CT treatment were polished in just two steps (P320, P400).

Figure 28: Polishing stage of Titanium samples

After polishing, the samples were washed in ultrasonic bath, arranged with the polished side upwards: the washing took place in acetone once for 5 min and in ultrapure water twice for 10 min, with rinsing step using ultrapure water between each wash.

Samples were finally dried under biological hood and Ti64 intended for CT ones were ready for the chemical treatment.

3.1.3 Fibrinogen

Fibrinogen from bovine plasma (F8630-1G) was purchased by Sigma-Aldrich, St. Louis, USA in form of powder and stored in freezer.

3.1.4 Chemical treatment

Ti64 intended for CT were subjected to the chemical treatment which, being an acid process, needed to be conducted under a specific hood (Pratika, Ferraro arredi tecnici). The treatment, which is protected by European patent coverage (EP2214732B1) was performed on the polished surface and included a first step of acid etching using a hydrofluoric acid (HF) solution with the aim of removing the native oxide surface layer; then a controlled oxidation in hydrogen peroxide (H_2O_2) solution was carried out so that an oxidation on a nanometer scale could occur in a way that the surface exposed a strongly bioactive complex topography with a specific nanoporous pattern.

At the end of the treatment, the samples were dried under the hood: half of them were stored in 24-multiwell, while the other half were subjected to fibrinogen adsorption, equally to SiO_2 and PP samples.

Figure 29: Titanium samples after chemical treatment

In this case, a distinction between wet and dry samples was made too: when wet, the samples were identified with the suffix "_w".

Table 1: Samples identification codes

SAMPLES IDENTIFICATION CODES	
FB	Fibrinogen solution
FB_p	Fibrinogen powder
FB_p_deg	Degraded fibrinogen powder
SiO_2	Silica
SiO_2_w	Wet silica
SiO_2_FB	Silica with fibrinogen
SiO_2_FB_w	Wet silica with fibrinogen
PP	Polypropylene
PP_w	Wet polypropylene
PP_FB	Polypropylene with fibrinogen
PP_FB_w	Wet polypropylene with fibrinogen
Ti64	Ti6Al4V alloy
Ti64_FB	Ti6Al4V alloy with fibrinogen
Ti64_FB_w	Wet Ti6Al4V alloy with fibrinogen
CT	Chemical treated Ti6Al4V alloy
CT_FB	Chemical treated Ti6Al4V alloy with fibrinogen
CT_FB_w	Wet chemical treated Ti6Al4V alloy with fibrinogen

3.2 Methods

3.2.1 Fibrinogen adsorption

A 3 mg/ml fibrinogen solution (physiological concentration, [4]) was prepared by dissolving fibrinogen powder in sodium chloride (NaCl) 0.9% solution, previously placed in incubator to 37 °C, in order to make fibrinogen soluble and adsorbable. The total volume of the solution was obtained considering the quantity of 1 ml of solution per well with a small excess in that a quantity of liquid is lost as a result of the next filtering process.

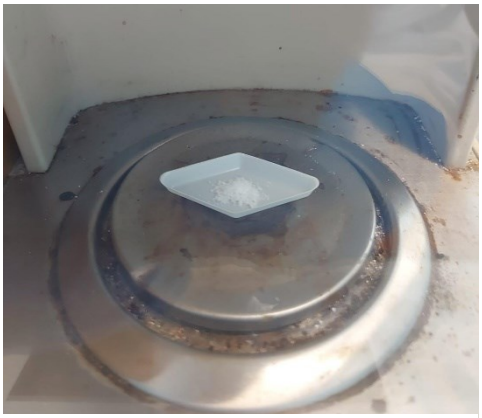

Figure 30: Fibrinogen powder weighing

The solution in fact was filtered thanks to a syringe with a filter (0.20 µm) and it was injected in the 24-multiwell (1 ml per well), totally covering the samples that were finally put in incubator at 37 °C for 2 h to allow the fibrinogen adsorption on their surface.

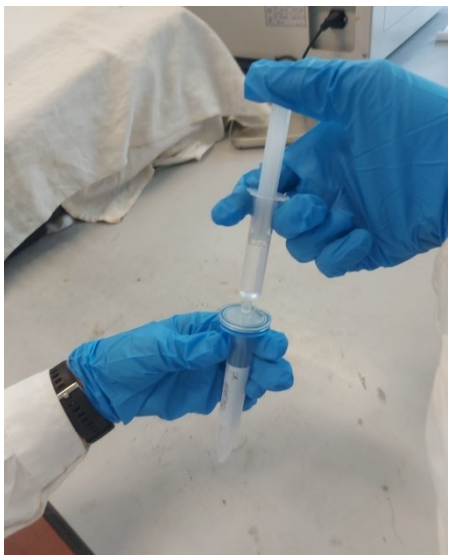

Figure 31: Filtering stage

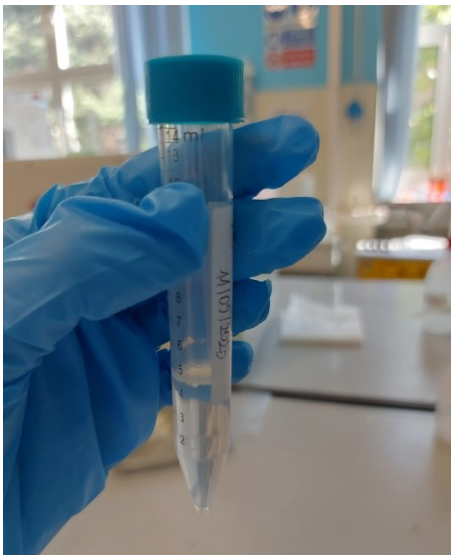

Figure 32: Fibrinogen solution

After the adsorption step, the samples were removed from the multiwell, subjected to three rinsing steps using ultrapure water and dried under biological hood for 10 min. The samples were finally stored into different 24-multiwell, separating SiO_2_FB, PP_FB, Ti64_FB and CT_FB which had to be kept in the fridge.

It is important to underline that some of the analyses needed wet samples, in that drying could determine unpredictable effects; moreover, the aim of the work is not related to the study of a pre-adsorbed material but it regards the investigation of specific materials behavior and their interaction with plasma fibrinogen after implantation. For this reason, not all the samples were dried under biological hood, but some of them were directly tested after the adsorption protocol for what concerns samples that underwent fibrinogen adsorption. The speech is similar for the samples that were not subjected to adsorption: in this case, in order to obtain wet samples, they were immersed in NaCl 0.9% without fibrinogen and placed in incubator to 37 °C for 2 h, after which they were subjected to three rinsing steps using ultrapure water. These samples were directly tested without waiting for the drying.

3.3 Surface characterization

3.3.1 Scanning Electron Microscopy/Energy-Dispersive X-ray Spectroscopy

Scanning Electron Microscopy (SEM) is an analysis which allows to obtain surfaces images with a magnification level and a really high resolution not attainable with traditional instruments, in order to acquire qualitative information about the topography and the external morphology of the samples [40]–[42]. The setup includes a source of electrons, electromagnetic lenses for the electrons focus, electron detectors, sample chambers, computers and displays for the visualization of the images [43].

Electrons generated by a specific source are accelerated and pushed through a system of lenses and apertures in order to produce a fine beam of electrons that, impacting on the sample surface which is installed on a movable stage under vacuum, enables its scanning on a defined area. The images derive from the detection of the signals generated by the interaction between the electron beam and the samples through the activity of specific detectors [43].

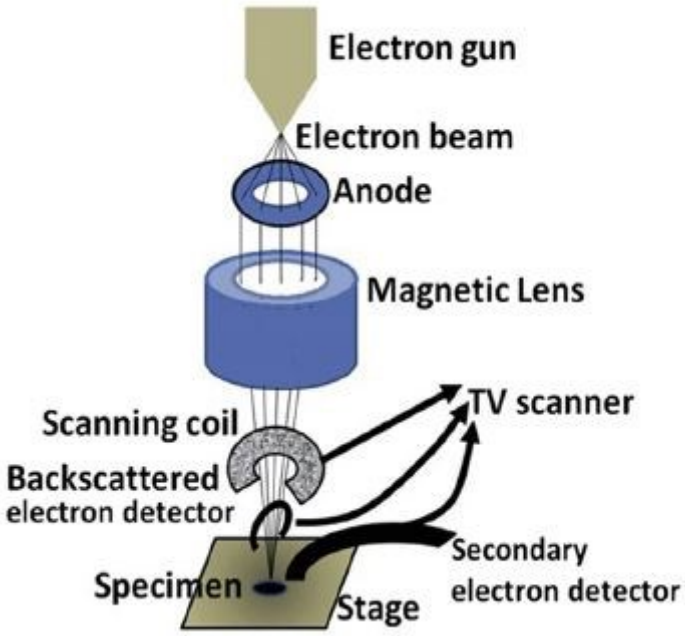

Figure 33: SEM setup [43]

In some cases, SEM can be associated to a further system known as “Energy-Dispersive X-ray Spectroscopy (EDS)”: it is able to quantitatively analyze the energy spectrum of the material, providing information about the chemical composition of the sample, thanks to a mechanism able to discriminates the X-rays received, that are specific for specific chemical elements [41]–[43].

SEM/EDS (Geol JCM 6000+) were performed on both SiO_2 and PP samples (with and without fibrinogen), working in triplicate: since the surfaces were not conductive, they firstly had to be metallized. For the metallization (Quorum Q150T S) the samples were placed on stubs thanks to a double-sided tape and they underwent a Platinum sputtering program for 20 s: this creates a very thin metal layer on the surface which does not affect the sample morphology but makes it conductive.

A magnification of 1000x was set for both SEM and EDS analysis while regarding the voltage it was about 5 kV for the imaging and 15 kV in the second case, as a result of which, information on the element’s atomic percentage was obtained.

Figure 34: SEM instrument [77]

3.3.2 Field Emission Scanning Electron Microscopy

Field Emission Scanning Electron Microscopy is an innovative microscopy technique able to generate, compared to conventional SEM, clearer and less electrostatically distorted images, with a better spatial resolution [44]. As the operating mechanism is similar to that of the SEM, the samples must be conductive but the main difference between the two techniques is that the FESEM electron generation system involves the implementation of a potential gradient to emit the electron beam, through a Field Emission Gun, then the electrons are accelerated toward a high electrical field gradient [45], [46]. The electrons are deflected thanks to an electronic lens present in the high vacuum column in which they are focused, in order to bombard the samples; for this reason, the samples can emit secondary electrons with different trajectory speed and angle that are finally caught by a detector, generating an electronic signal. Finally, this signal is converted into a video-scan image, so that it can be displayed on a monitor [46].

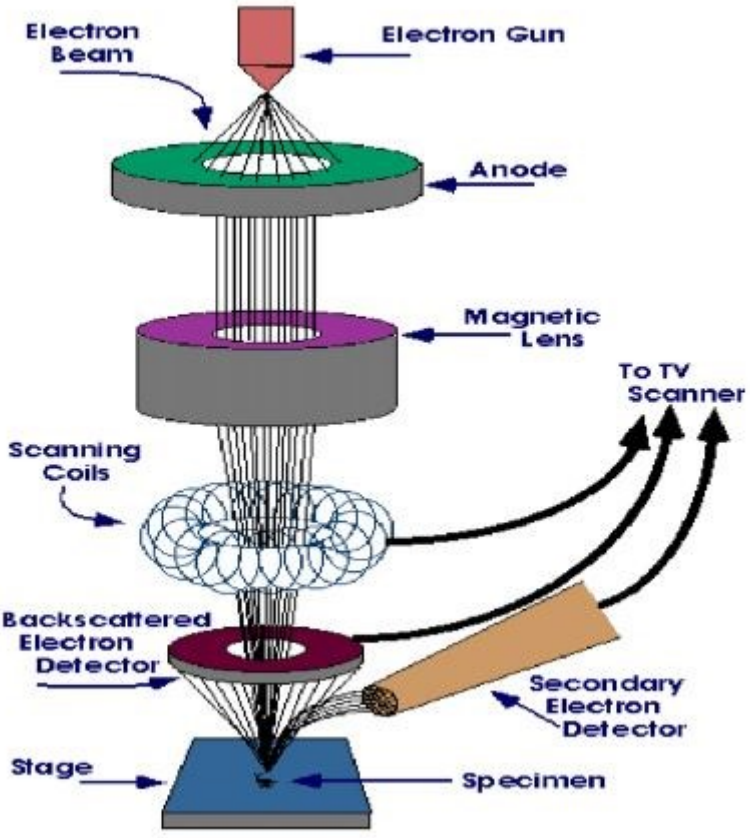

Figure 35: FESEM setup [78]

FESEM (Supra 40, Zeiss) analysis was applied to SiO_2 and PP samples, with and without fibrinogen: the metallization process was the same as that described for SEM. The samples were observed using four different magnification levels (10k, 50k, 100k, 250k) for SiO_2 and PP and six different magnification levels (5k, 10k, 25k, 50k, 100k, 250k) for SiO_2_FB and PP_FB.

Figure 36: FESEM instrument [79]

3.3.3 Fourier-Transform Infrared Spectroscopy

Fourier-Transform Infrared Spectroscopy (FTIR) is the most common form of infrared spectroscopy. Its main operation principle is that a portion of the infrared radiation (IR) that targets a sample is absorbed and the portion of the radiation that passes through the sample is recorded in order to acquire a spectrum which is used to obtain information about the chemical composition of the samples themselves, in that it is characteristic of the bonds in molecular species [47], [48]. In fact, the radiation absorption of a molecule's covalent bond happens for a specific wavelength and it changes the vibrational energy in the bond; depending on the atoms in the bond, a different type of vibration (stretching or bending) may occur and this aspect leads to a specific transmittance (or, complementarily,

absorbance) pattern, characterized by several peaks, each of them specific for a specific group or bond [47].

The infrared source, commonly known as "Michelson interferometer", generates the beam of IR radiation which falls on a beam splitter so that it is divided into two beams with equal intensities. After the generation of two reflected beams thanks to the action of two specific mirrors, they are properly recombined and directed to a detector, which create a signal known as "interferogram" [49]. Lastly, the interferogram is converted into the final spectrum graph thanks to the Fourier transform, a mathematical function able to return the frequency of the wave based on time, after taking them apart [47].

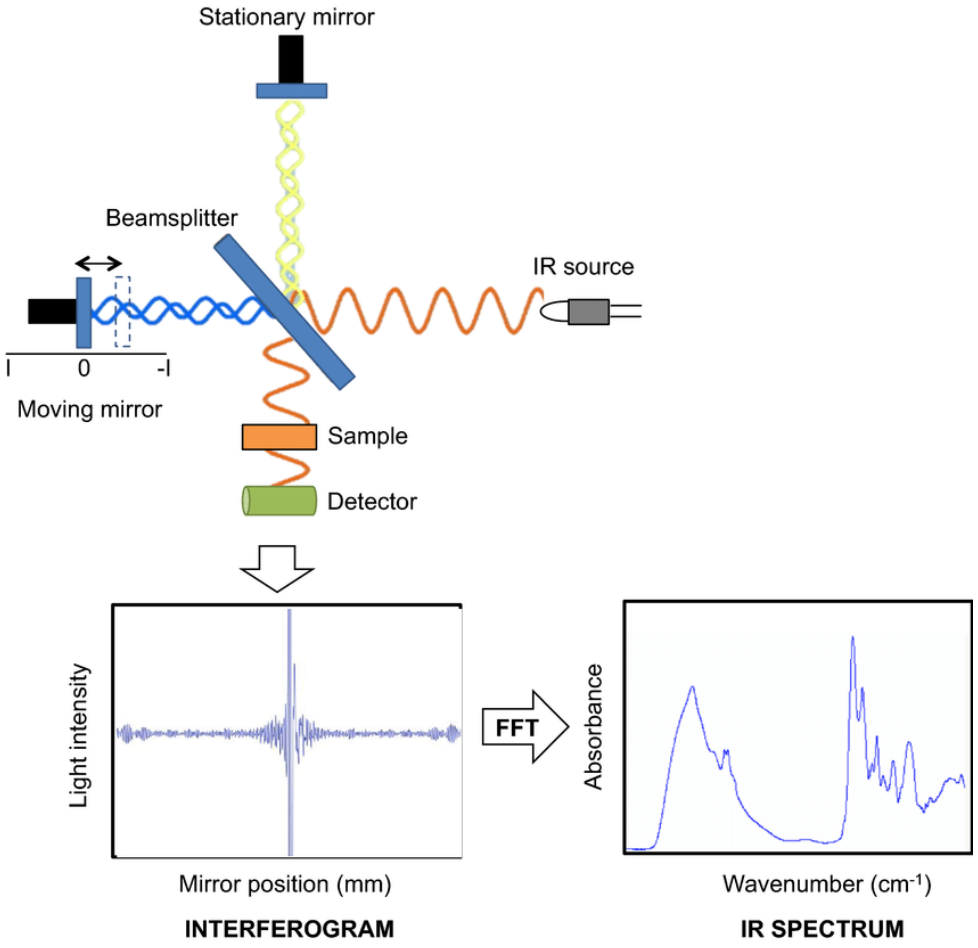

Figure 37: Schematization of FTIR process [80]

FTIR (Nicolet IS50 FT-IR, Thermo Scientific) was applied to SiO_2, SiO_2_FB, PP and PP_FB: the number of scanners is set to 64 to have a better resolution, which was of 4 cm^{-1}, and the measurement was carried out in absorbance. After obtaining the

background spectrum that must be subtracted from the final spectrum to exclude any air contamination, the sample was positioned upside down so that the surface to be analyzed was in contact with the detector and it was pushed on it, so as to improve contact and thus the measurement, which is based on ATR (Attenuated Total Reflection). Finally, the spectrum was obtained and it was properly studied.

Figure 38: FTIR instrument

3.3.4 Profilometry

Profilometry is a kind of contact microscopy able to measure the profile of a surface through the use of a metallic probe (a stylus) which scans it. The instrument, known as "profilometer", gives information about the surface roughness or the surface finish which depend on the several peaks and valleys with varying height, depth and spacing that compose the surface itself [50], [51].

Its operation is based on a mechanism whereby surface height variations are registered electrically through the stylus movement when it rides in a line across the surface: this movement is transmitted and amplified by a cantilever to identify a specific line which represents a reference to define the surface variations as notches/pits or asperities [50], [51].

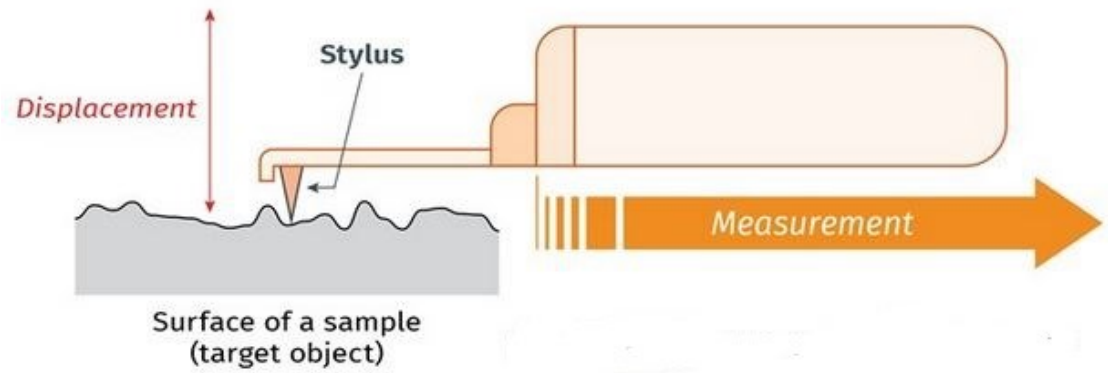

Figure 39: Schematization of profilometry measurement [50]

Profilometry (Intra Touch, Taylor Hobson) was carried out on SiO_2, SiO_2_FB, PP and PP_FB samples in triplicate: each sample was fixed on the support of the instrument thanks to a double-sided tape. Once the cantilever was positioned (z direction) with the tip as close to the sample as possible (distance between them ~0 µm), a length of 3 mm and a run-up of 0.05 mm were set while start and end points of the measurement were configured. The tip moved along the x axis, while the support along the y one.

The profilometer provided profile images that had to be "corrected" through the use of a high-pass filter and a low-pass filter in order to remove background noise and waviness respectively.

In addition, the measurement also provided several roughness values among which Ra was more frequently considered: it is defined as "the arithmetic average of the absolute values of the profile height deviations from the mean line, recorded within the evaluation length" [52].

Figure 40: Profilometry instrument

3.3.5 Confocal microscopy

Confocal microscopy is a modern microscopy technique able to provide very high-quality images with fine detail and more contrast than conventional microscopy; moreover, it can be used in order to obtain virtual 3D images of the samples thanks to a mechanism of combination of different sections [53].

Differing from the conventional microscopy, the confocal microscopy overcomes the problem related to the blur or the obscuration that the image can meet because of the scattering of the reflected light [53]. This is possible thanks to the presence of a screen that blocks the scattered light and allows only the passage of a diffraction-limited spot of light through a pinhole aperture which cuts off signals that are out of focus and sends them to a light detector, avoiding the whole sample illumination at once [53]–[55]. In this way, the light is collected from a highly focused point [53].

A modern confocal microscope consists of some pinholes, objective lenses and low-noise detectors; in addition, fast scanning mirrors, filters for wavelength selection and laser illumination may be present [56].

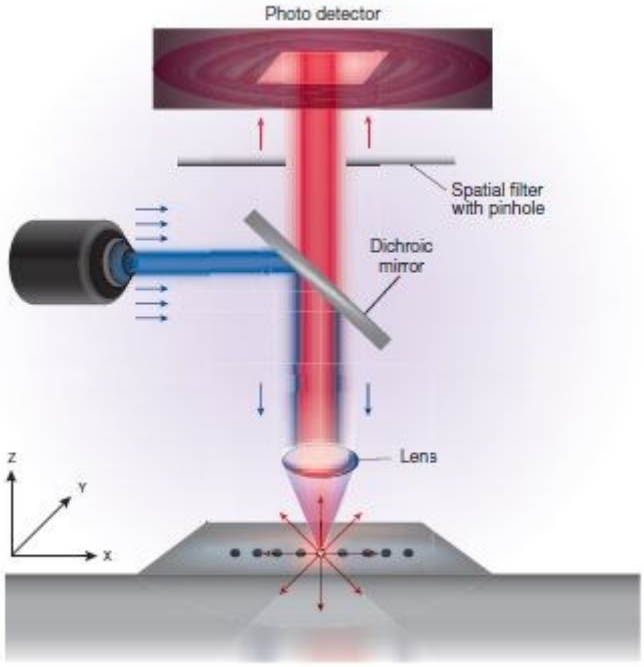

Figure 41: Confocal microscopy setup [53]

SiO_2, SiO_2_FB, PP and PP_FB samples were observed under confocal microscope (LSM 900, Zeiss) with two different analyses: roughness and topography.

For what concerns the topography a magnification of 50x, a laser power of 30% and a pinhole of 54 µm were set; the analysis range was selected to have a number of 70÷120 slices. Once the image was obtained, it underwent a smoothing, then the 3D structure was obtained too and the final image was properly colored to be easier to observe.

About the roughness a magnification of 20x, a laser power of 20% and a pinhole of 29 µm were set. In this case a filter for the waviness (8 µm) and a gaussian filter for the roughness (the cut-off was selected in function of the roughness Ra, by consulting ISO 4288 tables) were applied and the number of slices was about 70÷120 as previously.

The measurement provided several roughness values among which Sa was considered in triplicate: differing from the profilometry, in fact, in this case the roughness value was about a whole surface.

Figure 42: Confocal microscopy instrument

3.3.6 Contact angle

The deposition of a specific liquid drop on the surface leads to the formation of an angle θ between the surface and the tangent to the drop. This angle, which is inside the drop and depends on the equilibrium condition reached between three interfacial tensions which are γ_{lv} (liquid-vapor), γ_{sv} (solid-vapor) and γ_{sl} (solid-liquid), will identify the hydrophobic ($\theta \geq 90°$, the surface does not interact with the liquid and the drop shape remains strongly spherical) or hydrophilic ($\theta < 90°$, the interaction between the liquid and the surface gives the drop a more flattened shape on the surface itself) surface behavior [57], [58].

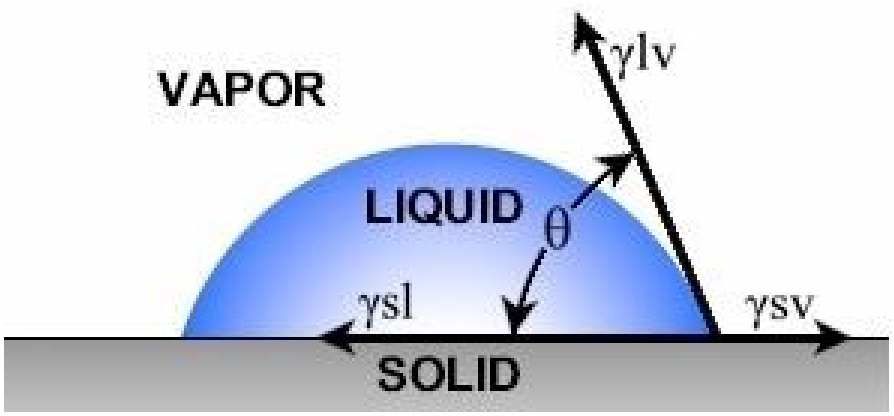

Figure 43: Schematization of the contact angle measurement [81]

The contact angle (Drop Shape Analyzer KRÜSS DSA100) of all SiO_2 and PP samples with and without fibrinogen was measured to obtain information about their surface's wettability. They were placed on the support of the instrument: samples were analyzed both when wet and dry to make a better comparison, using three different types of liquid (drop volume 10 µl) which are ultrapure water, fetal bovine serum (FBS) and fibrinogen solution. On the other hand, Ti64, Ti64_FB, CT and CT_FB were analyzed when dry, using only fibrinogen solution. Thanks to a cam, the program provided the contact angle values that were calculated in triplicate.

Figure 44: Contact angle instrument

A further analysis in triplicate was conducted by Messina University using drops of human blood from healthy donor to investigate the interaction between the blood and SiO_2, SiO_2_FB, PP and PP_FB surfaces too when they were dry.

Furthermore, the contact angle was measured in triplicate on fibrinogen powder (FB_p) using ultrapure water, FBS and fibrinogen solution: to easily analyze the powder, some o-rings were cut with a height of 0.5 cm and attached on the flat side of a petri dish using double-side tape, then the powder was located into the ring and pressed with a spatula. Finally, the o-ring was removed and the powder was analyzed.

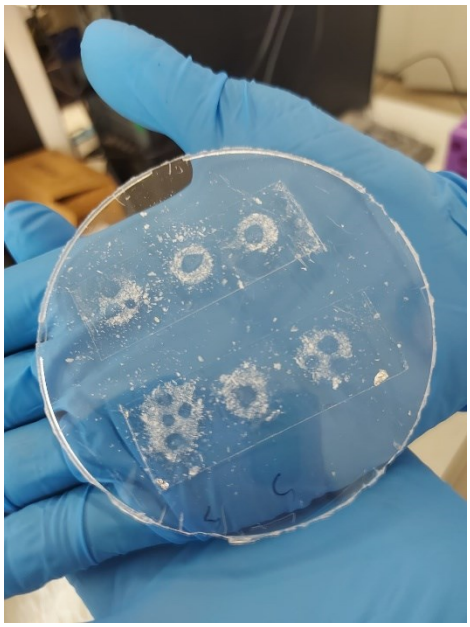

Figure 45: Illustration of the preparation of powder fibrinogen samples for the evaluation of contact angle

3.3.7 Zeta potential

When a material comes into contact with water-based media (e.g. physiological fluids), a counterions distribution in the liquid leads to the development of a surface charge at solid-liquid interface which strongly depends on the surface features. For example, the generation of this charge can be a consequence of the replacement of the adsorbed water molecules with ions (OH^-, H_3O^+) in case of absence of functional groups on the surface or alternatively be a result of different types of acid-basic reactions between the medium and any functional groups on the surface, such as protonation of the amine groups or dissociation of the hydroxyl groups [59].

According to the "*Electrochemical Double Layer (EDL) model*", the counterions that compensate the surface charge can be divided into a "*stationary layer*" (immobile) and a "*diffuse layer*" (mobile): the potential at the outside of the stationary layer is the zeta potential ζ [59].

Zeta potential measurement also allows to identify the so-called "*isoelectric point (IEP)*", which is defined as the pH value for which the net charge of a specific molecule is zero (neutral charge) [60].

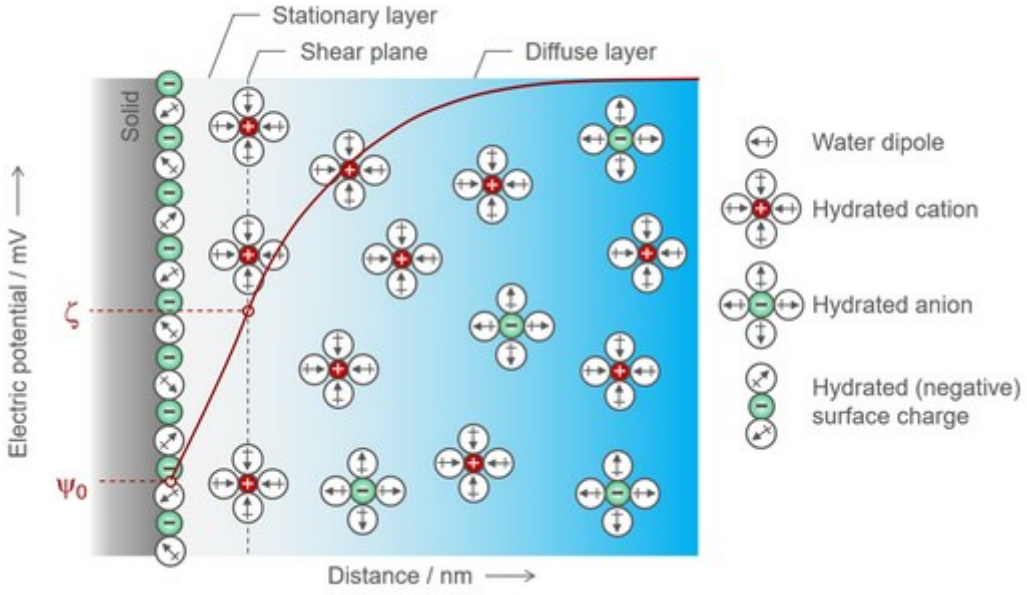

Figure 46: Schematization of EDL model [82]

Zeta potential (SurPASS electrokinetic analyzer, Anton Paar) was measured on SiO_2, SiO_2_FB, SiO_2_FB_w, PP, PP_FB, PP_FB_w, Ti64_FB_w, and CT_FB_w samples' surfaces (in polypropylene case, samples without Titanium support were considered). The samples were directly fixed on two supports thanks to a specific double-sided tape, so that their surfaces were parallel to each other, with a gap of ~100 μm.

After mounting the cell, the device was prepared for the measurement, starting from a first essential step of cleaning.

A filling step allowed to obtain the electrolytic solution of interest, a KCl 0.001 M solution made by dissolving 45 mg of KCl in 600 ml of ultrapure water thanks to a magnetic stirrer. A pH meter and a conductivity probe permitted the continuous monitoring of pH and conductivity respectively: thanks to a check of the conductivity, it was maintained in the range of 15 ÷ 20 mS/m.

Then there was the rinsing step, during which the gap was monitored and set to the right value.

The next stop was the flow check, during which the pressure value was set in order to obtain an electrolyte flow of 100 ml/min.

After setting the pressure value, the measurement started: it was based on two separate processes of basic and acid titration, using NaOH 0.05 M and HCl 0.05 M respectively, changing the samples between the two measurements.

The instrument provided a curve describing the trend of the potential as a function of pH and finally a last cleaning step was essential.

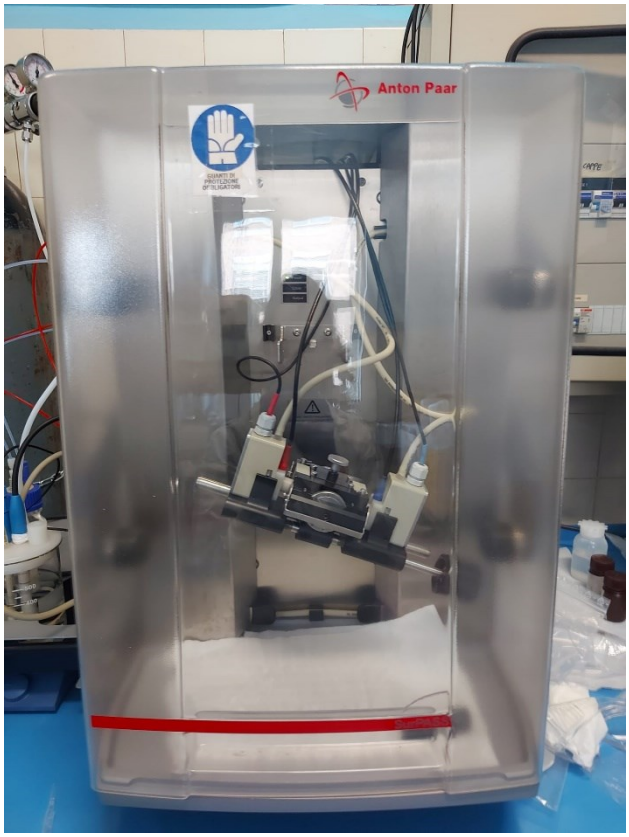

Figure 47: Zeta potential instrument

4 RESULTS AND DISCUSSION

4.1 Materials

4.1.1 Silica

Silica, also known as silicon dioxide (SiO_2) is a solid compound present in many different crystalline or amorphous allotropic forms [61].

Silica-based materials are extremely used in biomedical field, especially for the implementation of drug-delivery systems and bone-repairing devices [62]. In fact, nano- and micro-sized silica present a high surface area, an excellent biocompatibility, adjustable surface or pore morphological structures and rich functionality [63].

These materials are also characterized by a great bioactivity, defined as the ability of the material to incorporate into the living tissue through a series of chemical processes. These processes involve the nucleation (thanks to silanol groups -Si-OH- which act as nucleation sites and make silica hydrophilic) and growth on the material surface of a layer of carbonated hydroxyapatite with low-crystallinity and close-related to the mineral phase of the bone tissue (the nucleation rate strongly depends on pore size and volume) [62], [63].

Silica can be used in form of amorphous silica spheres, as constituent of bioglasses or ordered mesoporous materials [62].

4.1.2 Polypropylene

Polypropylene is a polymer which derives from a polymerization process starting from propylene, an ethylene with one methyl group attached, in a way that in polypropylene all the methyl groups are oriented in the same direction [64].

It is widely used in different branches, especially in biomedical one, thanks to its low cost, good plastic toughness and high light transmission [65]. Its main advantages, for what concerns biomedical applications, are the high biocompatibility and the ability to be autoclaved [64], [65].

It is generally used in form of meshes, alone or in combination with other materials [64].

4.1.3 6-4 Titanium alloy

Titanium and its alloys are characterized by good mechanical properties and biocompatibility, so that they are extremely used in biomedical field to realize dental orthopedic or cardiovascular implants [66], [67].

Titanium implants are also characterized by the formation of corrosion resistant layer of TiO_2 on their surface, thanks to the high chemical affinity between Oxygen and Titanium itself: this feature makes the Titanium and its alloys extremely resistant to corrosion [67].

6-4 Titanium alloy (Ti6Al4V, α+β biphasic alloy) is the most widely used Titanium alloy: Aluminum has a crucial role in the passivation layer formation and in the stabilization of α phase, while Vanadium leads to a biphasic structure and to the stabilization of β phase as well as an improvement of mechanical properties [68], [69].

4.2 Fibrinogen adsorption

After the fibrinogen adsorption, some of the PP_FB samples showed on their surface circular shapes, while other samples showed radial patterns. This can be considered a first qualitative demonstration of the presence of fibrinogen on the samples' surface.

The shape of the fibrinogen deposits can derive from the drying conditions which are not completely controlled in our protocol.

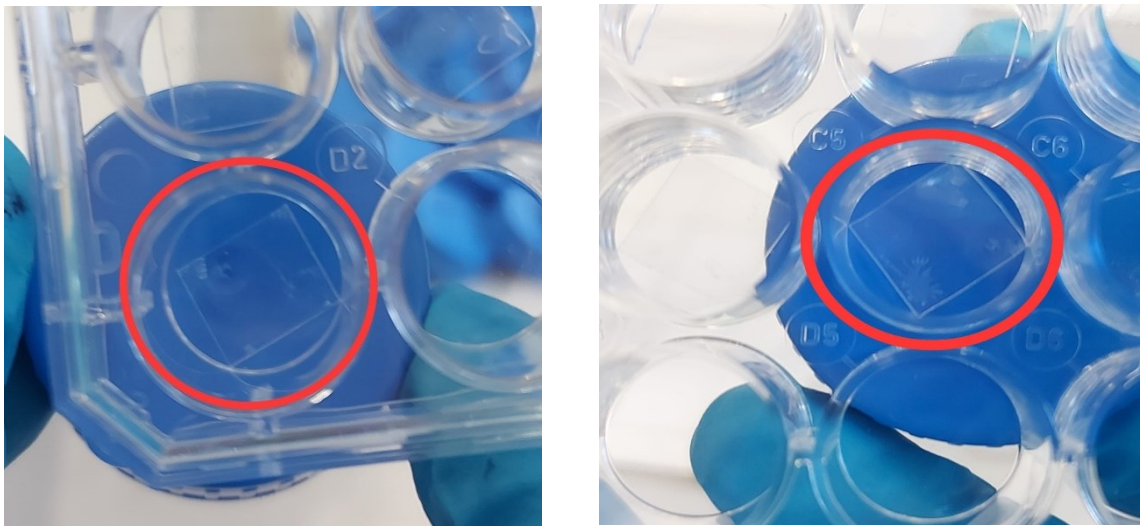

Figure 48: Circular shapes on PP_FB samples (sx); radial patterns on PP_FB samples (dx)

4.3 Surface characterization

It is necessary to premise that wet samples data are mainly interesting for the purpose of this thesis, which is to investigate the materials behavior and their interaction with plasma fibrinogen after implantation. In case of dry materials, the inevitable drying effect should be considered: for this reason, dry samples characterization might be useful in order to understand a pre-adsorbed material, which is implanted at a later time, but this is not our aim. On the other side, some characterization techniques cannot be applied or give no significant data on wet samples. In this case, dried samples were used taking into account that they can be affected by drying.

Techniques that have not been successful such as SEM/EDS, FESEM and FTIR are firstly reported: in this case they have not been applied to other materials; on the other hand, profilometry, confocal microscopy, contact angle and zeta potential showed more interesting results, so that their application was extended to Ti64 and CT too.

4.3.1 Scanning Electron Microscopy/Energy-Dispersive X-ray Spectroscopy

SEM/EDS were applied both on silica and polypropylene samples and it was possible to make observations related to the degree of covering of fibrinogen on the samples surface. Atomic percentage of different elements and SEM images with a magnification of 1000x are reported for both SiO_2 and SiO_2_FB.

Table 2: Atom % SiO_2

SiO_2		
Element	**Atom % (Average)**	**Standard Deviation**
C	3.42	2.96
N	0	0
O	62.49	1.41
Si	33.67	1.56
Pt	0.43	0.011

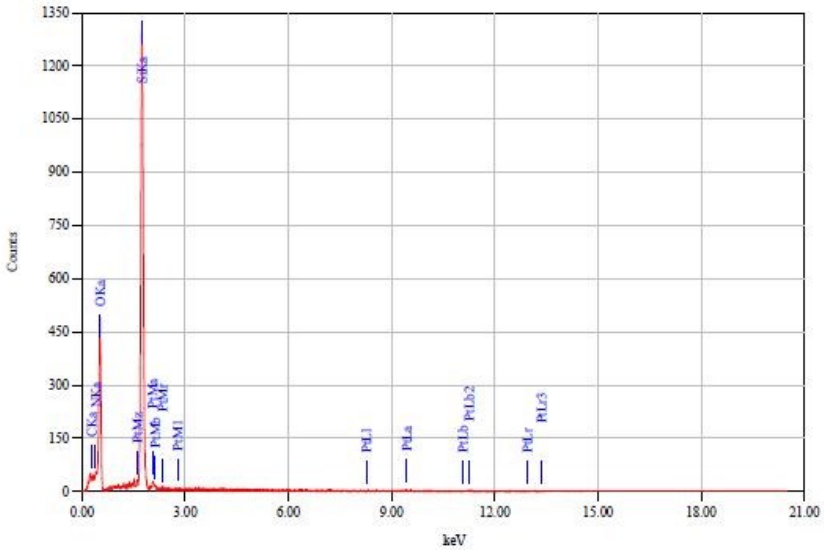

Figure 49: EDS spectrum SiO_2

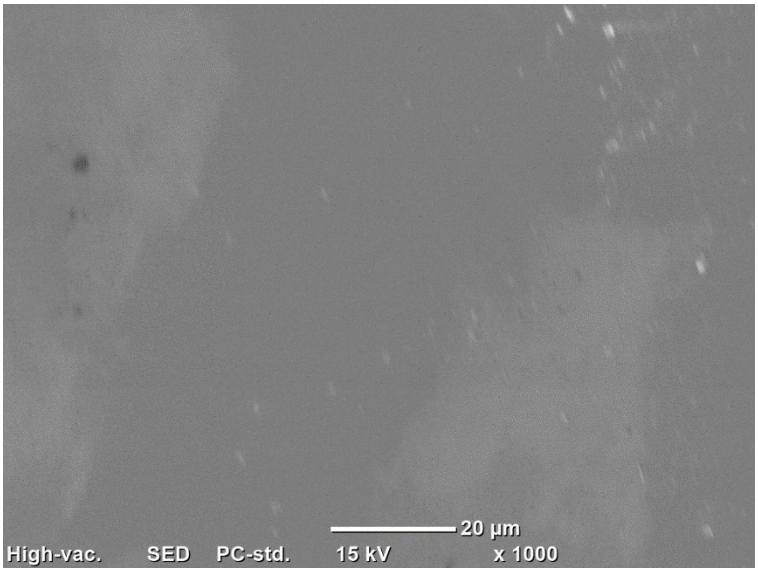

Figure 50: SEM image SiO_2

Table 3: Atom % SiO_2_FB

SiO_2_FB		
Element	**Atom % (Average)**	**Standard Deviation**
C	7.06	5.26
N	0	0
O	60.11	2.64
Si	32.28	2.64
Pt	0.37	0.10
Na	0.17	0.057
Cl	0.075	0.11

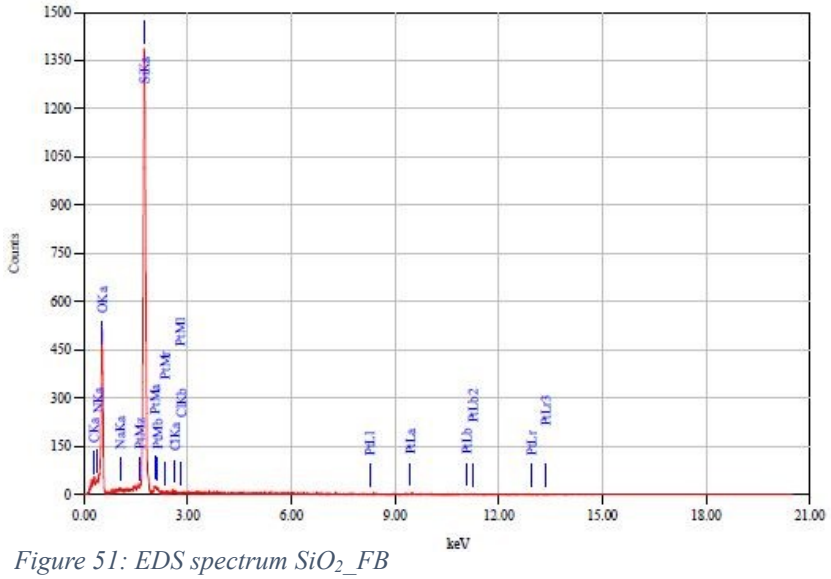

Figure 51: EDS spectrum SiO_2_FB

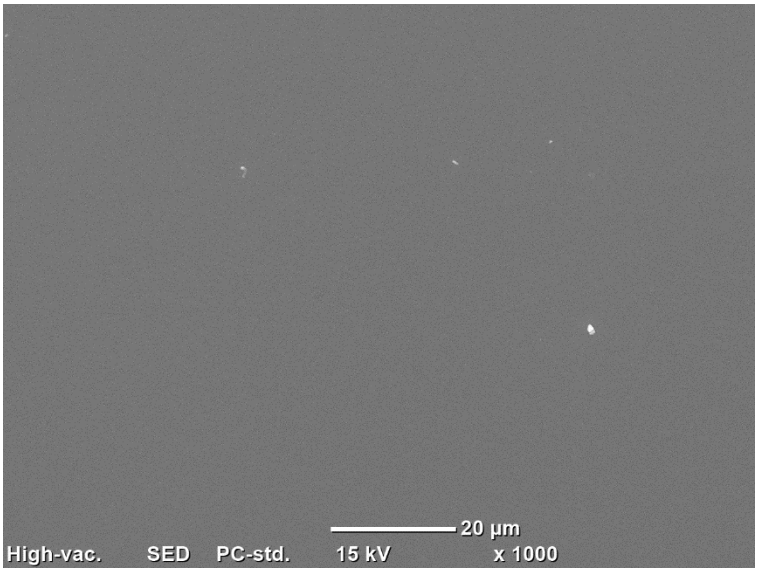

Figure 52: SEM image SiO_2_FB

SiO_2 and SiO_2_FB resulted to have a similar composition and the comparison between them underlined a specific trend, characterized by an increase in the quantity of Carbon (C) in the second case, with a decrease of Oxygen (O) and Silicon (Si), although these differences are not significant. In addition, in both cases Platinum was present as a consequence of the metallization process. As regards imaging, there were not evident qualitative differences between the two images.

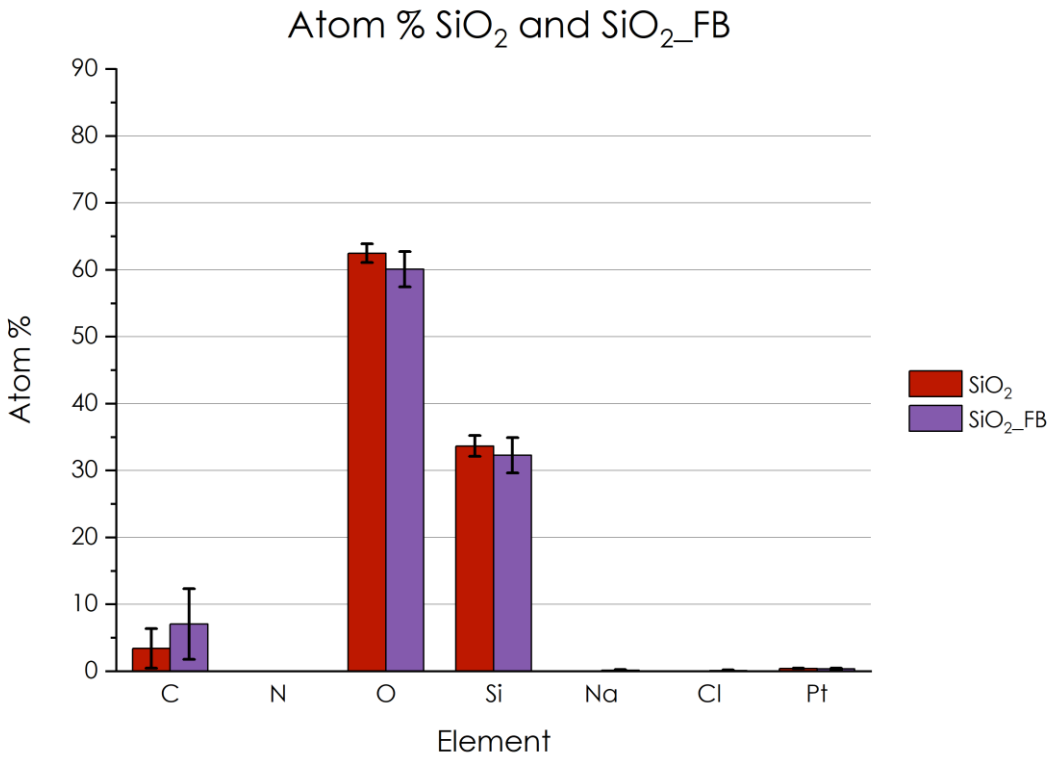

Figure 53: Atom % SiO_2 and SiO_2_FB

In SiO_2_FB samples a great presence of Sodium (Na) and Chlorine (Cl) was identified in specific zones: it could be considered as a demonstration of the presence of salt (also visible by the images), due to the use of NaCl solution for the adsorption protocol. These elements were not equally present in samples without the protein.

Table 4: Atom % SiO_2_FB (salt)

SiO_2_FB (salt)	
Element	**Atom %**
C	24.38
N	5.6
O	44.99
Si	8.37
Pt	0.34
Na	10.89
Cl	5.44

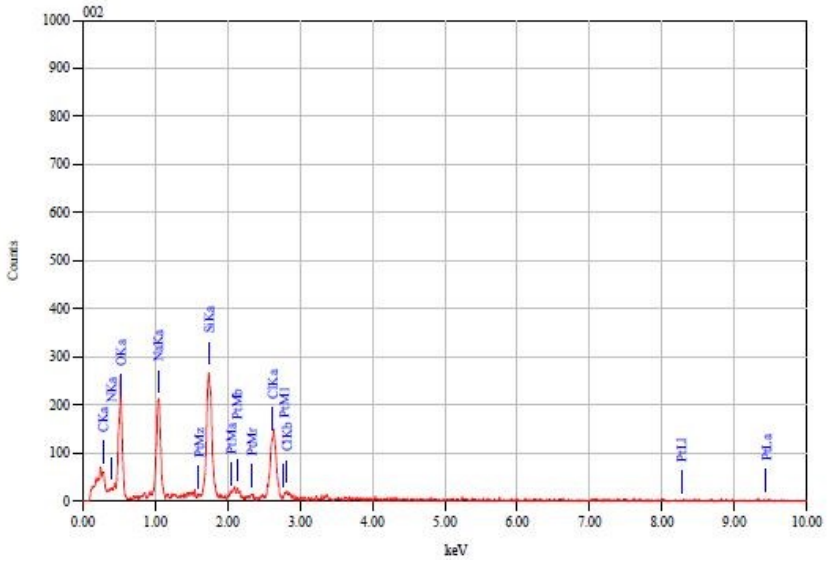

Figure 54: EDS spectrum SiO_2_FB (salt)

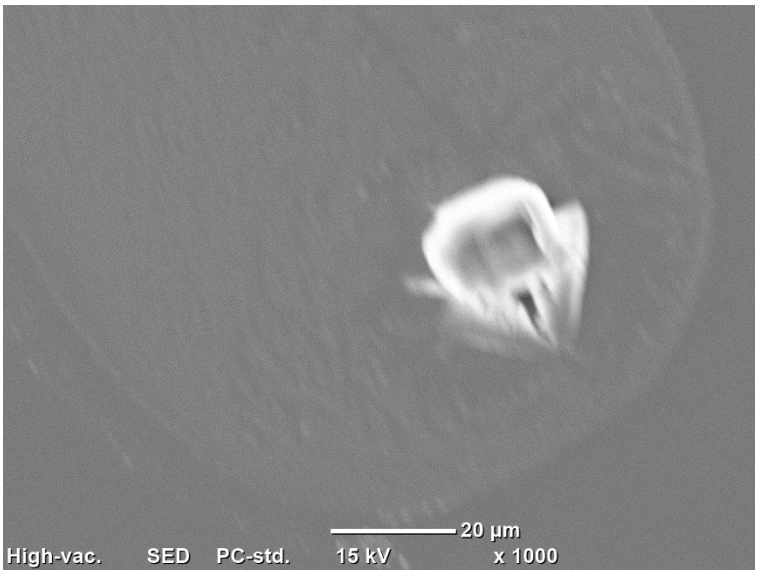

Figure 55: SEM image SiO_2_FB (salt)

Atomic percentage of different elements and SEM images with a magnification of 1000x are also reported for both PP and PP_FB.

Table 5: Atom % PP

PP		
Element	**Atom % (Average)**	**Standard Deviation**
C	85	1.44
N	13.04	1.70
O	1.45	0.27
Pt	0.5	0.017

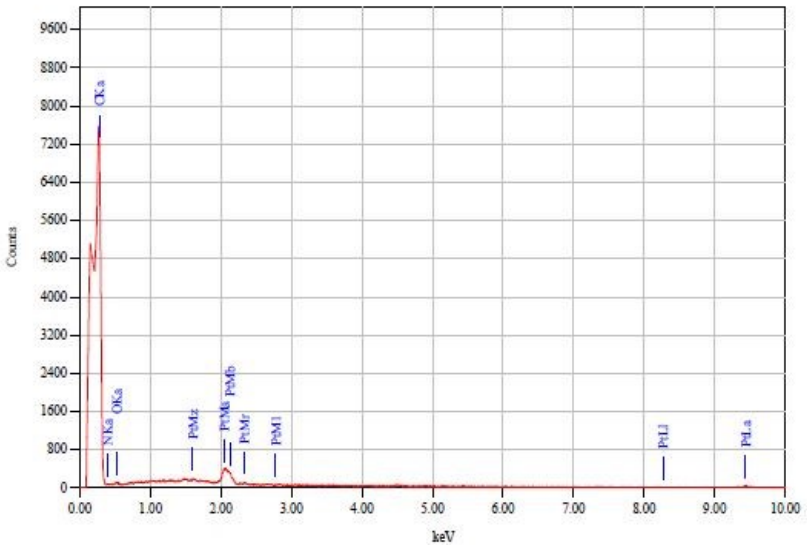

Figure 56: EDS spectrum PP

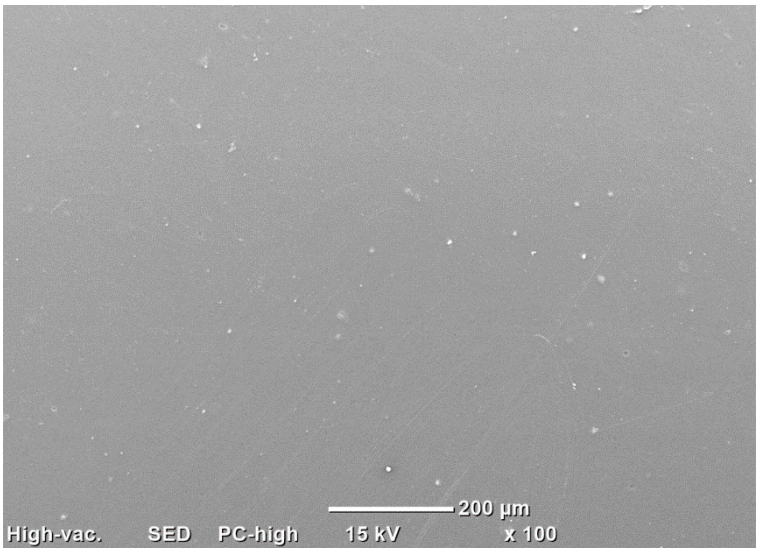

Figure 57: SEM image PP

Table 6: Atom % PP_FB

PP_FB		
Element	**Atom % (Average)**	**Standard Deviation**
C	80.75	1.34
N	16.50	1.27
O	2.21	0.074
Pt	0.36	0.15

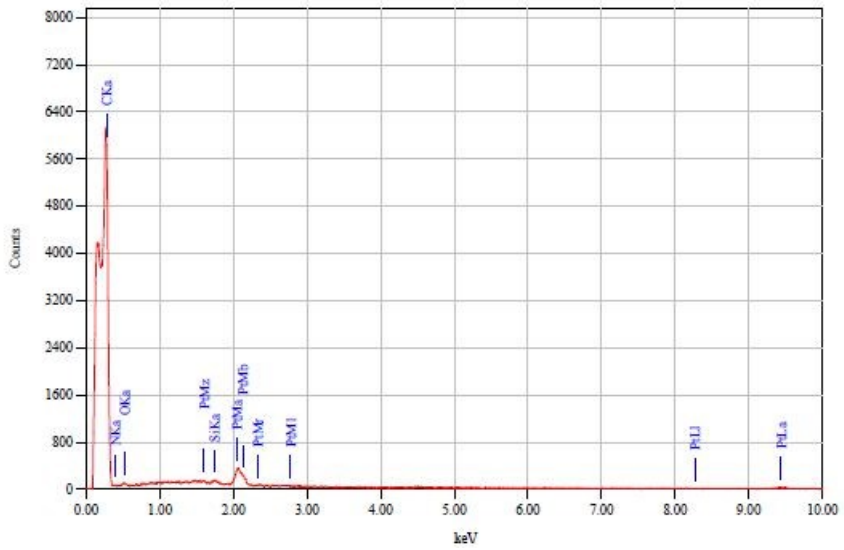

Figure 58: EDS spectrum PP_FB

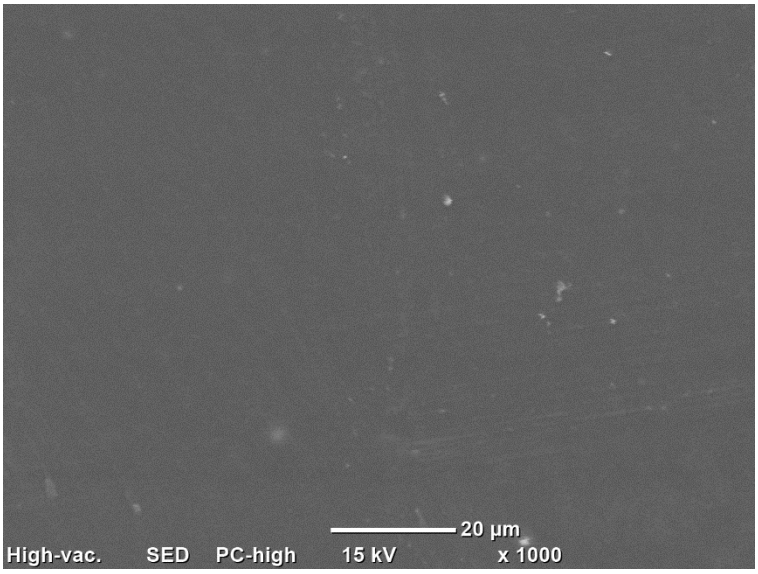

Figure 59: SEM image PP_FB

PP and PP_FB resulted to have a similar composition and the comparison between them underlined a specific trend, characterized by an increase in the quantity of Oxygen (O) in the second case, with a decrease of Carbon (O) and Nitrogen (N), although these differences are not significative. In addition, in both cases Platinum was present as a consequence of the metallization process.

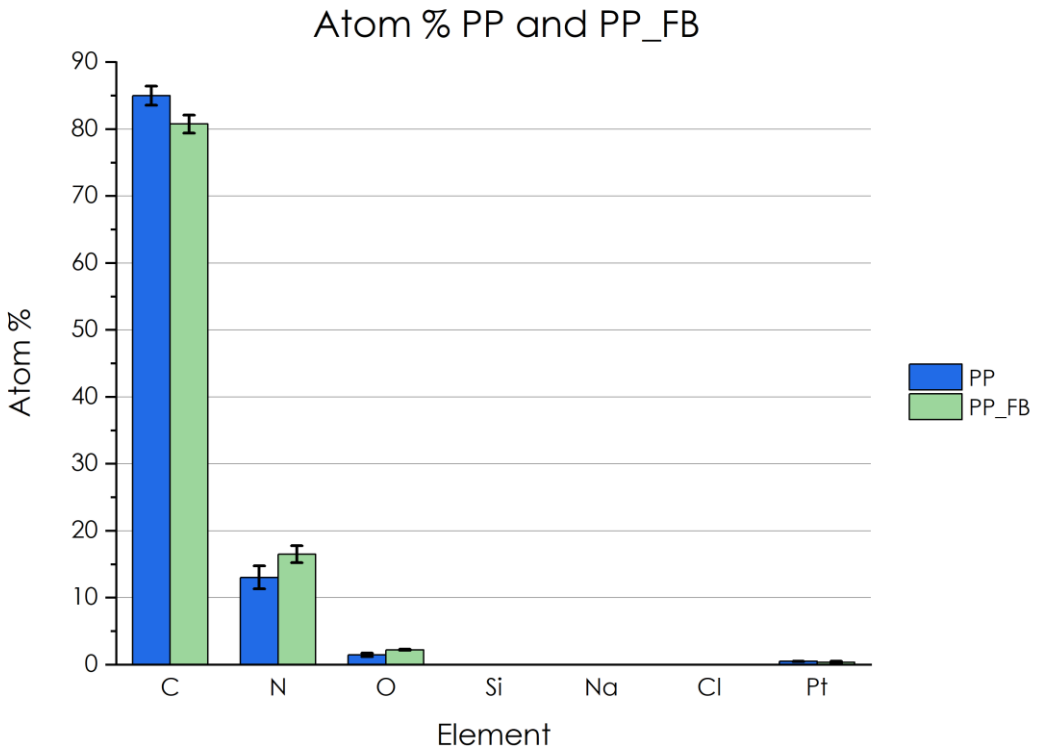

Figure 60: Atom % PP and PP_FB

Some agglomerations were easily viewable in SEM images of PP_FB samples: studying them it was possible to distinguish between two different zones. The first zone (blue) showed Silicon (Si) contamination, while the second zone (red) a salt.

Table 7: Atom % PP_FB (contamination, sx); atom % PP_FB (salt, dx)

PP_FB (contamination)	
Element	**Atom %**
C	54.41
N	18.36
O	18.74
Na	0.26
Si	7.59
S	0.04
Cl	0.11
Ca	0.18
Pt	0.3

PP_FB (salt)	
Element	**Atom %**
C	38.81
N	27.4
O	30.67
Na	1.38
Si	0.1
S	0.23
Cl	0.55
Ca	0.45
Pt	0.4

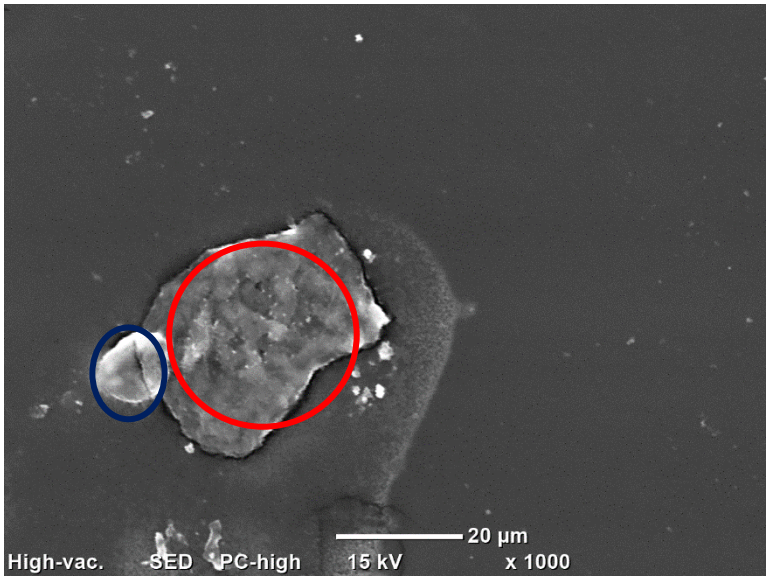

Figure 61: SEM image PP_FB (salt, red) and PP_FB (contamination, blue)

SEM/EDS technique is not useful for the characterization of these samples, in that drying effects may create morphological artefacts and EDS is too penetrating (1 - 1.5 µm) to allow to observe significative compositional differences.

4.3.2 Field Emission Scanning Electron Microscopy

FESEM images were obtained for SiO_2, SiO_2_FB, PP and PP_FB samples at different magnification levels (10k, 50k, 100k, 250k for the samples without fibrinogen, 5k, 10k, 25k, 50k, 100k, 250k for the samples with fibrinogen).

SiO_2

The surface appeared smooth.

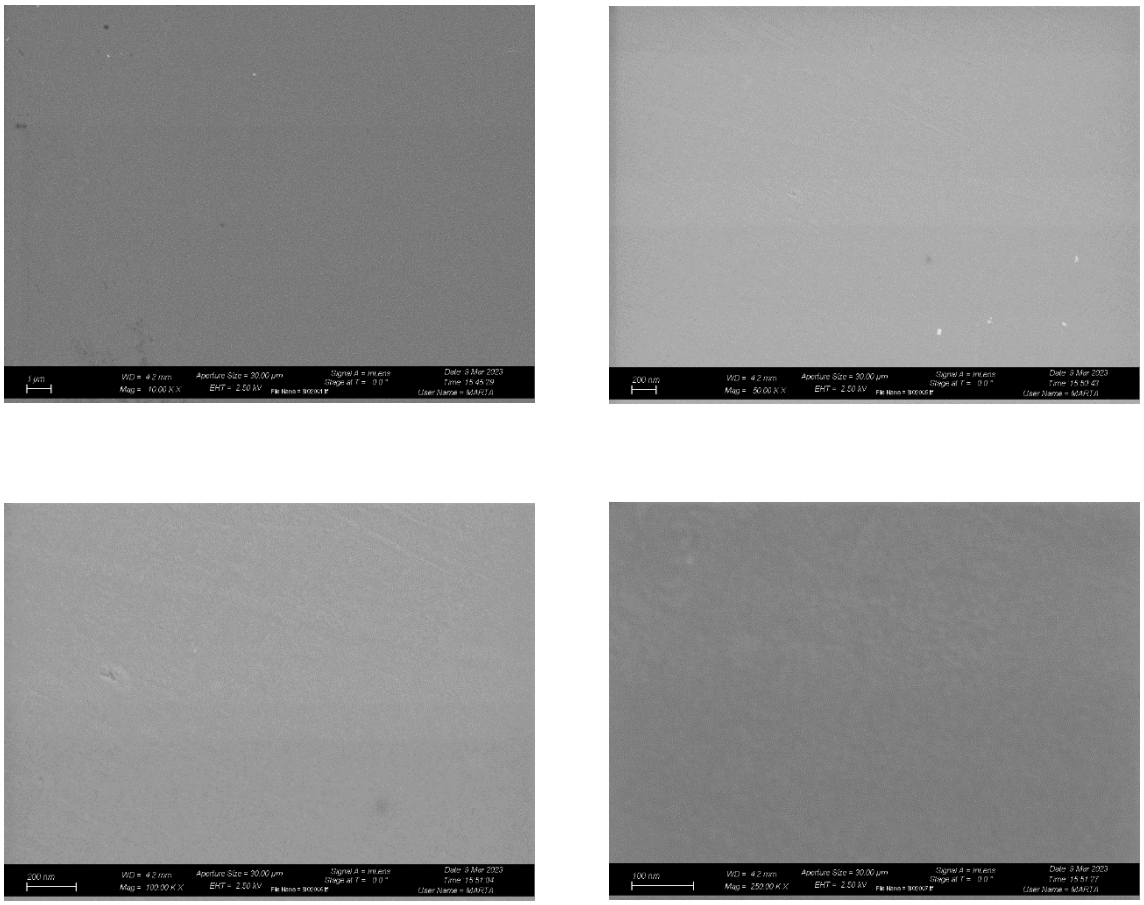

Figure 62: FESEM images SiO_2

SiO_2_FB

The sample's surface resulted to be irregular and rough, with the presence of salt crystals and branched structures, in line with Ra and Sa data (paragraphs 4.3.4 and 4.3.5).

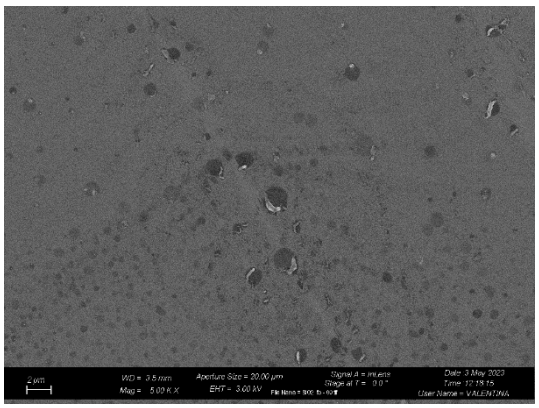

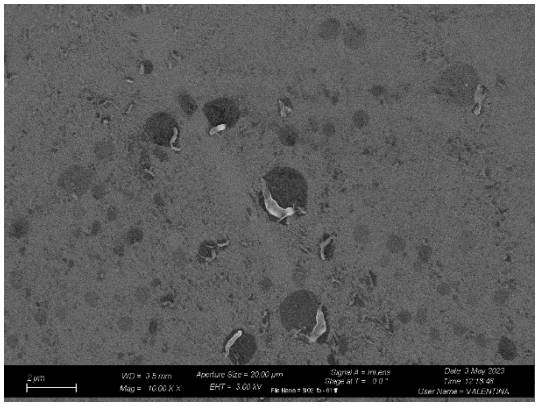

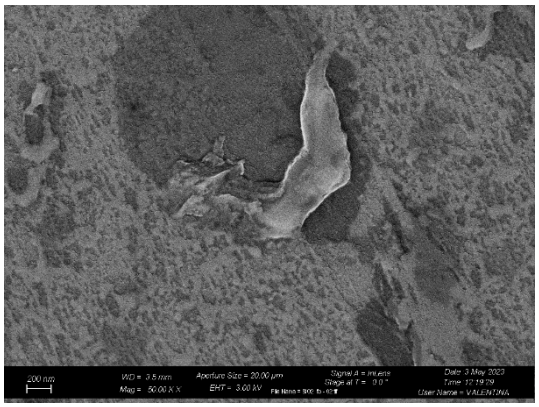

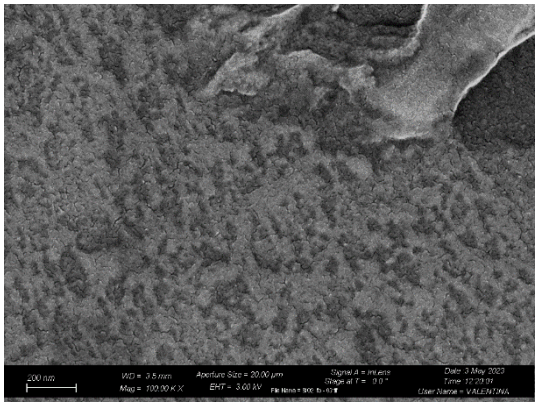

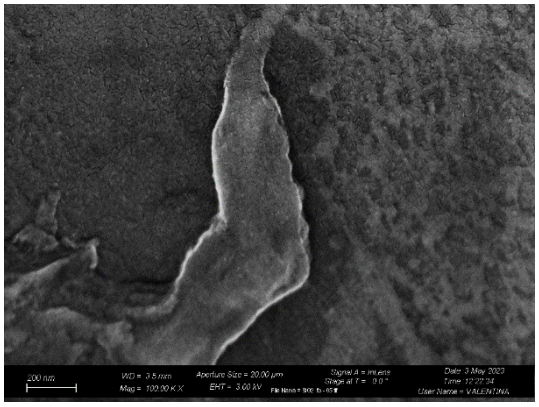

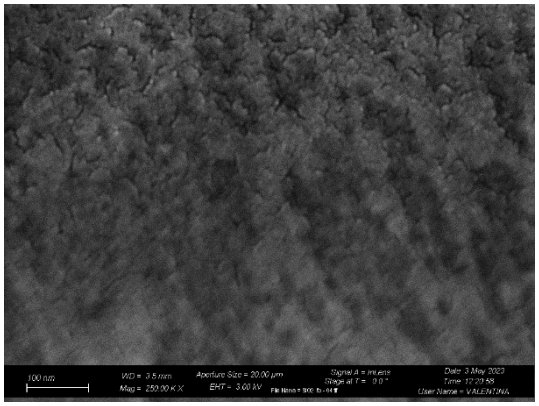

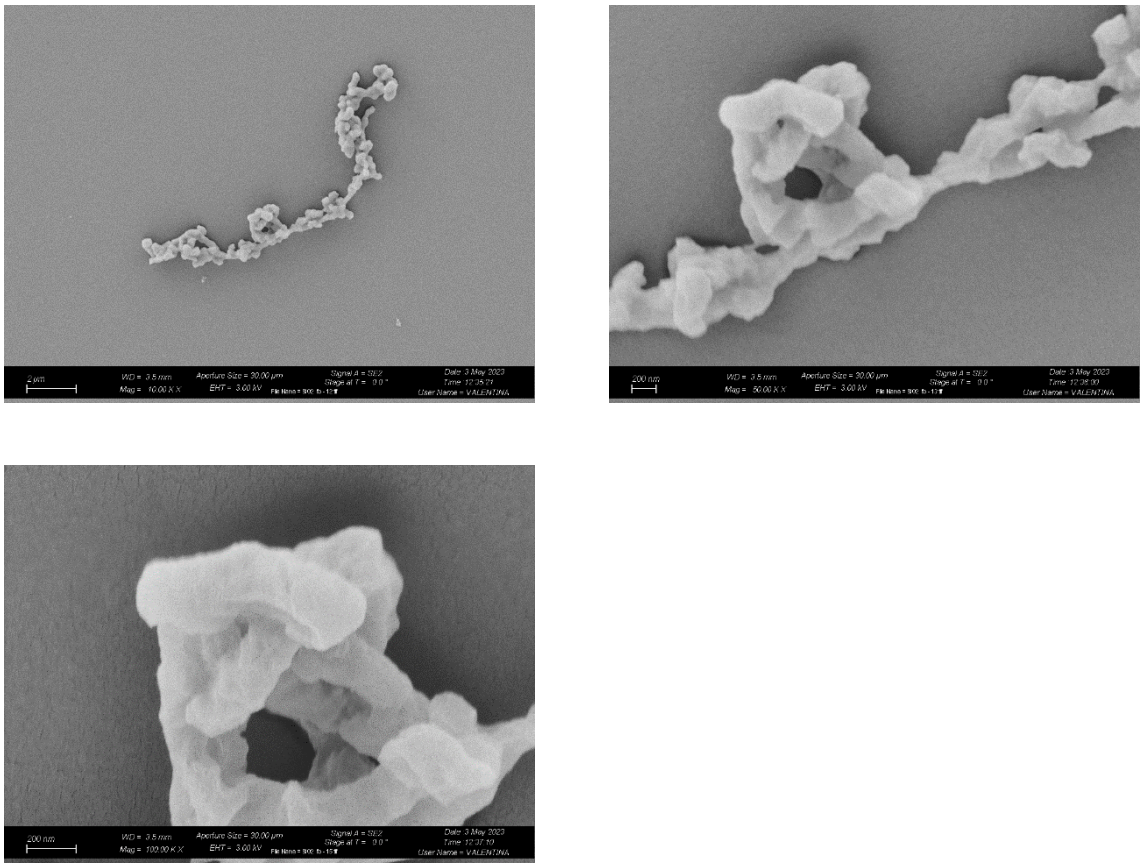

Figure 63: FESEM images SiO_2_FB

PP

The surface was slightly rough, in accordance with Ra and Sa measurements (paragraphs 4.3.4 and 4.3.5).

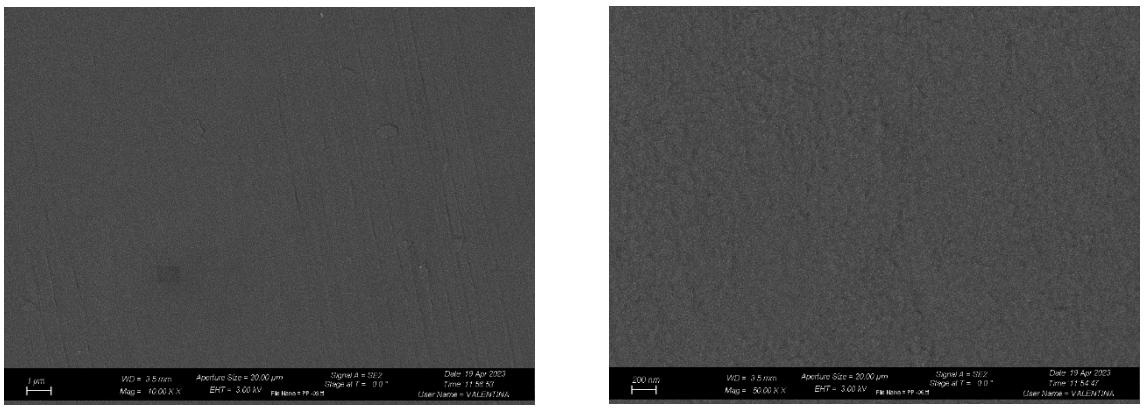

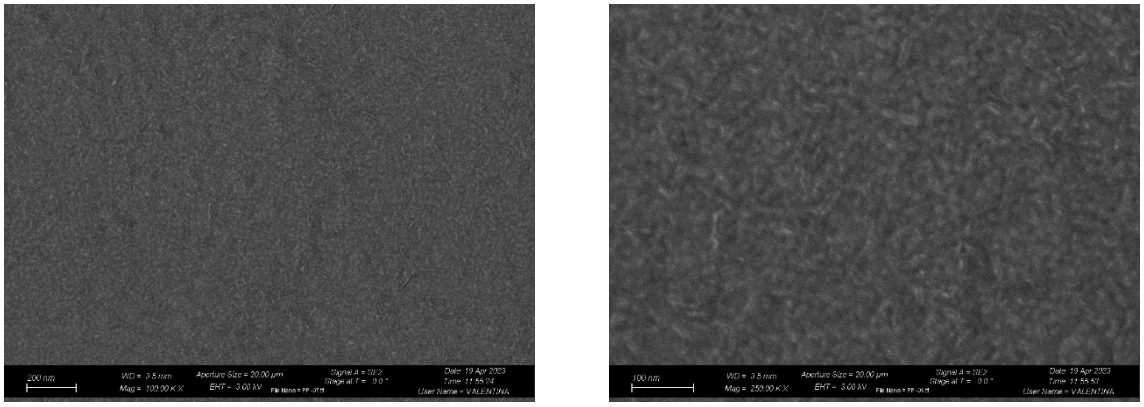

Figure 64: FESEM images PP

PP_FB

The images showed structures characterized by aligned crystals and a roughness comparable to that of PP samples. The surface was extremely inhomogeneous after the fibrinogen adsorption.

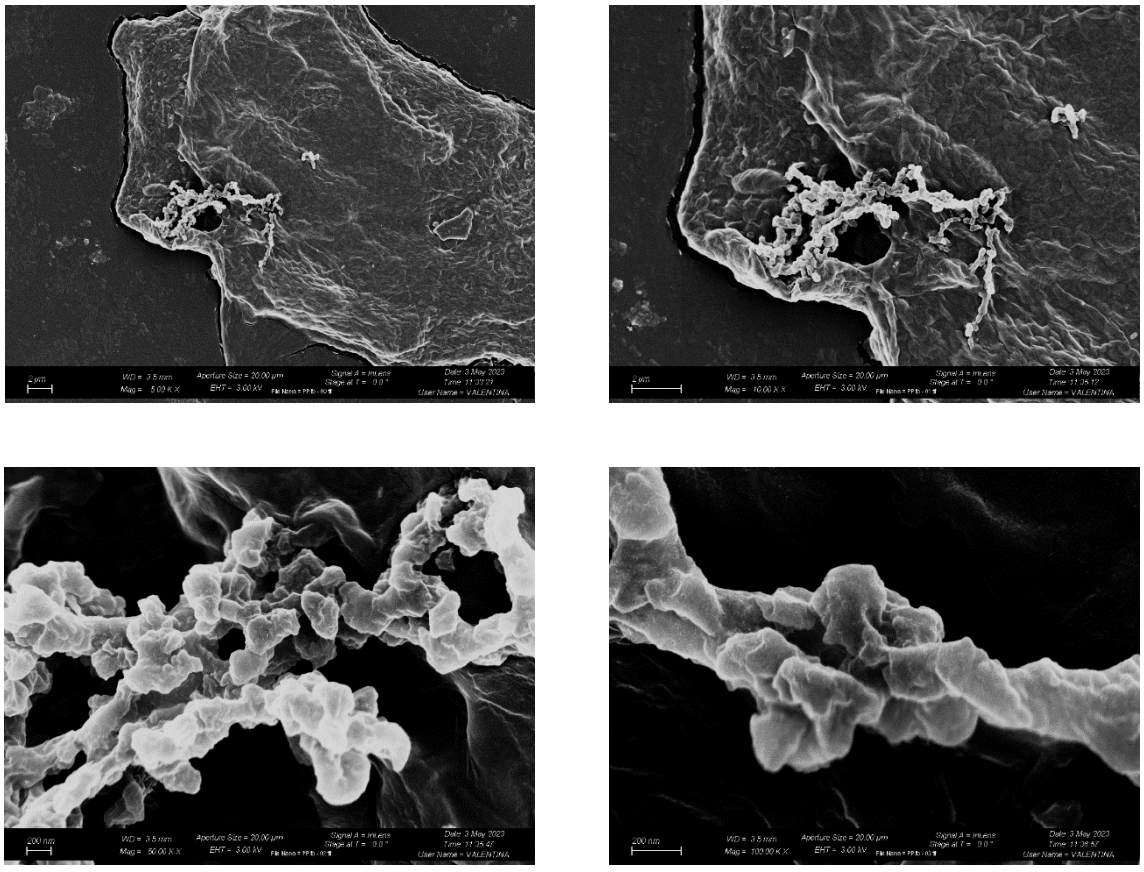

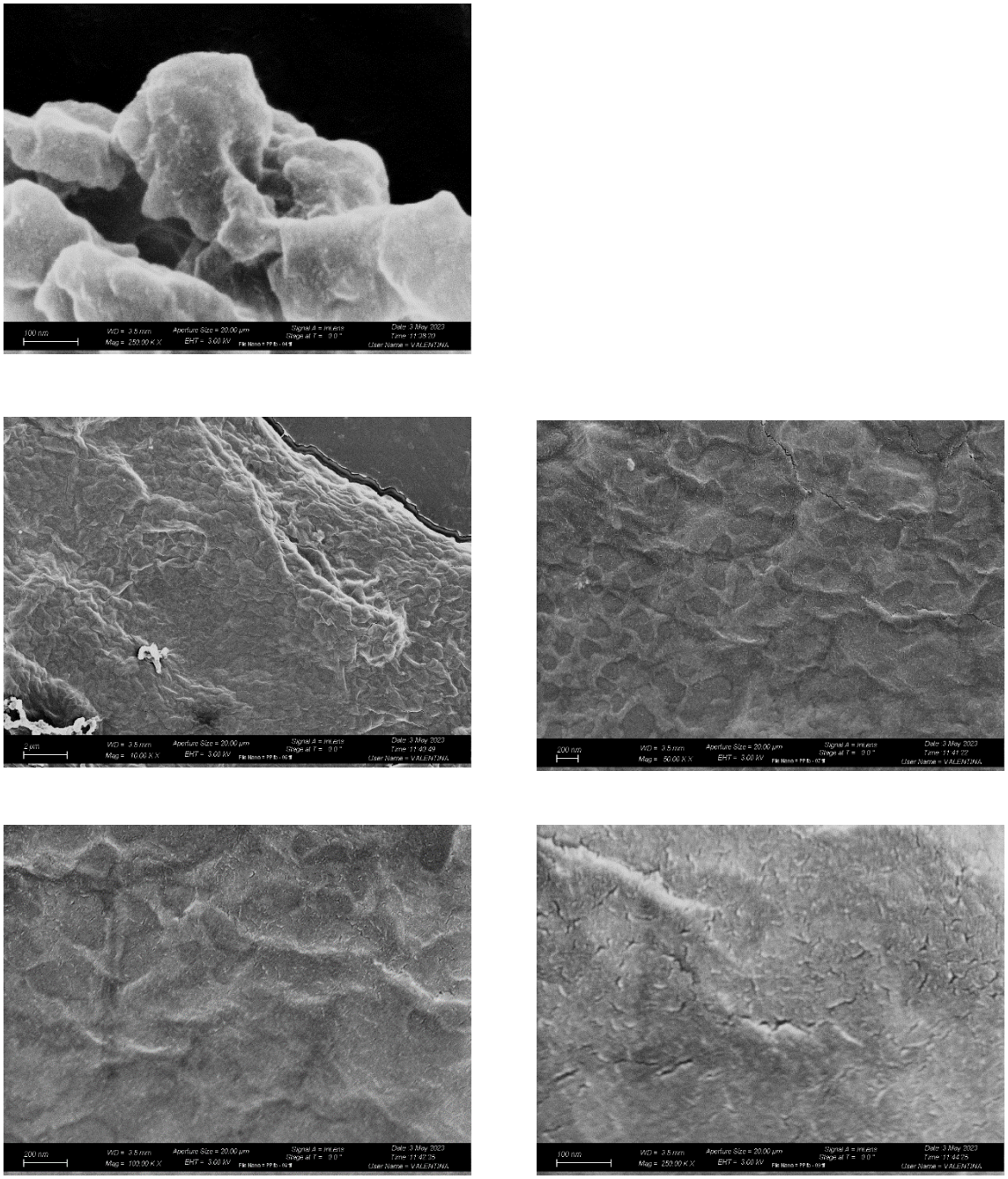

Figure 65: FESEM images PP_FB

CT FESEM images with four different magnification levels (10k, 50k, 100k, 250k) are reported too[1]: the surface nanostructure generated by the chemical treatment is easily viewable.

[1] These images were not obtained during this thesis but they are part of Camilla Reggio's PhD thesis

CT

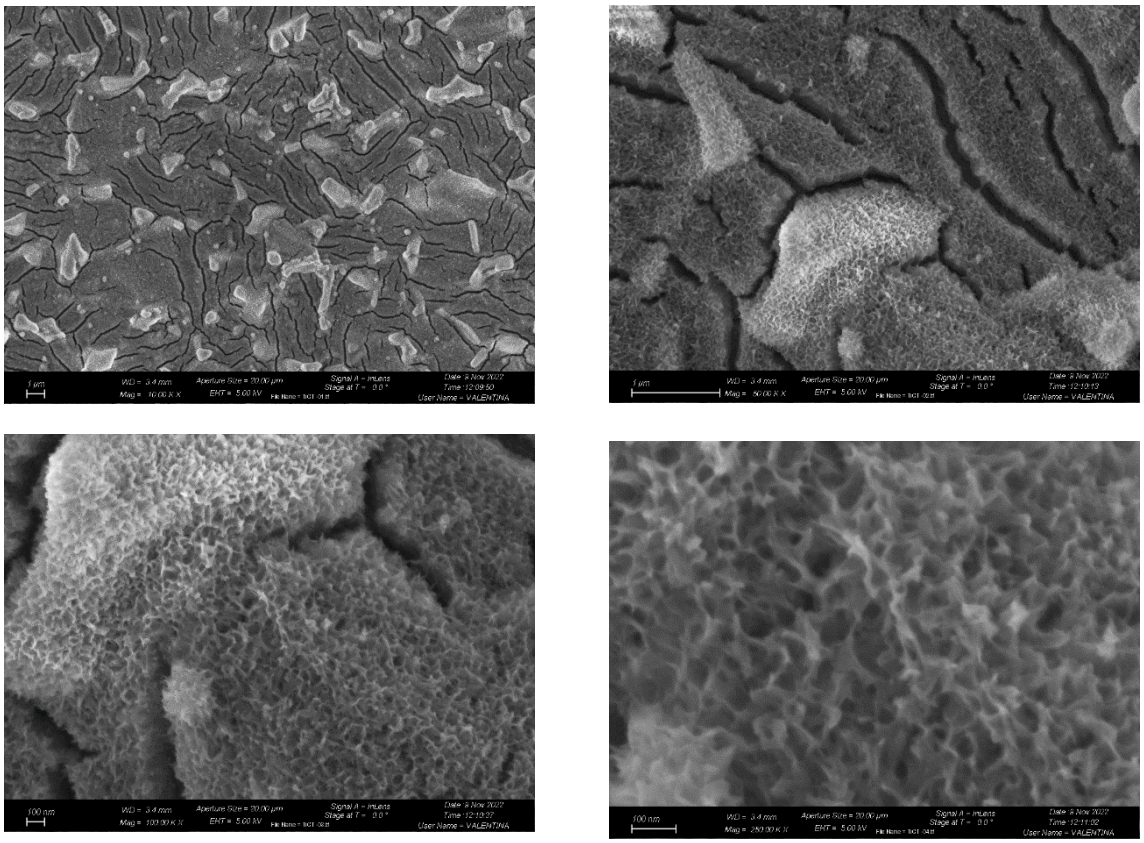

Figure 66: FESEM images CT

4.3.3 Fourier-Transform Infrared Spectroscopy

FTIR spectroscopy was firstly applied on FB_p and FB_p_deg.

FB_p_deg spectrum showed a peak in 1137 cm^{-1} that was not similarly present in FB_spectrum.

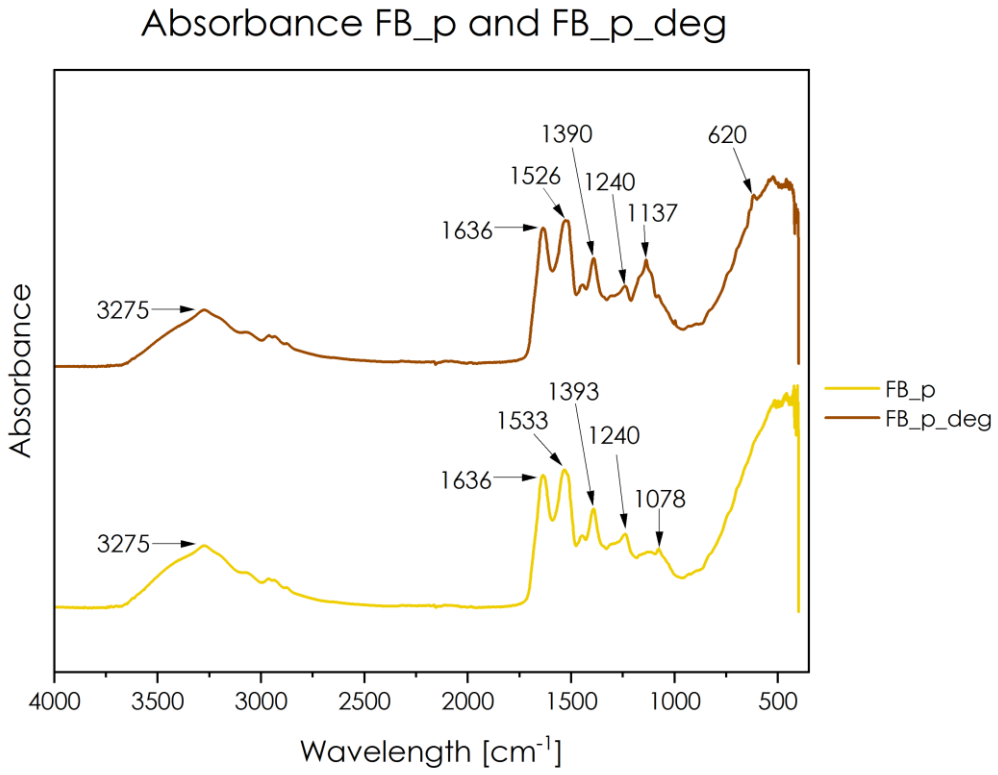

Figure 67: FTIR spectrum FB_p and FB_p_deg

Peaks assignment [cm^{-1}]

Table 8: Peaks assignment FB_p and FB_p_deg

Wavelength FB_p [cm^{-1}]	**Wavelength FB_p_deg [cm^{-1}]**	**Comments**
3275	3275	N-H and C-H stretching vibrations
1636	1636	Amide I band (~80% C-O stretching, ~10% C-N stretching, ~10% N-H bending vibrations), with predominance of β sheet
1533	1526	Amide II band (~60% N-H bending, ~40% C-N stretching vibrations) with predominance of β sheet
1393	1390	Amide III band
1240	1240	Amide III band (30% C-N stretching, 30% N-H bending, 10% C-O stretching, 10% O=C-N bending vibrations, rest other vibs), with predominance of random chain
/	1137	
1078	/	C-N stretching in aliphatic amides

FTIR Spectroscopy was applied both on SiO_2 and SiO_2_FB samples.

There were not evident differences between the two spectra.

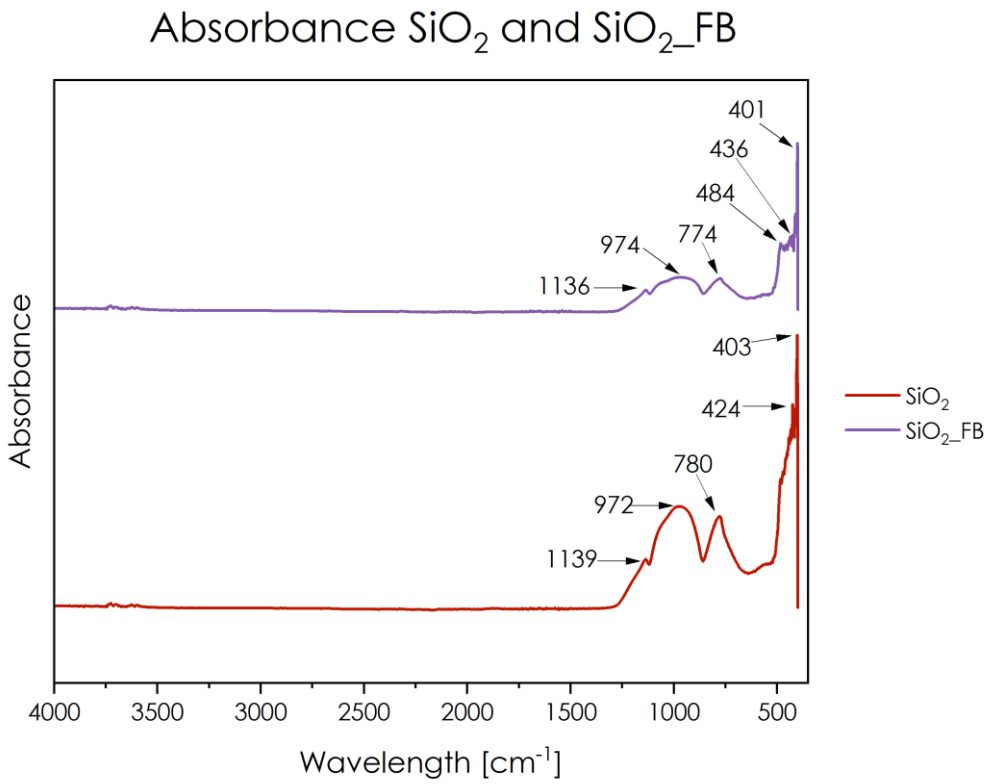

Figure 68: FTIR spectrum SiO_2 and SiO_2_FB

Peaks assignment [cm^{-1}]

Table 9: Peaks assignment SiO_2 and SiO_2_FB

Wavelength SiO_2 [cm^{-1}]	**Wavelength SiO_2_FB [cm^{-1}]**	**Comments**
1139	1136	Anti-symmetric stretching vibration of the bridging vibrations of Si-O-Si.
972	974	Stretching vibration Si-O^- of the non-bridging Oxygen atoms.
780	774	Bending vibration Si-O-Si
/	484	Bending (rocking) vibration Si-O-Si
424	436	Stretching vibration Si-Si
403	401	Bending vibration Si-O-Si

FTIR Spectroscopy was applied both on PP and PP_FB samples.

The presence of fibrinogen in PP_FB determined the formation of a peak (red ring) that was absent in PP. The same peak was not present on SiO_2_FB surface, probably because of a lower thinness or discontinuity of the adsorbed layer.

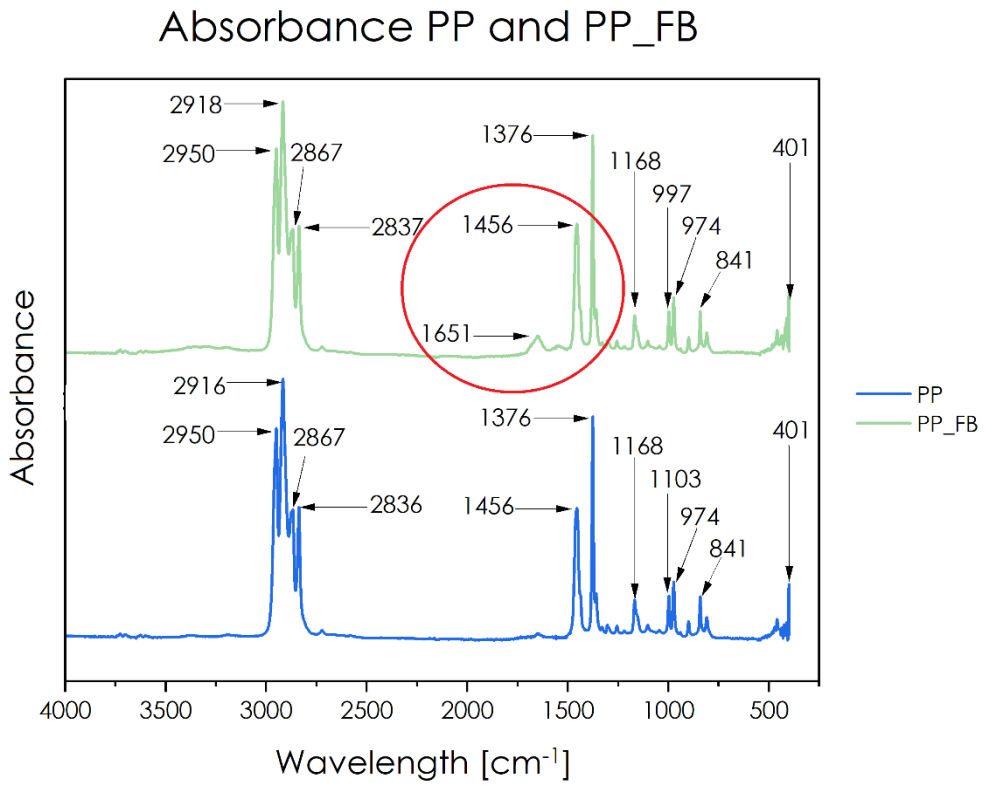

Figure 69: FTIR spectrum PP and PP_FB

Peaks assignment [cm^{-1}]

Table 10: Peaks assignment PP and PP_FB

Wavelength PP [cm^{-1}]	**Wavelength PP_FB [cm^{-1}]**	**Comments**
2950	2950	Anti-symmetric stretching vibration of CH3
2916	2918	Anti-symmetric stretching vibration of CH_2
2867	2867	Symmetric stretching vibration of CH_3
2836	2837	Symmetric stretching vibration of CH_2
/	1651	Amide I band, with predominance of α-helix structure
1456	1456	Anti-symmetric bending vibration of CH_3
1376	1376	Symmetric bending vibration of CH_3
1168	1168	Wagging vibration of C-H
1103	997	Anti-symmetric bending (rocking) vibration of CH_3
974	974	Asymmetric bending (rocking) vibration of CH_3
841	841	Bending (rocking) vibration of CH_2

In conclusion, the fact that fibrinogen was more easily visible on PP_FB rather than SiO_2_FB may be seen as a further confirmation of the fact that, in general, the adsorption is greater on hydrophobic surfaces compared to hydrophilic ones.

The analyses described above have not been successful, so they have not been applied to other materials; those described from this point onwards resulted to be more interesting and, for this reason, Ti64 and CT data are reported too.

4.3.4 Profilometry

Profilometry was applied both on SiO_2 and SiO_2_FB samples: the analysis allowed to obtain different types of roughness parameter, but Ra was mainly considered.

Table 11: Roughness parameters SiO_2

SiO_2		
Roughness Parameter	**Roughness (Average)**	**Standard Deviation**
Rp (µm)	0.052	0.0076
Rv (µm)	0.056	0.0071
Rz (µm)	0.11	0.014
Rc (µm)	0.037	0.0034
Rt (µm)	0.11	0.015
Ra (µm)	0.012	0.0015
Rq (µm)	0.015	0.0019
Rsk	-0.11	0.081
Rku	3.22	0.0265
Rms (%)	100	0
Rdc (µm)	0.024	0.0025

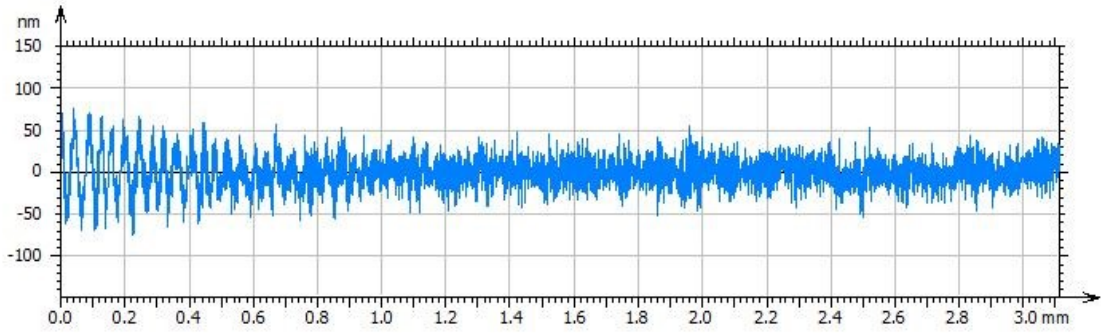

Figure 70: Roughness spectrum SiO_2

Table 12: Roughness parameters SiO_2_FB

SiO_2_FB		
Roughness Parameter	**Roughness (Average)**	**Standard Deviation**
Rp (µm)	0.076	0.033
Rv (µm)	0.069	0.026
Rz (µm)	0.15	0.059
Rc (µm)	0.038	0.0068
Rt (µm)	0.18	0.086
Ra (µm)	0.012	0.0018
Rq (µm)	0.015	0.0027
Rsk	-0.12	0.046
Rku	4.77	1.57
Rms (%)	100	0
Rdc (µm)	0.023	0.0028

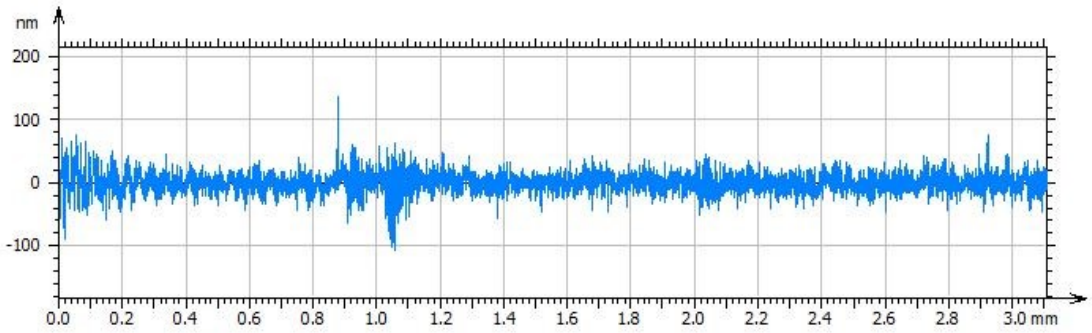

Figure 71: Roughness spectrum SiO_2_FB

Although the presence of fibrinogen in SiO_2_FB samples, the Ra value was similar to that of SiO_2 samples (~0.012 µm) as a demonstration of the fact that fibrinogen did not affect the surface roughness value.

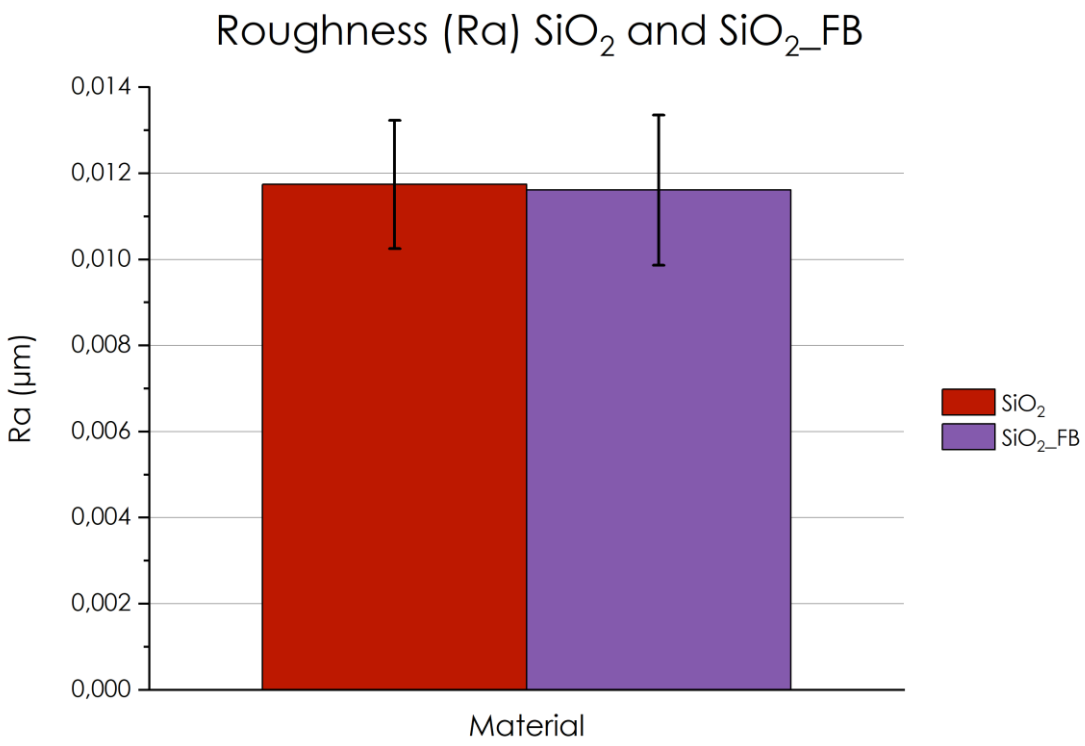

Figure 72: Roughness (Ra) SiO_2 and SiO_2_FB

The same comparison was made for PP and PP_FB samples evaluating all the roughness parameters, but mainly considering Ra as for the previous samples.

Table 13: Roughness parameters PP

PP		
Roughness Parameter	**Roughness (Average)**	**Standard Deviation**
Rp (µm)	0.47	0.25
Rv (µm)	0.19	0.029
Rz (µm)	0.66	0.25
Rc (µm)	0.20	0.15
Rt (µm)	0.88	0.45
Ra (µm)	0.083	0.014
Rq (µm)	0.11	0.027
Rsk	1.28	0.53
Rku	6.65	5.33
Rms (%)	69.71	52.46
Rdc (µm)	0.159	0.040

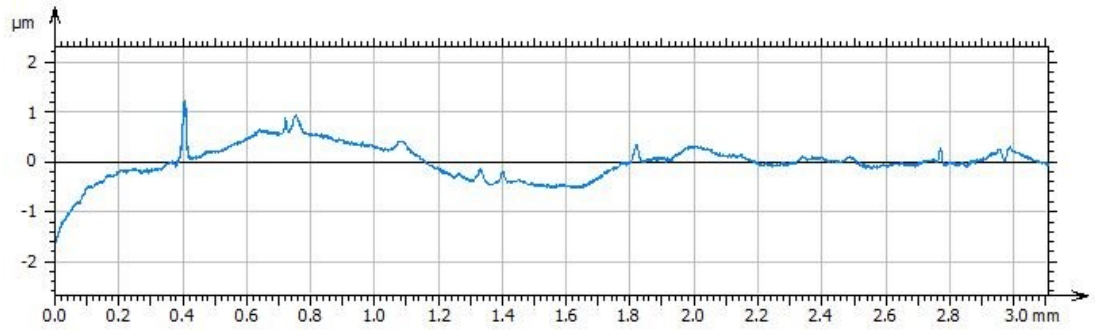

Figure 73: Roughness spectrum PP

Table 14: Roughness parameters PP_FB

PP_FB		
Roughness Parameter	**Roughness (Average)**	**Standard Deviation**
Rp (µm)	0.561	0.54
Rv (µm)	0.21	0.069
Rz (µm)	0.77	0.60
Rc (µm)	0.32	0.34
Rt (µm)	1.32	0.95
Ra (µm)	0.075	0.024
Rq (µm)	0.11	0.053
Rsk	1.32	1.74
Rku	11.49	12.41
Rms (%)	66.80	57.50
Rdc (µm)	0.16	0.032

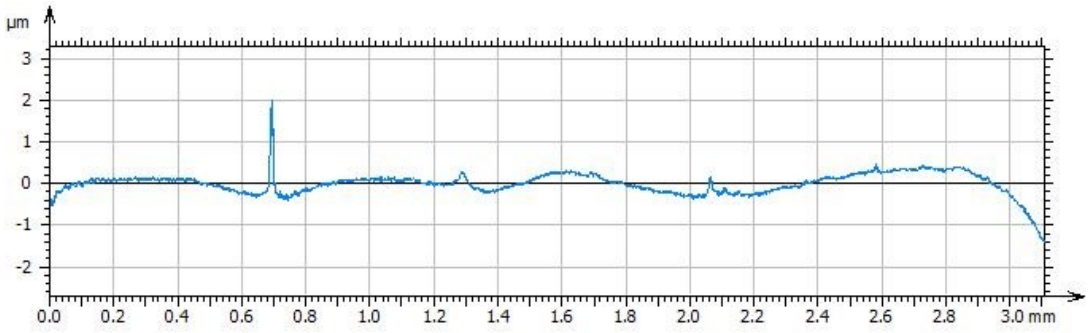

Figure 74: Roughness spectrum PP_FB

The presence of fibrinogen on the surface did not affect the roughness parameter which remains similar in the two situations (~0.08 µm).

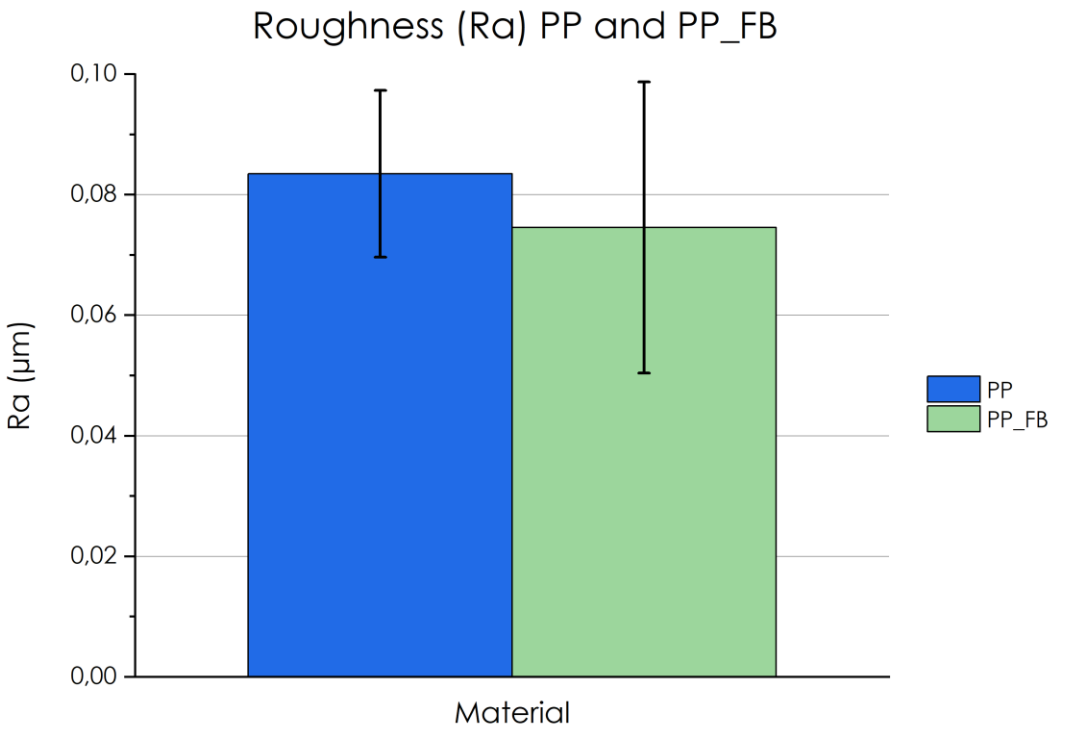

Figure 75: Roughness (Ra) PP and PP_FB

Finally, a comparison between all the samples could be made: it was possible to observe that PP and PP_FB were rougher than SiO_2 and SiO_2_FB.

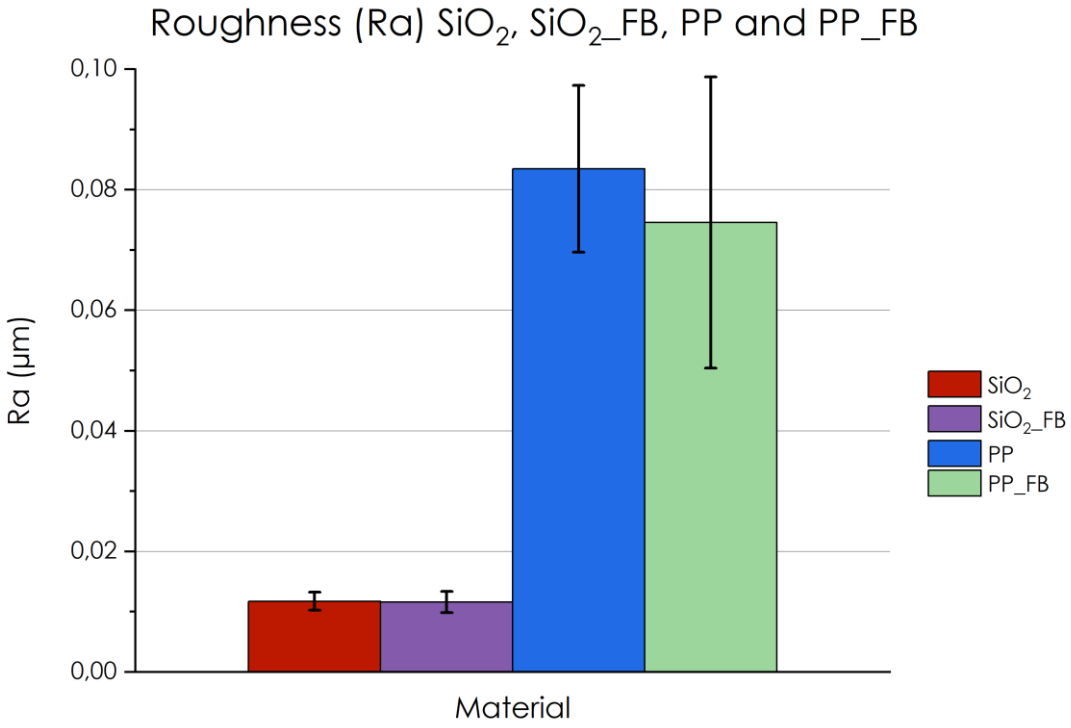

Figure 76: Roughness (Ra) SiO_2, SiO_2_FB, PP and PP_FB

4.3.5 Confocal microscopy

Confocal microscopy was applied both on SiO_2 and SiO_2_FB samples in order to obtain information about the topography and the surface roughness values. Different types of roughness parameter were evaluated, but Sa was mainly considered; in addition, microscopy images and 3D reconstruction of the surface samples are reported.

Optical images in SiO_2 case did not show surface features.

Table 15: Roughness parameters SiO_2

SiO_2		
Roughness Parameter	**Roughness (Average)**	**Standard Deviation**
Sq (µm)	0.011	0.00036
Ssk	-2.01	1.81
Sku	51.85	75.87
Sp (µm)	0.045	0.0032
Sv (µm)	0.25	0.28
Sz (µm)	0.30	0.28
Sa (µm)	0.0085	0.00021

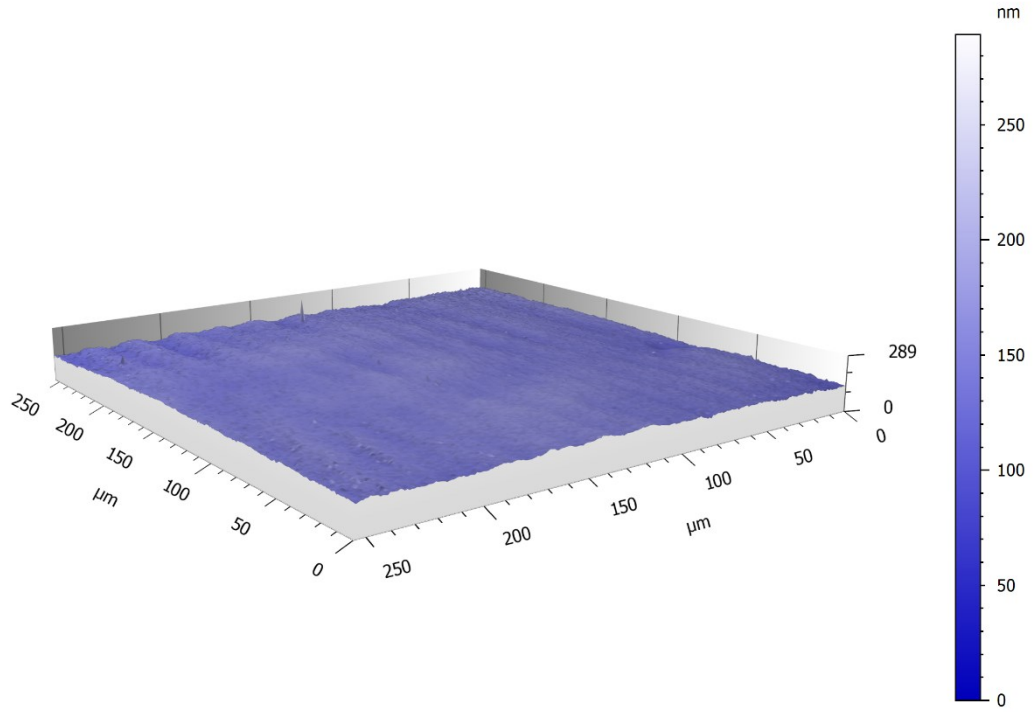

Figure 77: 3D surface reconstruction SiO_2

Two different areas were analyzed in SiO_2_FB samples: in the first area there were not important peculiarities in topography.

Table 16: Roughness parameters SiO_2_FB (1)

SiO_2_FB (1)		
Roughness Parameter	**Roughness (Average)**	**Standard Deviation**
Sq (µm)	0.018	0.0062
Ssk	24.68	23.75
Sku	1665.29	1633.20
Sp (µm)	1.31	1.02
Sv (µm)	0.11	0.012
Sz (µm)	1.42	1.03
Sa (µm)	0.0088	0.00058

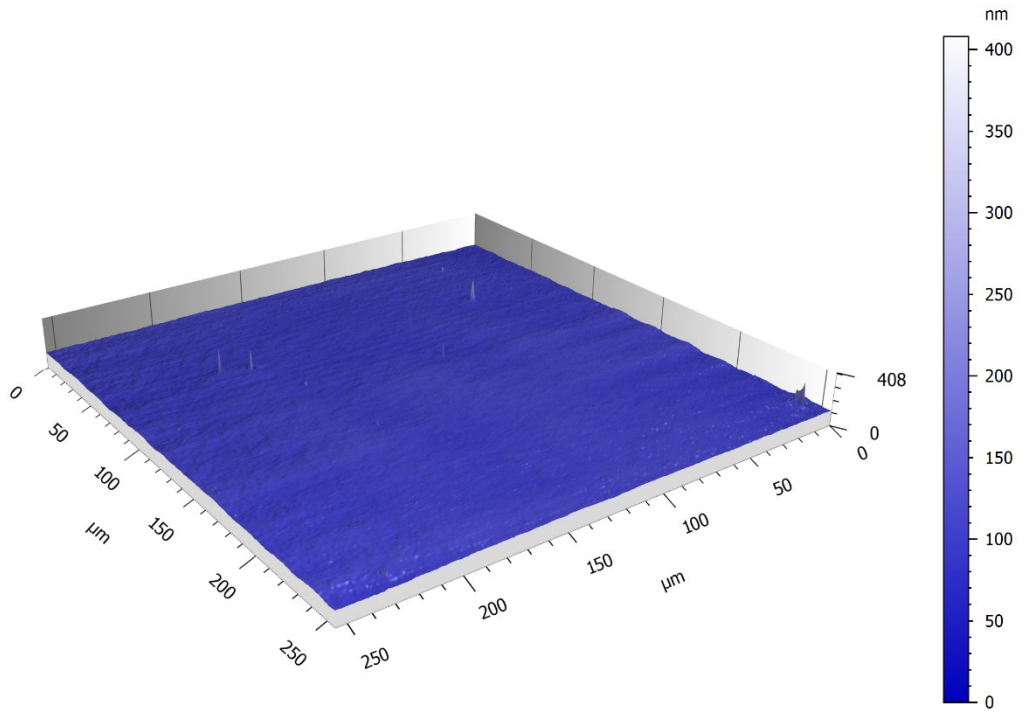

Figure 78: 3D surface reconstruction SiO_2_FB (1)

The second area showed an evident dendritic structure: the fibrinogen disposed on the surface according to branched structures, easily visible from both the confocal microscope images with a magnification of 50x and the 3D images.

Table 17: Roughness parameters SiO_2_FB (2)

SiO_2_FB (2)		
Roughness Parameter	**Roughness (Average)**	**Standard Deviation**
Sq (µm)	0.089	0.013
Ssk	18.60	3.33
Sku	479.55	192.60
Sp (µm)	3.52	1.05
Sv (µm)	0.17	0.020
Sz (µm)	3.69	1.03
Sa (µm)	0.023	0.0014

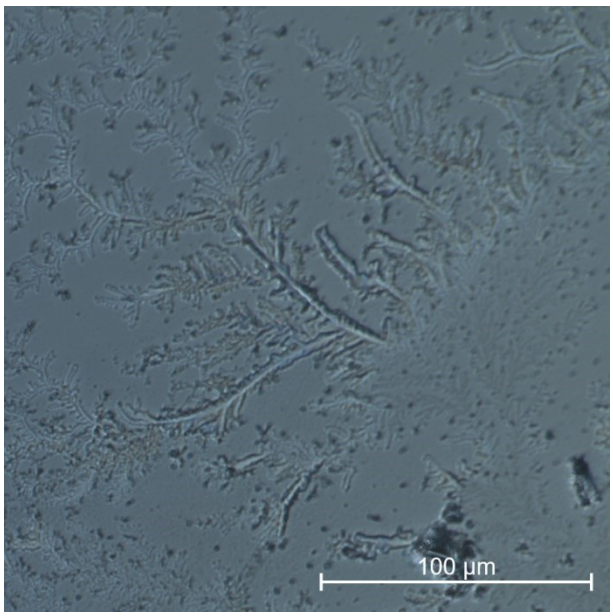

Figure 79: Confocal microscopy image SiO_2_FB (2)

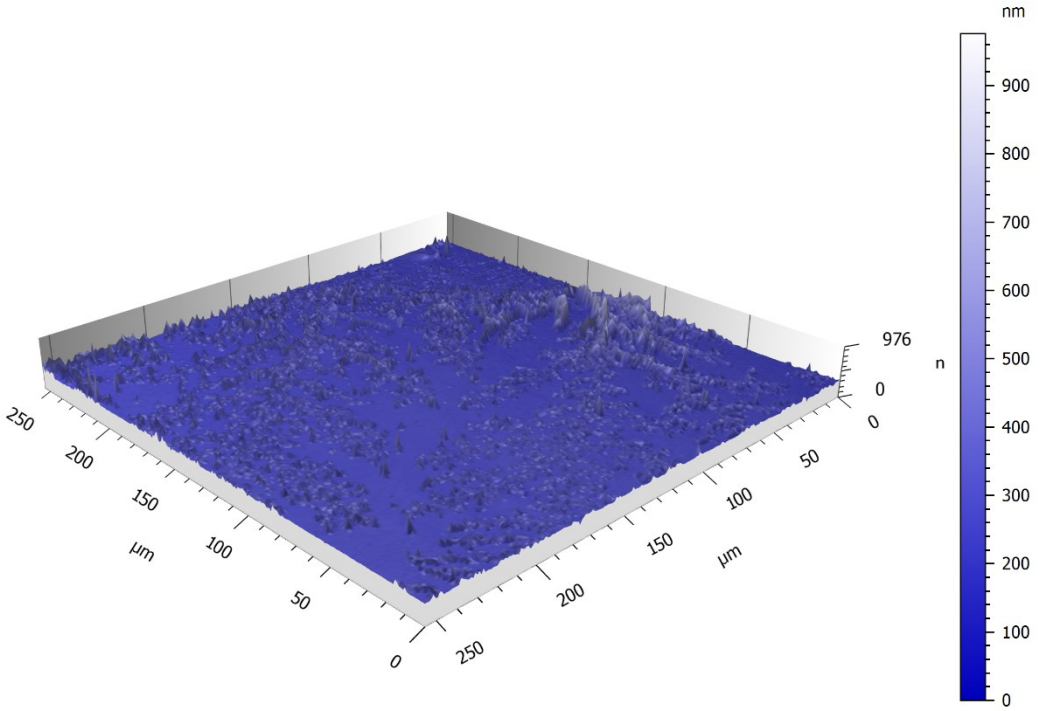

Figure 80: 3D surface reconstruction SiO_2_FB (2)

The comparison between SiO_2, SiO_2_FB (1) and SiO_2_FB (2) allowed to affirm that the presence of fibrinogen on the surface caused an increase in surface roughness. This aspect was further confirmed by the fact that the first area in the sample with fibrinogen, which had no differences in topography compared to that without the protein showed a roughness value similar to the original one in SiO_2 sample.

In the second area, in which the fibrinogen was clearly visible by the images, the roughness grows prominently.

Actually, the formation of dendritic structure could be connected to the shrinkage effect of the fibrinogen layer which was adsorbed on the silica's surface.

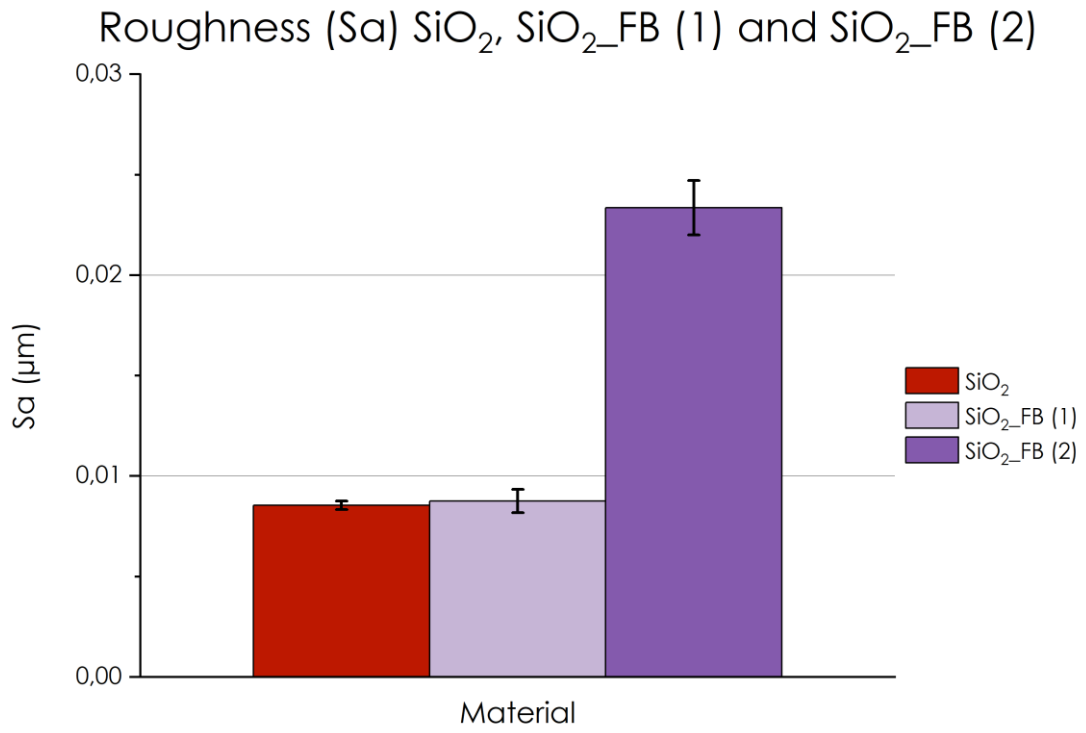

Figure 81: Roughness (Sa) SiO_2, SiO_2_FB (1) and SiO_2_FB (2)

In the same way, PP and PP_FB were observed under the confocal microscope: different types of roughness parameter were evaluated, but Sa was mainly considered; in addition, microscopy images and 3D reconstruction of the surface samples are reported.

Table 18: Roughness parameters PP

PP		
Roughness Parameter	**Roughness (Average)**	**Standard Deviation**
Sq (µm)	0.088	0.012
Ssk	4.49	2.15
Sku	54.21	42.84
Sp (µm)	1.75	0.71
Sv (µm)	0.57	0.11
Sz (µm)	2.32	0.68
Sa (µm)	0.053	0.0029

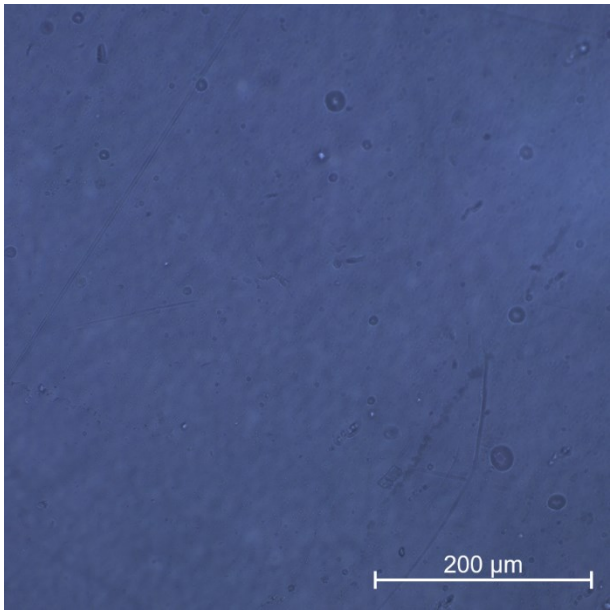

Figure 82: Confocal microscopy image PP

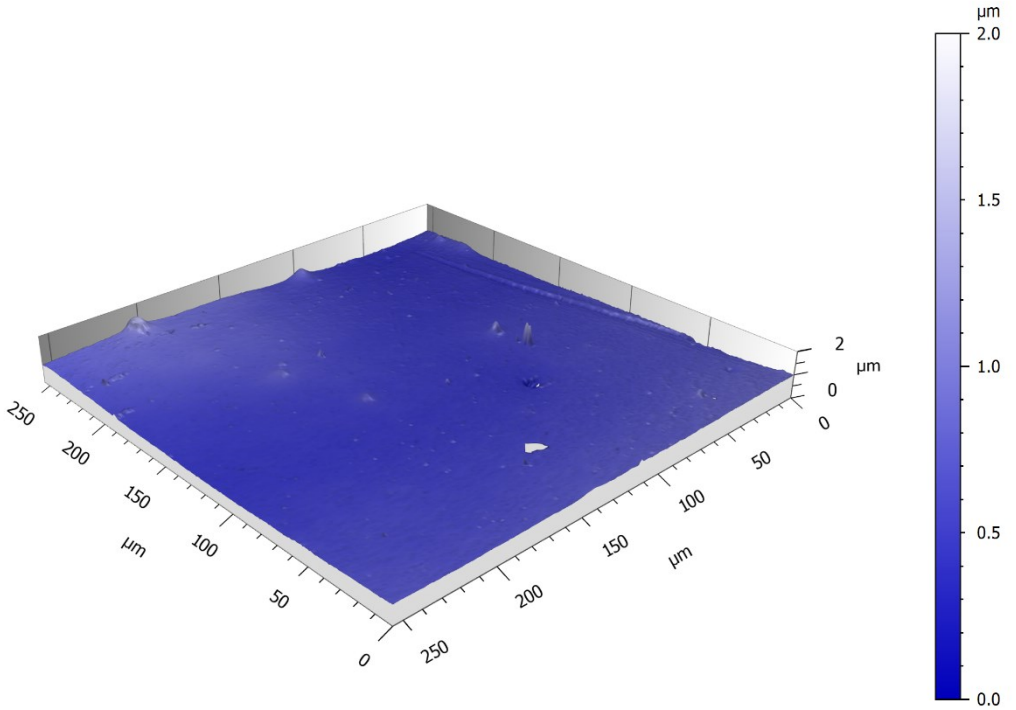

Figure 83: 3D surface reconstruction PP

Table 19: Roughness parameters PP_FB

PP_FB		
Roughness Parameter	**Roughness (Average)**	**Standard Deviation**
Sq (µm)	011	0.014
Ssk	7.38	4.34
Sku	124.19	117.99
Sp (µm)	2.67	0.70
Sv (µm)	0.57	0.21
Sz (µm)	3.24	0.76
Sa (µm)	0.058	0.0055

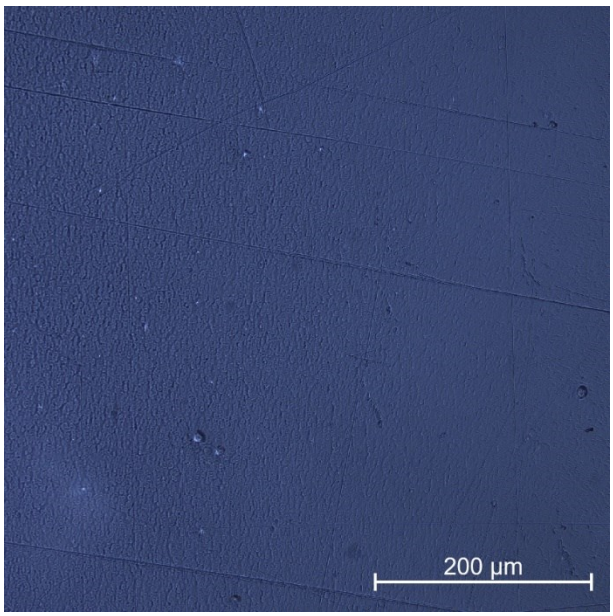

Figure 84: Confocal microscopy image PP_FB

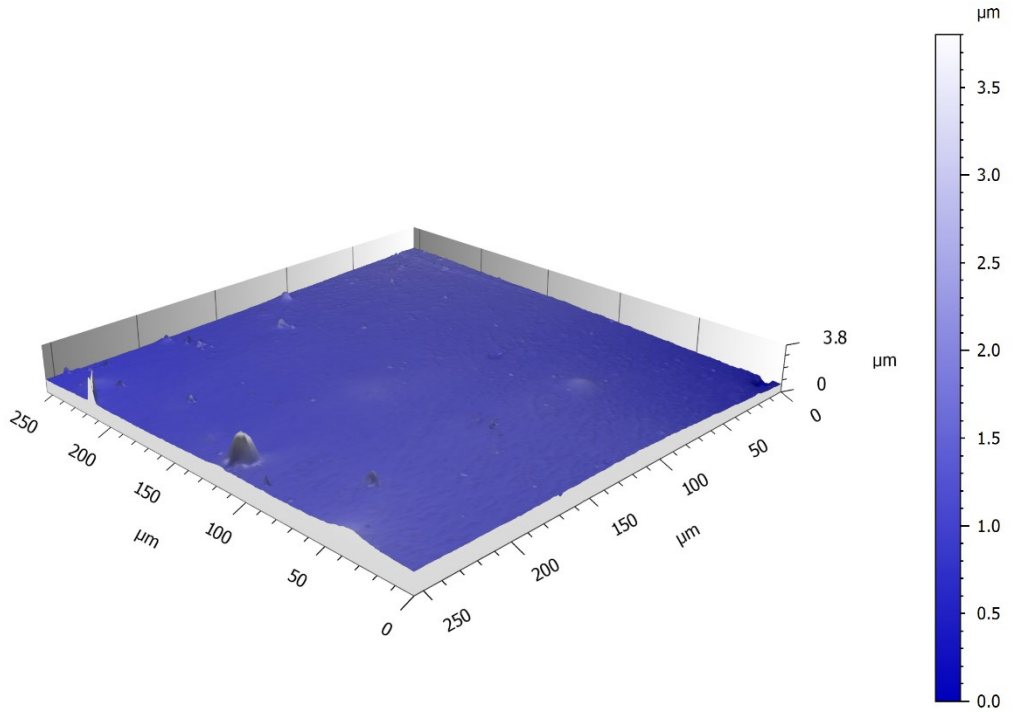

Figure 85: 3D surface reconstruction PP_FB

The presence of fibrinogen on the surface did not affect the surface roughness values which remained about 0.05÷0.06 µm.

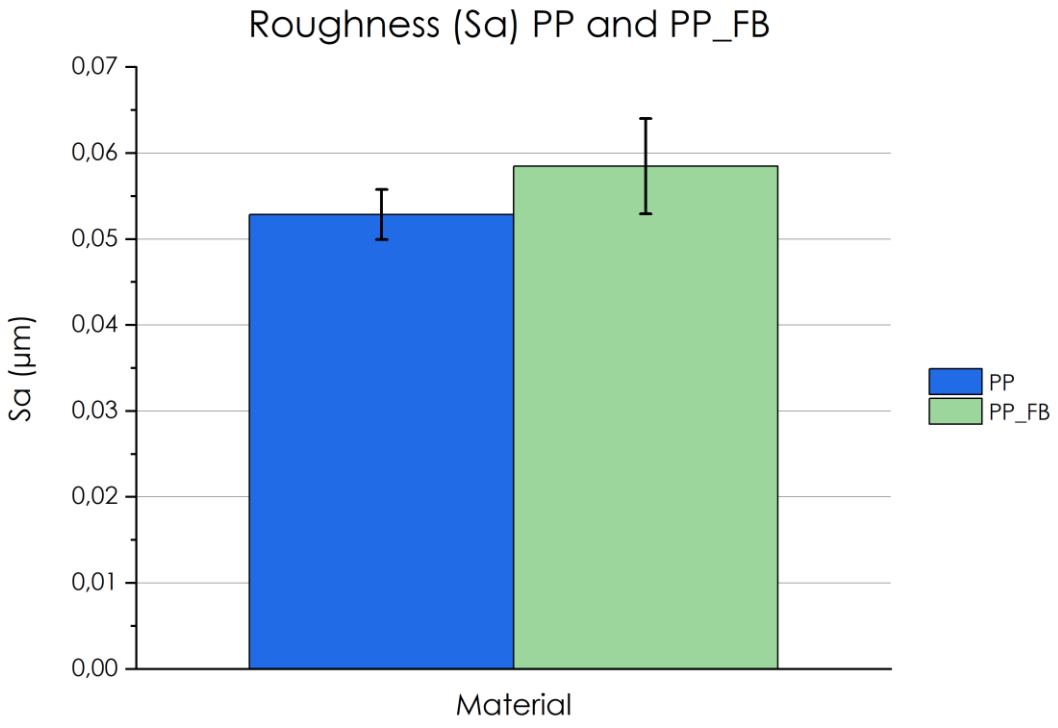

Figure 86: Roughness (Sa) PP and PP_FB

Finally, an overall comparison between SiO_2, SiO_2_FB, PP and PP_FB was drawn: the graph further confirmed a greater roughness value in case of PP and PP_FB, compared to SiO_2 and SiO_2_FB.

In conclusion it is possible to consider SiO_2 surface as a model for hydrophilic and smooth materials, while PP as a model for hydrophobic and nanostructured ones.

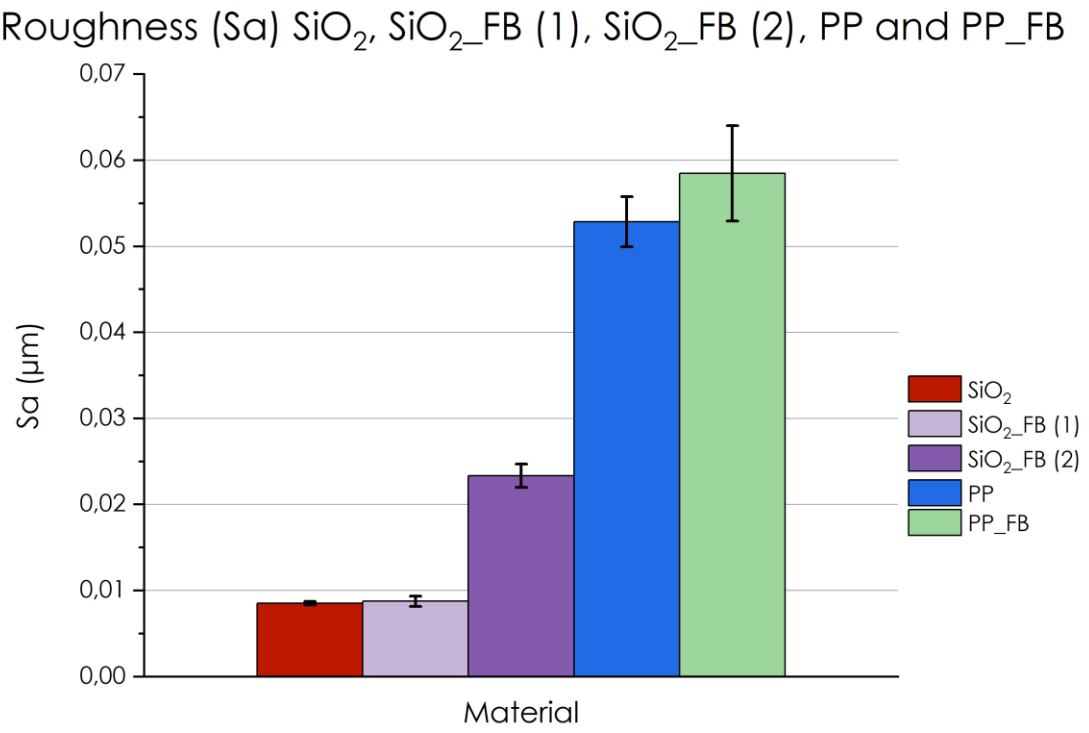

Figure 87: Roughness (Sa) SiO_2, SiO_2_FB (1), SiO_2_FB (2), PP and PP_FB

Confocal microscopy data related to Ti64 and CT are reported too [2].

Table 20: Roughness parameters Ti64

Ti64		
Roughness Parameter	**Roughness (Average)**	**Standard Deviation**
Sq (µm)	0.03	0.00
Ssk	0.71	1.07
Sku	32.85	37.95
Sp (µm)	0.95	0.30
Sv (µm)	0.19	0.05
Sz (µm)	1.14	0.34
Sa (µm)	0.02	0.00

[2] These measurements were not obtained during this thesis but they are part of Camilla Reggio's PhD thesis

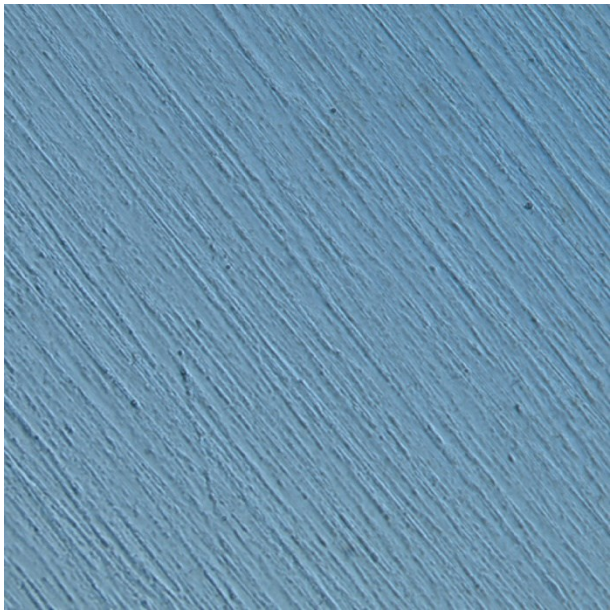

Figure 88: Confocal microscopy image Ti64

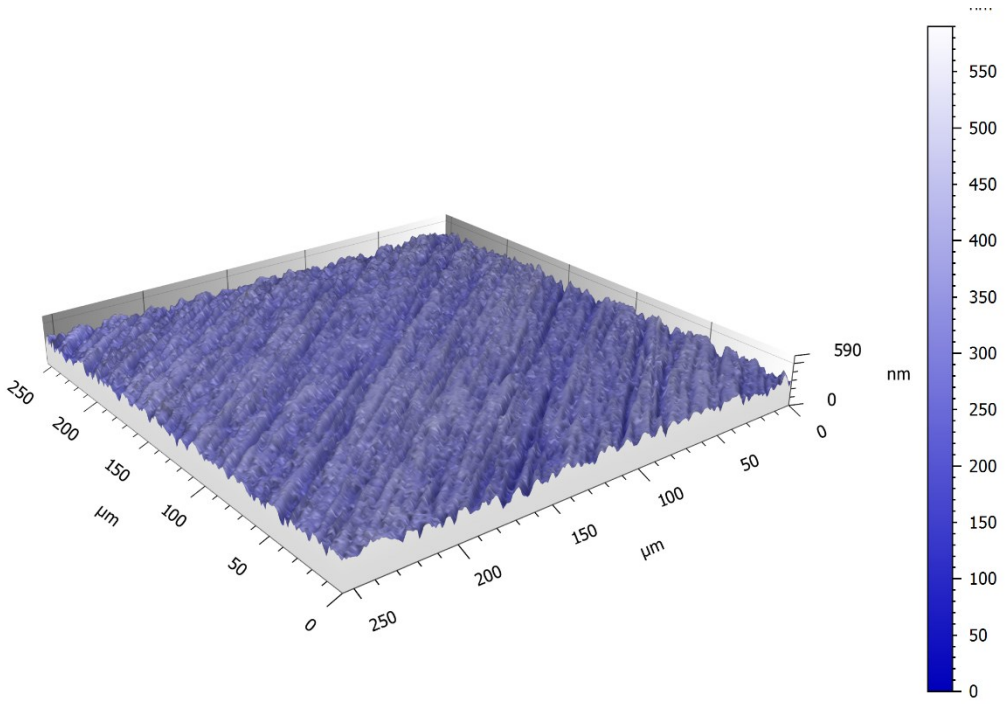

Figure 89: 3D surface reconstruction Ti64

Table 21: Roughness parameters Ti64_FB

Ti64_FB		
Roughness Parameter	**Roughness (Average)**	**Standard Deviation**
Sq (µm)	0.02	0.01
Ssk	5.67	9.47
Sku	271.83	452.53
Sp (µm)	0.94	1.04
Sv (µm)	0.19	0.09
Sz (µm)	1.13	1.12
Sa (µm)	0.02	0.00

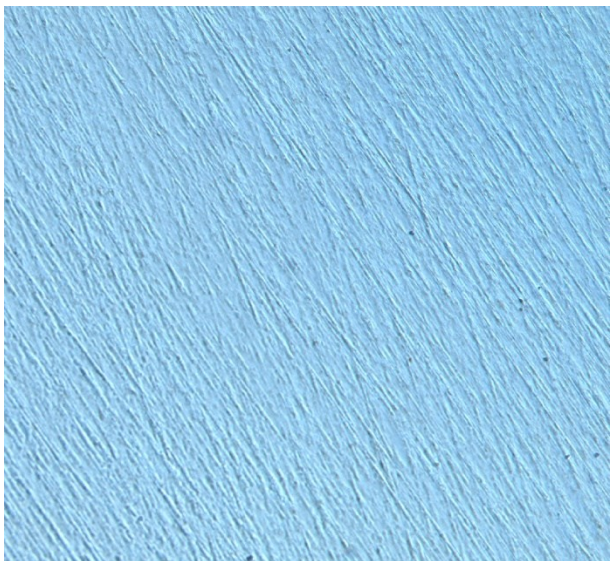

Figure 90: Confocal microscopy image Ti64_FB

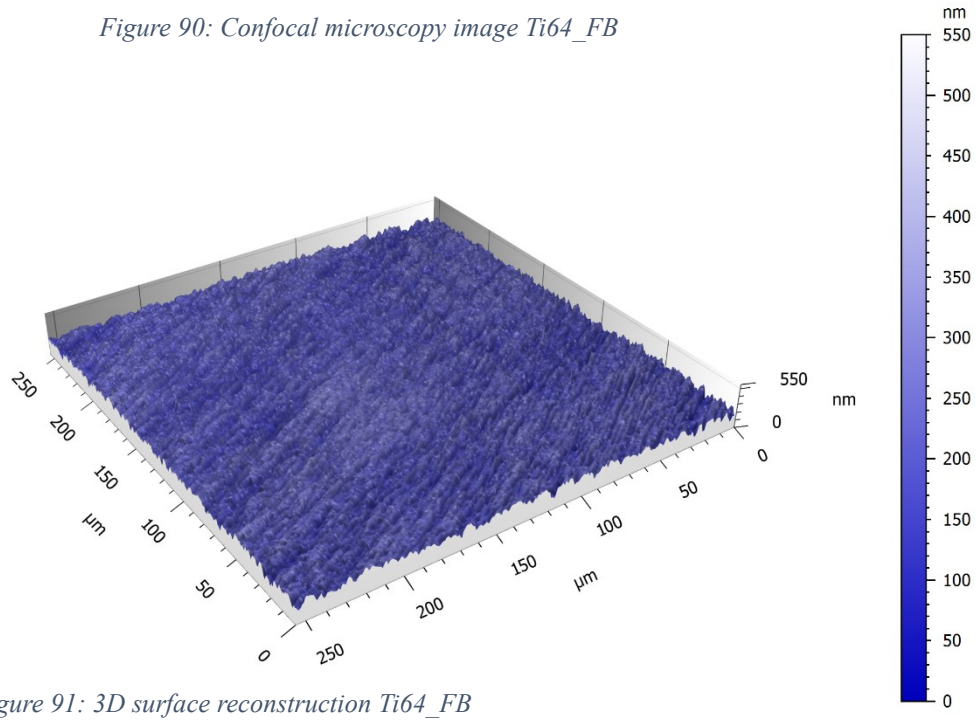

Figure 91: 3D surface reconstruction Ti64_FB

Table 22: Roughness parameters CT

CT		
Roughness Parameter	**Roughness (Average)**	**Standard Deviation**
Sq (µm)	0.20	0.01
Ssk	-0.63	0.23
Sku	8.77	7.48
Sp (µm)	2.12	1.78
Sv (µm)	1.59	0.78
Sz (µm)	3.71	2.55
Sa (µm)	0.16	0.01

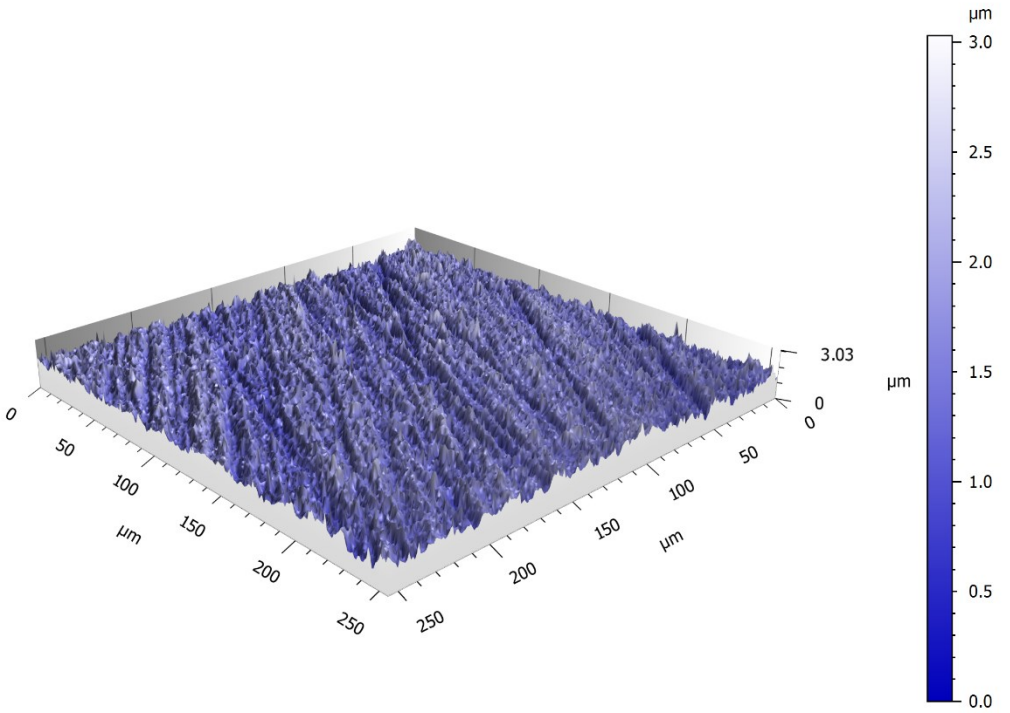

Figure 92: 3D surface reconstruction CT

Table 23: Roughness parameters CT_FB

CT_FB		
Roughness Parameter	**Roughness (Average)**	**Standard Deviation**
Sq (µm)	0.18	0.02
Ssk	-1.51	0.80
Sku	12.80	9.25
Sp (µm)	1.47	0.95
Sv (µm)	2.20	0.78
Sz (µm)	3.67	1.48
Sa (µm)	0.13	0.02

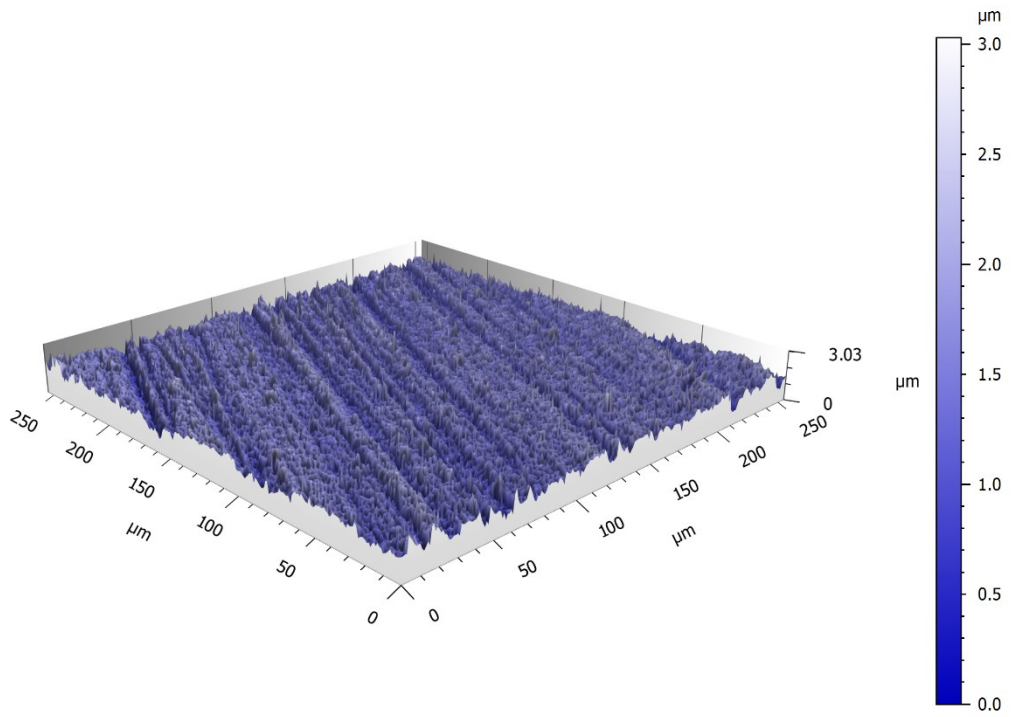

Figure 93: 3D surface reconstruction CT_FB

4.3.6 Contact angle

Contact angle was measured on SiO_2, SiO_2_w, SiO_2_FB, SiO_2_FB_w, PP, PP_w PP_FB and PP_FB_w samples, using ultrapure water, FBS and fibrinogen drops.

SiO_2 samples showed a strongly hydrophilic behavior because of the exposure of OH groups, slightly more evident in case of a fibrinogen drop, while SiO_2_FB a hydrophobic one, more obvious in case of a fibrinogen drop. Fibrinogen adsorption led to a variation in the surface wettability, not so much noticeable in case of wet samples: this is probably due to the fact that, during the analysis, the fibrinogen drop interacted with the water on the surface rather than with the surface itself. Results obtained for wet samples are still reported, although they do not have the same validity as the dry ones.

The contact angles for FB_p (fibrinogen powder, Table 1) are specified too: it is interesting to notice that the presence of fibrinogen on dry surfaces caused a decrease in the wettability, showing an angle value more similar to that of FB_p samples themselves.

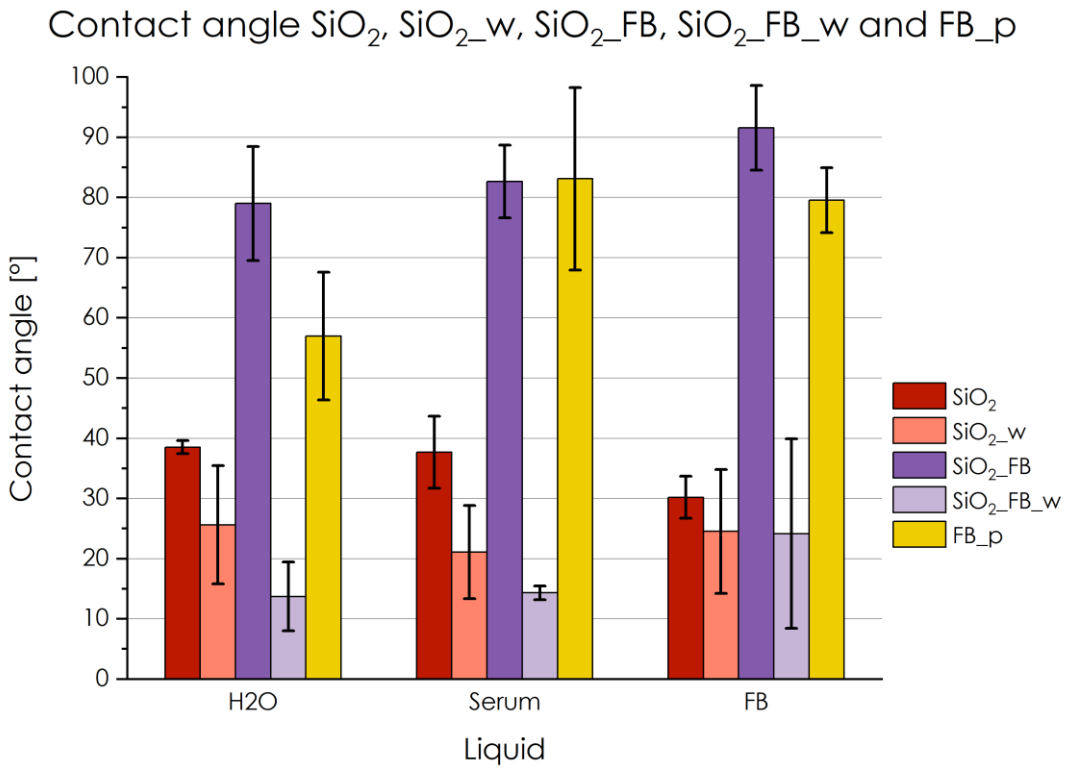

Figure 94: Contact angle SiO_2, SiO_2_w, SiO_2_FB, SiO_2_FB_w and FB_p

As regards PP samples, they had a hydrophobic behavior for all the liquids used; in this

case, PP_FB samples maintained these features, especially for water and FBS drops, while in case of fibrinogen drop, the contact angle value decreased.

PP _w samples maintained their hydrophobicity in case of FB drop, while they turned out to be slightly and strongly hydrophilic for serum and H_2O drops respectively.

As previously, results obtained for wet samples with fibrinogen are reported, although they do not have the same validity as the dry ones, in that they present a really low contact angle value, probably due to the water on the surface.

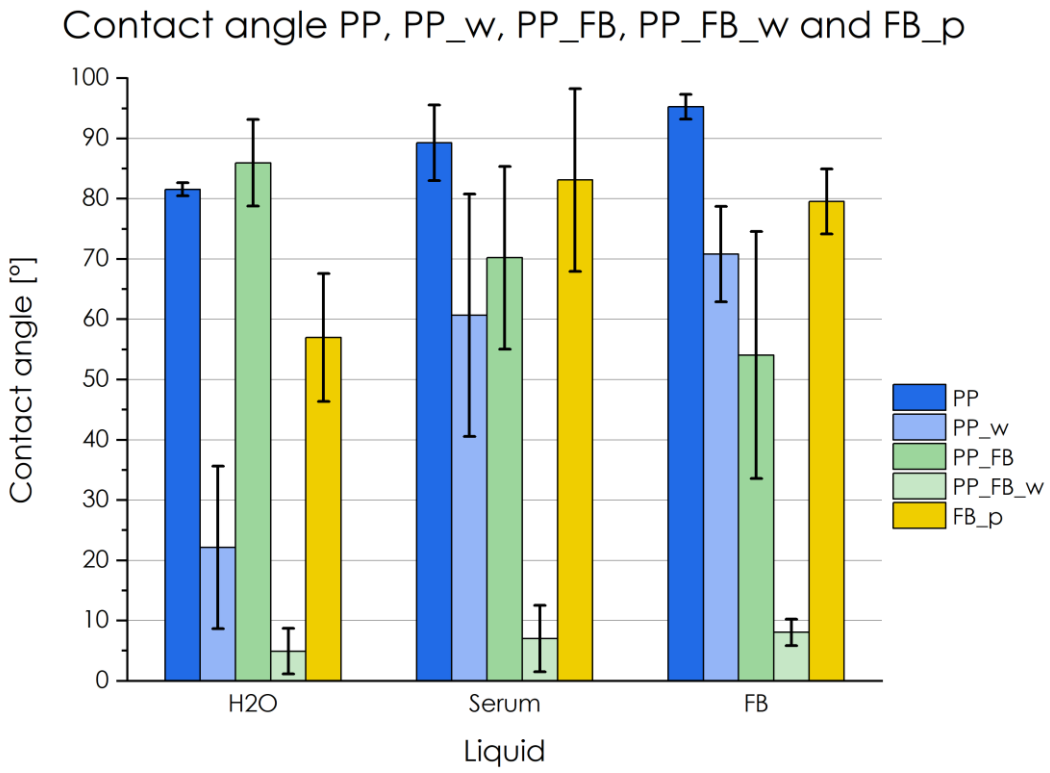

Figure 95: Contact angle PP, PP_w, PP_FB, PP_FB_w and FB_p

The contact angle measurement on Ti64 and CT with and without fibrinogen using drops of fibrinogen itself revealed a hydrophobic behavior in all cases. Considering the other liquids[3], CT behavior was different in all the cases since with the water drop it showed a hydrophilic behavior with a contact angle < 40°, while with the FBS drop the contact angle value rose to 70°.

[3] These measurements were not obtained during this thesis but they are part of Camilla Reggio's PhD thesis

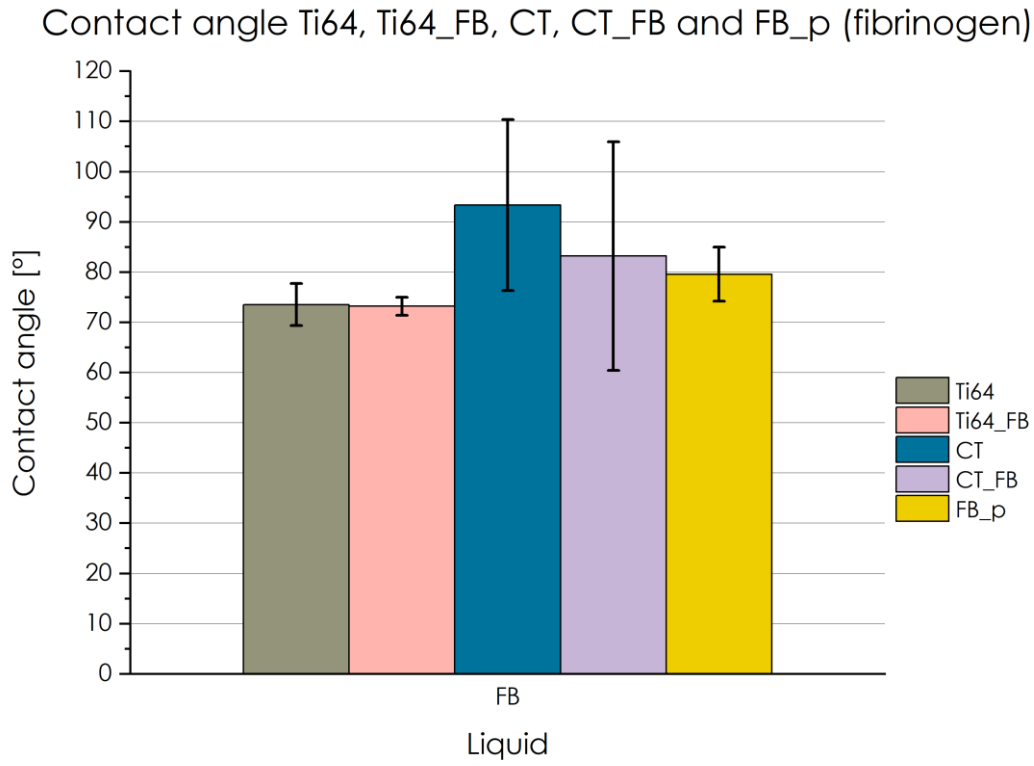

Figure 96: Contact angle Ti64, Ti64_FB, CT, CT_FB and FB_p (drop of fibrinogen)

The evaluation of contact angle using the drop of blood showed a hydrophilic behavior in case of SiO_2 samples and a hydrophobic one in case of PP samples. As previously, the presence of fibrinogen on the surface led to an increase in the angle value compared to the original value.

Ti64 and CT, with and without fibrinogen, had a hydrophobic behavior instead.

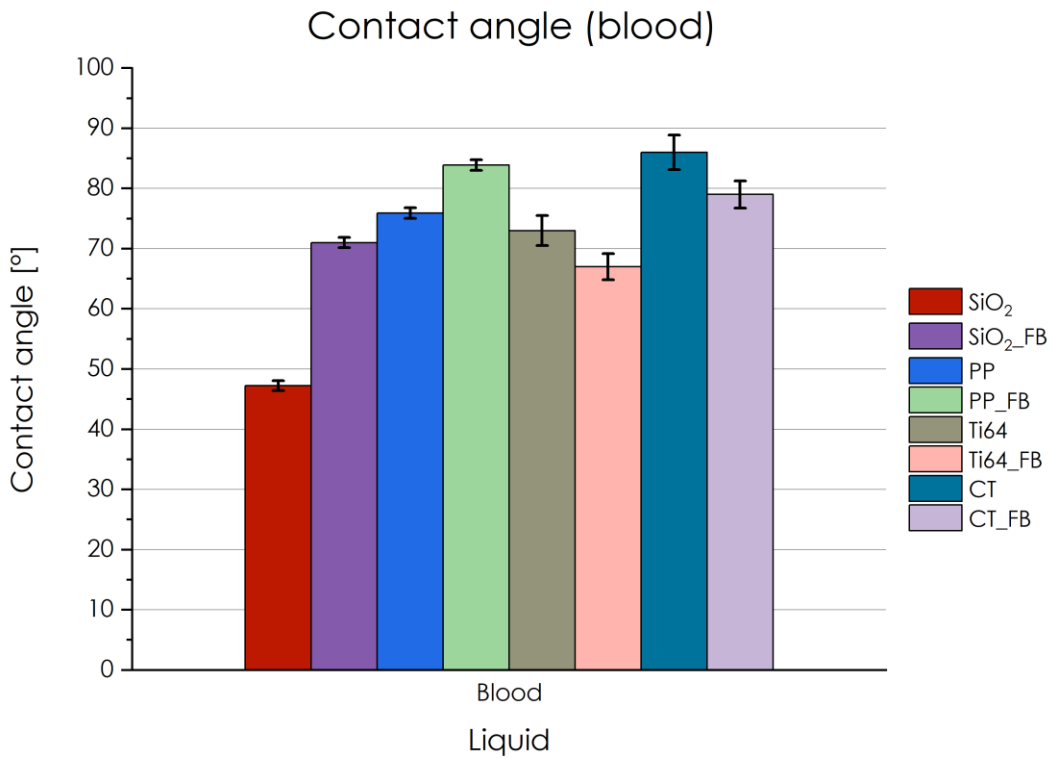

Figure 97: Contact angle SiO_2, SiO_2 _FB, PP, PP_FB, Ti64, Ti64_FB, CT and CT_FB (drop of blood)

An overall evaluation of the contact angle with ultrapure water, FBS and FB drops was conducted[4] on all the samples when dry.

While, in case of water drop, SiO_2 and CT had a hydrophilic behavior because of the presence of OH groups on their surfaces, PP and Ti64 had a hydrophobic one in that they did not expose polar functional groups. The same behavior occurred with the FBS and FB drop, except for CT for which wettability was not so high and close to PP and Ti64.

After fibrinogen adsorption, the contact angle values obtained with the water drop were similarly high for most of the surfaces. The behavior was different with the FBS drop for Ti64_FB and CT_FB which resulted hydrophilic, while SiO_2_FB and PP_FB resulted hydrophobic. Finally, as regards fibrinogen drop, SiO_2_FB, Ti64_FB and CT_FB had a

[4] Measurements about Ti64 and CT with and without fibrinogen, using water and FBS drops were not obtained during this thesis but they are part of Camilla Reggio's PhD thesis

hydrophobic behavior, while PP_FB contact angle was about ~55°, with an elevated standard deviation of ~20°.

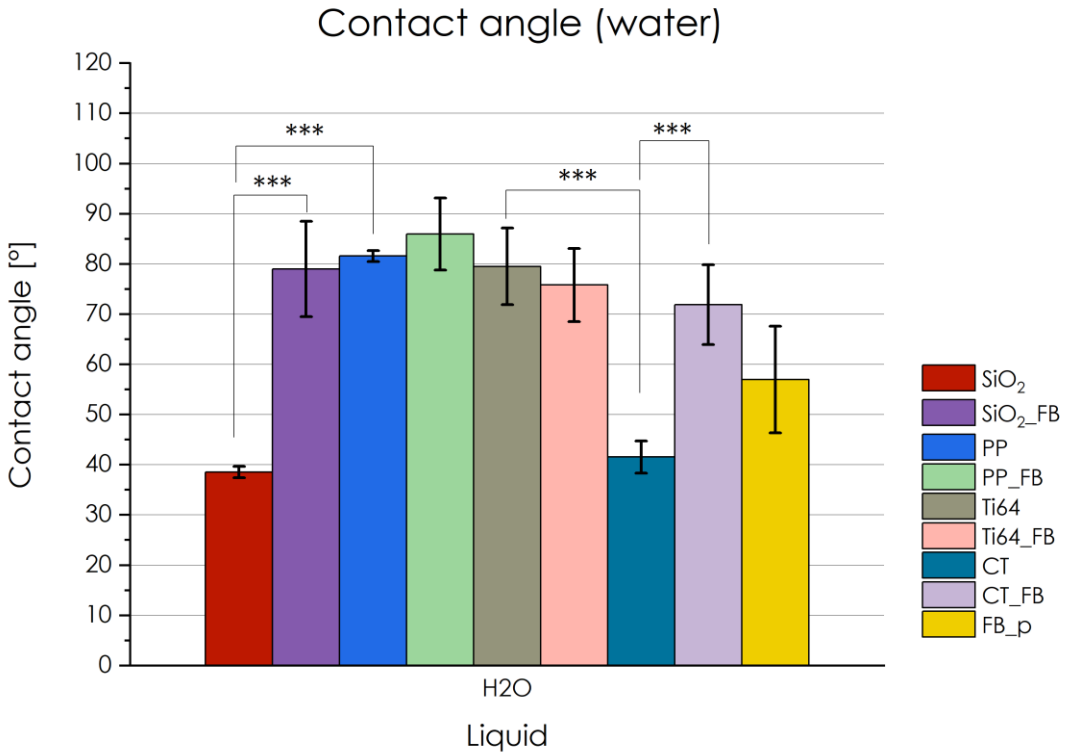

Figure 98: Contact angle SiO_2, SiO_2 _FB, PP, PP_FB, Ti64, Ti64_FB, CT, CT_FB and FB_p (drop of water)

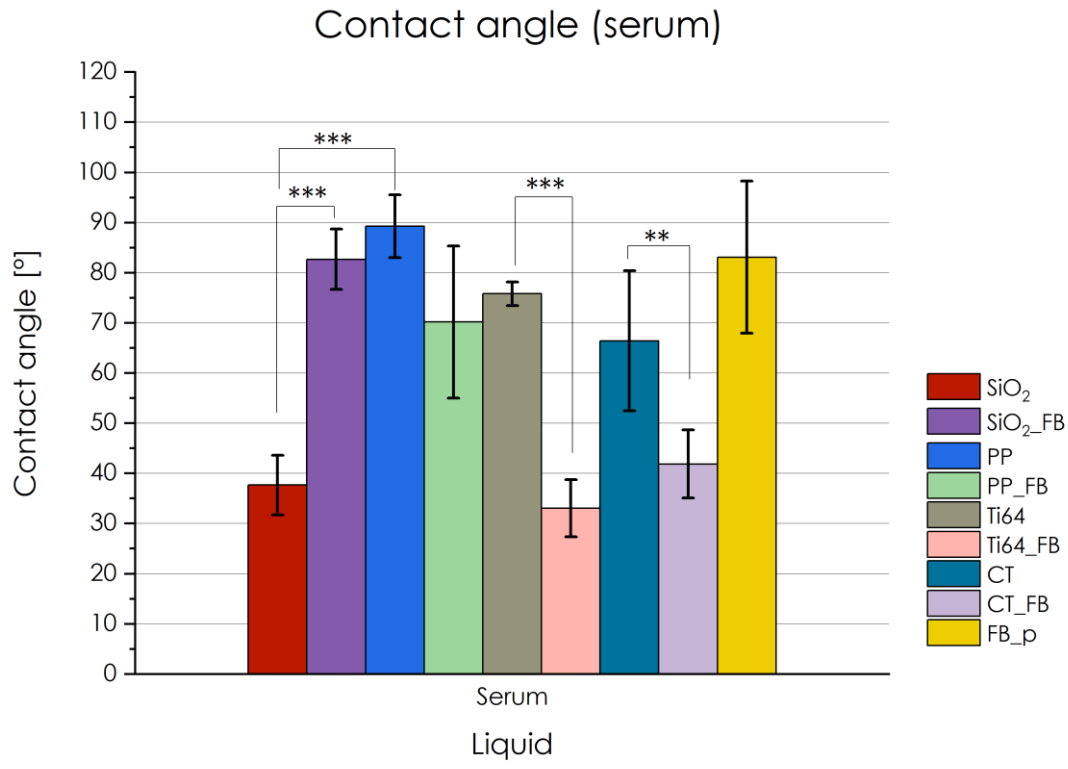

Figure 99: Contact angle SiO_2, SiO_2_FB, PP, PP_FB, Ti64, Ti64_FB, CT, CT_FB and FB_p (drop of serum)

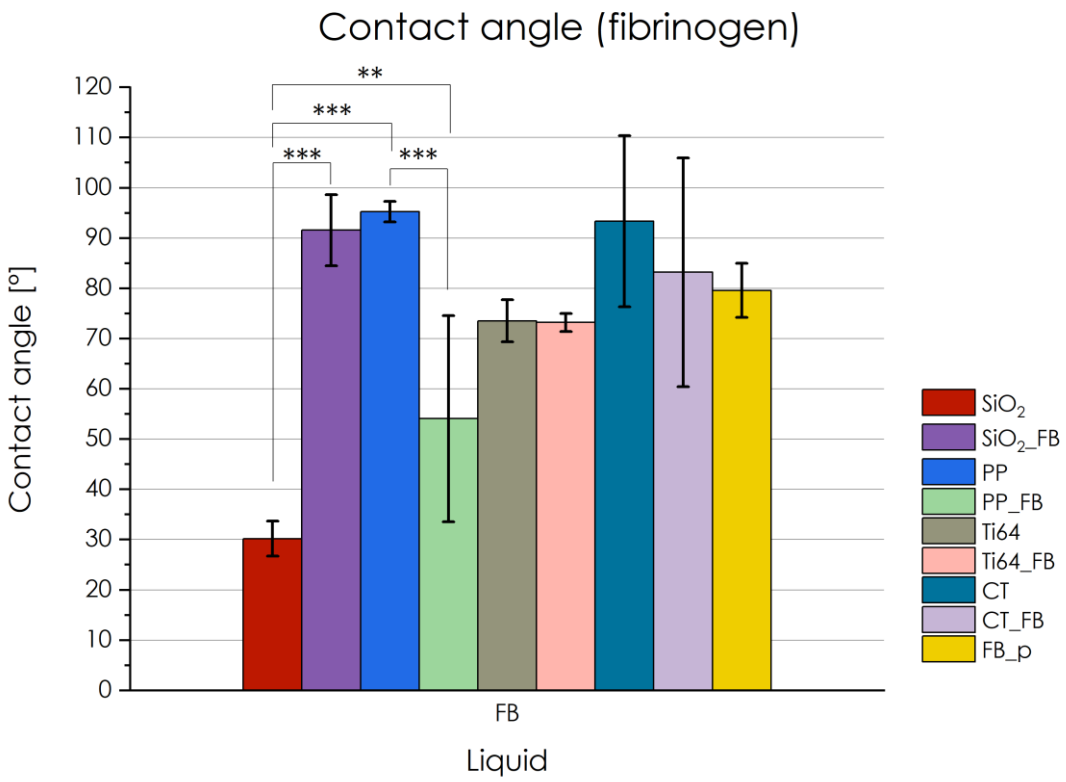

Figure 100: Contact angle SiO_2, SiO_2_FB, PP, PP_FB, Ti64, Ti64_FB, CT, CT_FB and FB_p (drop of fibrinogen)

Considering that the fibrinogen structure can be described as a cylinder with terminal flexible, hydrophilic and positively charged αC domains and a rigid structure in the middle characterized by a hydrophobic behavior and negatively charged D-E-D domains, wettability is an important parameter. In fact, it has been hypothesized that a hydrophobic surface allows the formation of a network of fibrinogen thanks to an adsorption process which occurs with central domains while αC ones interact with each other at the extremities. Hydrophilic surfaces, on the contrary, are characterized by the formation of single clusters of fibrinogen dispersed on the surfaces themselves in that αC domains, interacting with the OH groups of the surface, are not available to form a network.

Observations about the orientation must be reported too: in this case, nanostructured surfaces with high negative charge density allow a larger adsorption of fibrinogen, with an end-on configuration.

The measured contact angles cannot be used, at this stage, to confirm or refute these hypotheses. The roughness can affect contact angle values which are not significative only of the surface chemical composition.

A first observation is that silica could not be used as a model material for protein adsorption on CT even if SiO_2 and CT had a similar wettability by water. Wettability of CT by protein solutions (single protein-FB or a protein mixture-FBS) was much more similar to Ti64 and PP than to silica. This could be related to a larger and more uniform adsorption on a surface like CT with a high density of polar groups.

After FB adsorption, all the surfaces had a similar low wettability by water and FB. Metal substrates with adsorbed FB (Ti64_FB and CT_FB) were highly wettable by a protein mixture (FBS): this was not observed in the other cases.

4.3.7 Zeta potential

Zeta potential was firstly measured on fibrinogen: it showed a light predominance of positive functionalities, as it can be deduced by the IEP higher than 4 (IEP ~5.6) and, in solution, it was oriented by exposing the hydrophilic groups, as it can be deduced by the low slope of the curve around the IEP.

The presence of two plateau in the basic and acidic ranges is typical of a compound (like a protein) with both acidic (carboxylic) and basic (amines) functional groups.

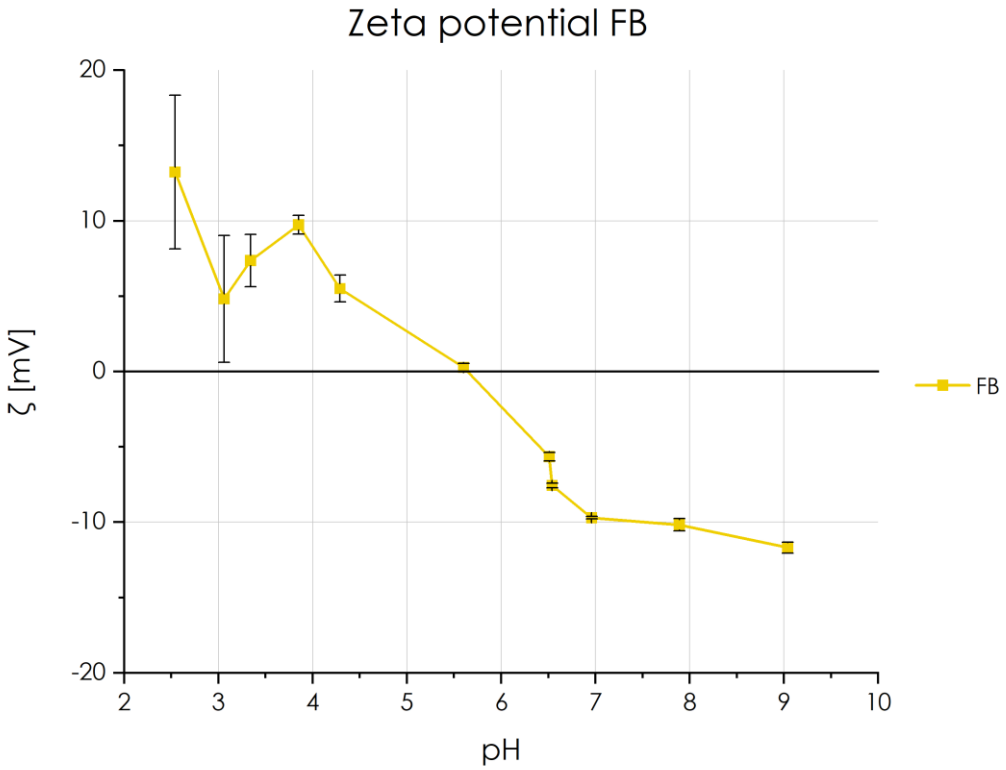

Figure 101: Zeta potential FB

Silica curve was typical of hydrophilic surfaces with acidic functional groups: IEP was 2÷3 as shown in the graph; the presence of fibrinogen on its surface, led to a great increase in IEP which becomes about 4.9 and 5.1 for dry and wet samples respectively. This difference was probably due to drying which might have shrinkage effects with partial exposure of silica substrate and subsequent IEP decrease and plateau in basic titration range.

The titration curve of SiO_2_FB had a high slope around the IEP, that is typical of hydrophobic surfaces. The zeta potential measurements are not affected by roughness and they can allow to make some hypothesis about the conformation of the adsorbed molecules. The presence of the two plateaus agreed with the basic (amino) and acidic (carboxyilic) groups of a protein.

The titration curve of SiO_2 had not an evident plateau. This is typical of a surface with OH groups with different acidic reactivity which are not completely deprotonated at a specific pH. SiO_2 is different from CT even if the IEP is similar. On CT (figure 106) a plateau is evident at pH around 5.5: in this case, all OH groups act as a strong acid and are completely deprotonated at a specific and low pH value.

Zeta potential value was extremely negative for SiO_2, mainly characterized by hydroxyl (OH) groups, while it was less negative for samples with fibrinogen, in particular for dry ones, that reached a plateau of only -30 mV for a pH value of ~6.5; on the other hand, a plateau of -60 mV was reached by SiO_2_FB_w samples for a pH ~7.2.

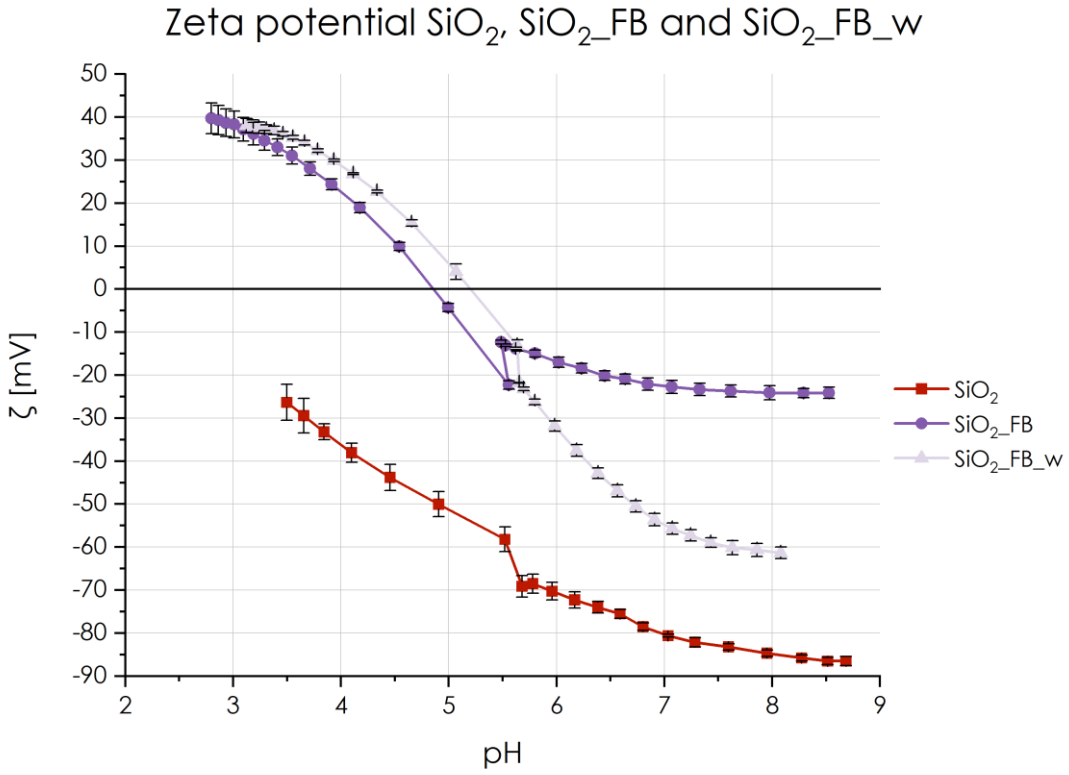

Figure 102: Zeta potential SiO_2, SiO_2_FB and SiO_2_FB_w

As regards PP, it had a typical titration curve of a hydrophobic surface with an IEP of ~4, which increased to ~5.5 in presence of fibrinogen on the surface for both wet and dry samples. Differing from the silica's case, for PP samples the plateau was reached to a pH value of ~6.5, regardless of the type of sample.

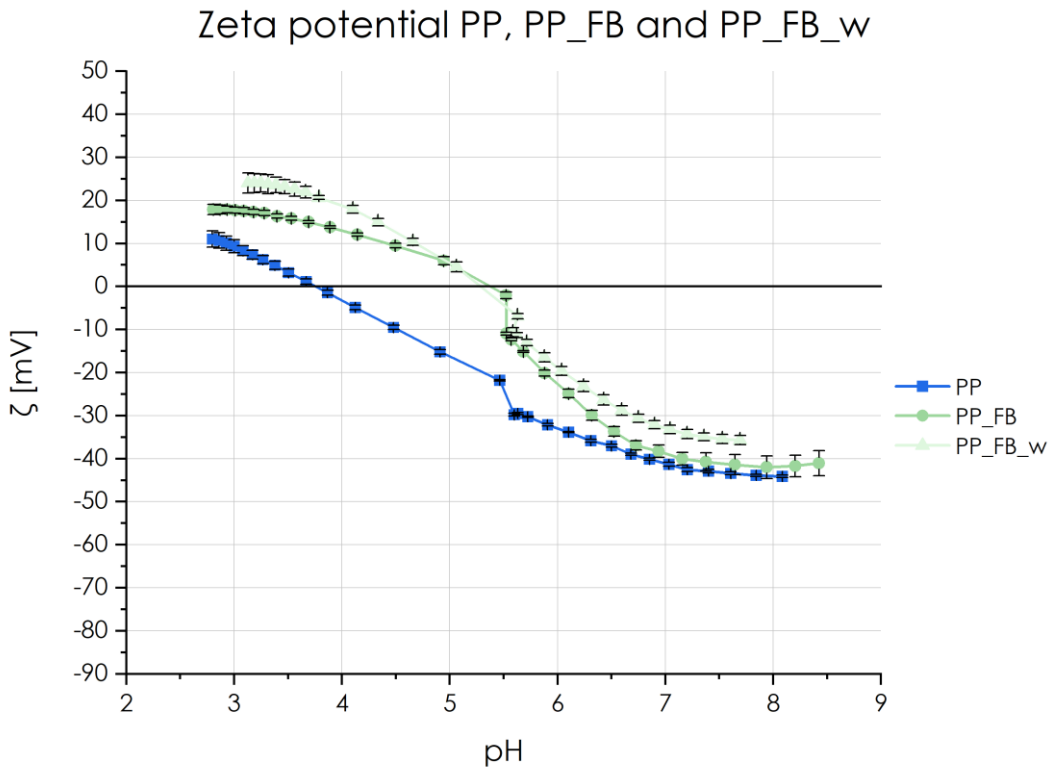

Figure 103: Zeta potential PP, PP_FB and PP_FB_w

An overall evaluation could be produced considering and comparing SiO_2, SiO_2_FB_w, PP, PP_FB_w and FB. In both SiO_2_FB_w and PP_FB_w, the presence of fibrinogen results in increased value of zeta potential, approaching the curve to that of fibrinogen; in addition, a shift in IEP, which resulted to be the same in SiO_2_FB_w and PP_FB_w was observable, as a demonstration of successful fibrinogen adsorption process.

Finally, the significant difference in the slope of the curves related to SiO_2_FB_w and PP_FB_w samples might be associated to a different orientation in fibrinogen on the surfaces.

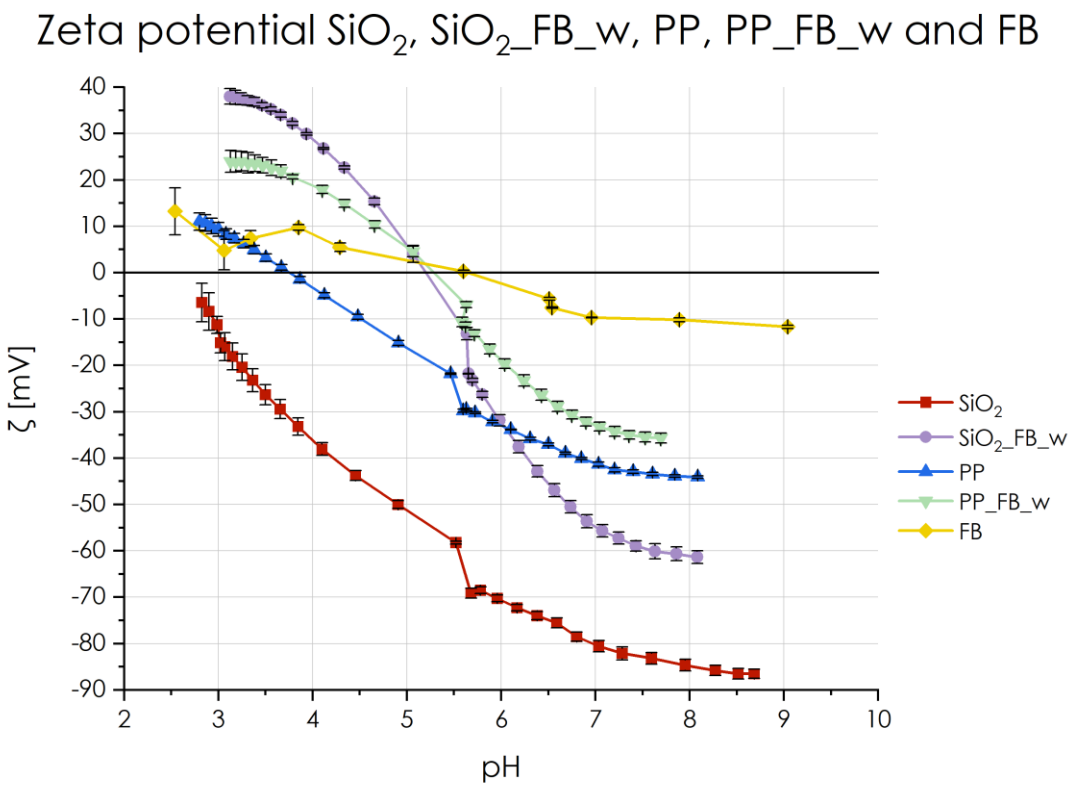

Figure 104: Zeta potential SiO_2, SiO_2_FB_w, PP, PP_FB_w and FB

The zeta potential measurement on Ti64_FB_w and CT_FB_w samples showed two very different behaviors: although in the acid range they had a similar trend with an IEP of ~5 and ~4.5 respectively, in the basic range CT_FB_w reached a plateau of -35 mV for a pH of ~7, while Ti64_FB_w decreased to -105 without an evident plateau.

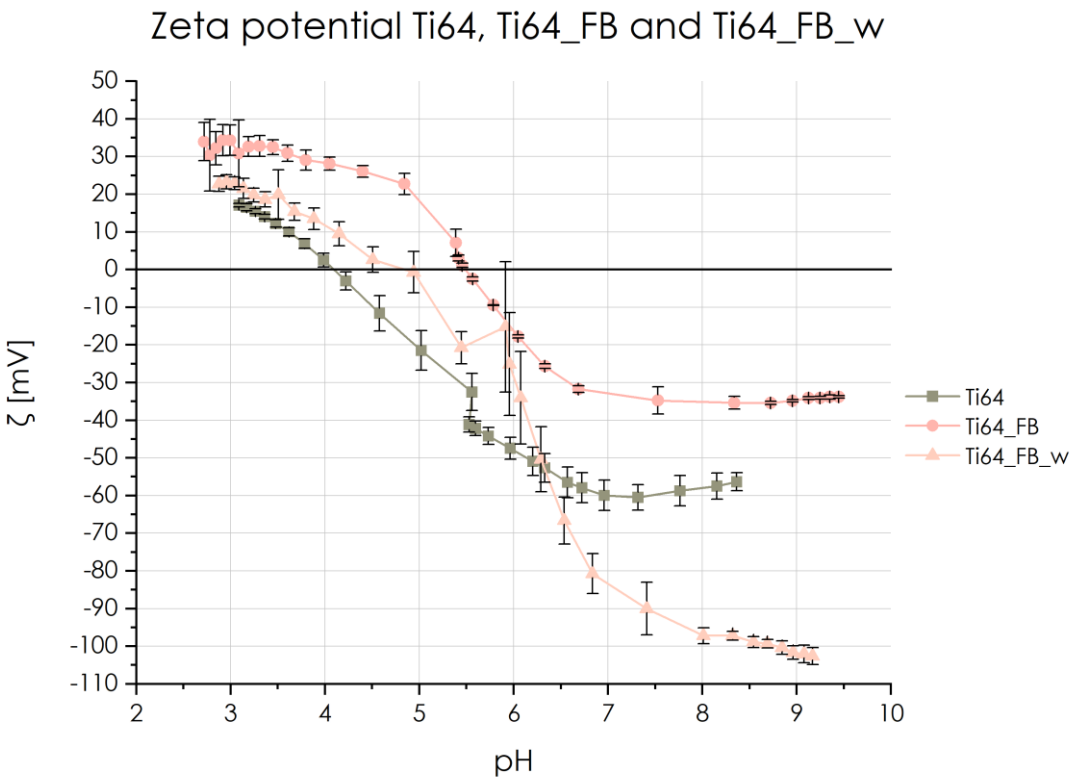

Figure 105: Zeta potential Ti64, Ti64_FB and Ti64_FB_w

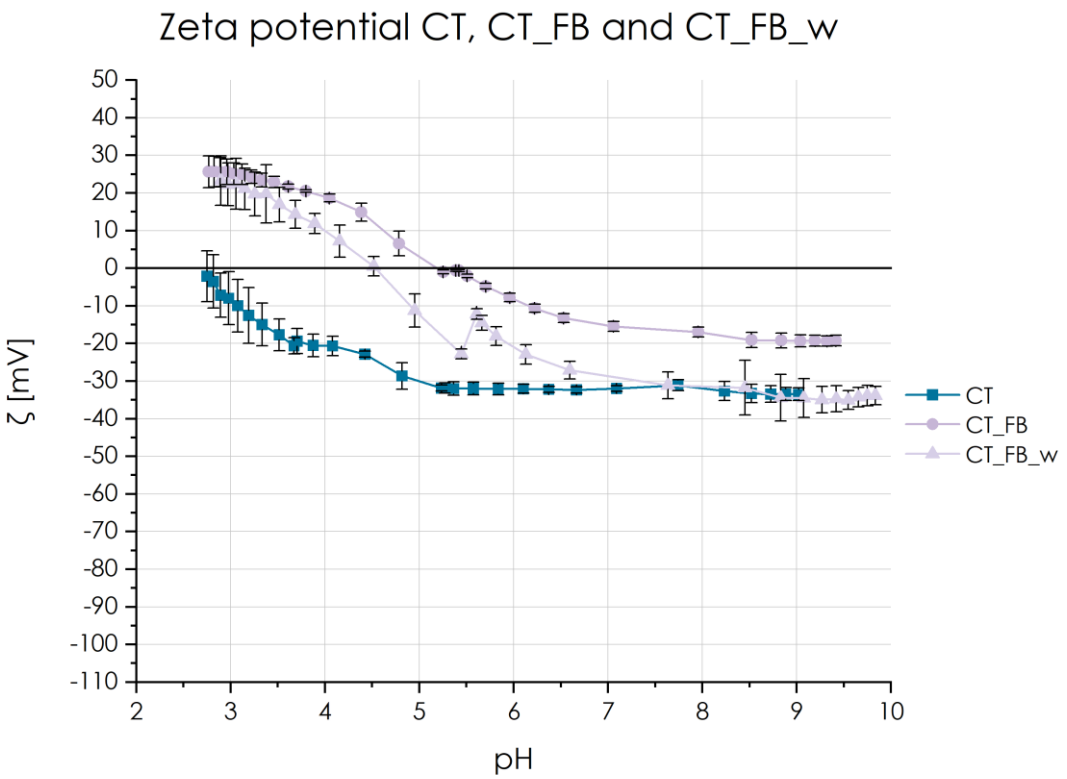

Figure 106: Zeta potential CT, CT_FB and CT_FB_w

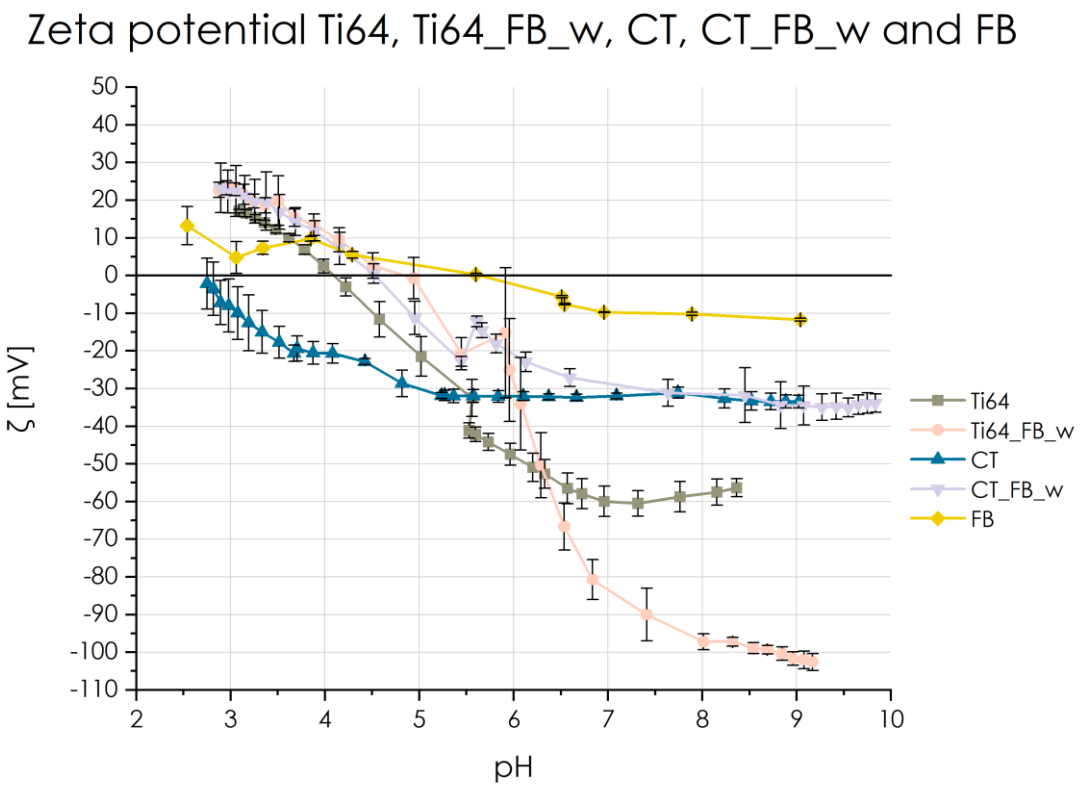

Figure 107: Zeta potential Ti64, Ti64_FB_w, CT, CT_FB_w and FB

A final overall evaluation is reported with zeta potential curves of SiO_2, PP, Ti64 and CT in figure 108 and SiO_2_FB_w, PP_FB_w, Ti64_FB_w, CT_FB_w and FB[5] in figure 110.

In general, the curves suggested that the adsorption was successful in all samples, in that the IEPs shifted if compared to the substrates and they became similar to the FB solution.

In case of CT_FB_w, whose curve was close to PP_FB_w one, there was probably a limited change in conformation and exposition of the functional groups of the adsorbed FB and this was suggested by the fact that the curve was also similar in shape to that related to fibrinogen.

Ti64_FB_w curve, by contrast, was significantly different from FB one. The lower isoelectric point of Ti64_FB_w vs CT_FB_w allows also to suppose that the surface

[5] Zeta potential measurements on Ti64 and CT were not obtained during this thesis but they are part of Camilla Reggio's PhD thesis

coverage of the first surface was not complete. This agrees with the literature: a high density of surface polar groups increases protein adsorption.

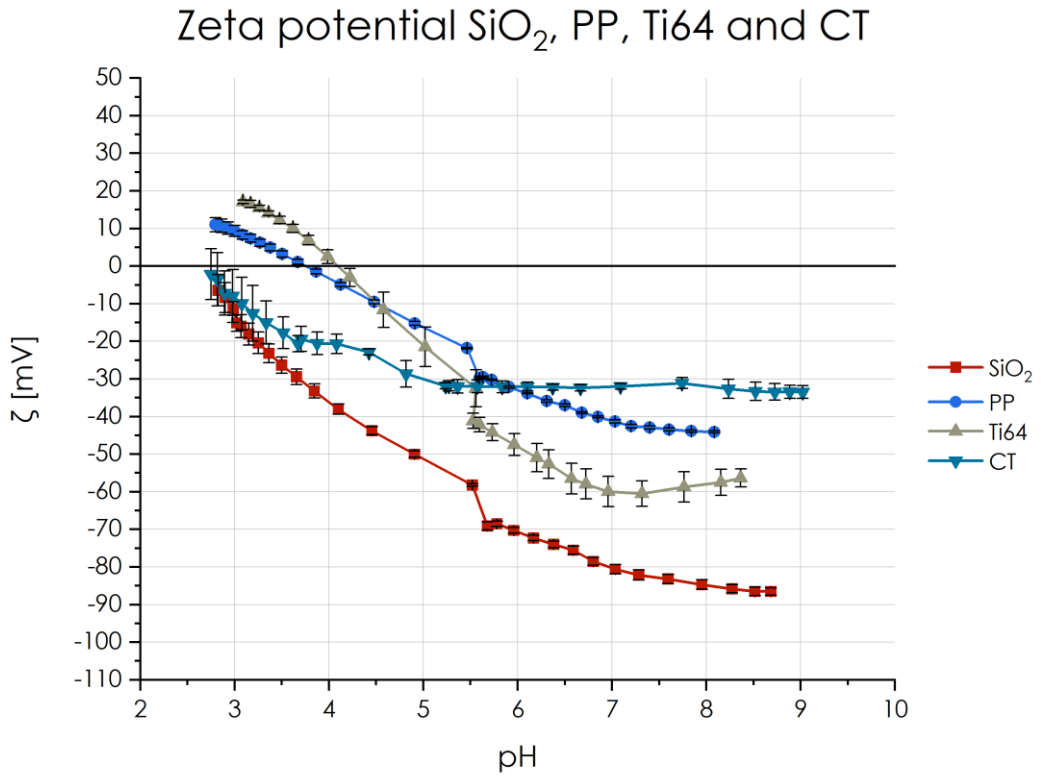

Figure 108: Zeta potential SiO_2, PP, Ti64 and CT

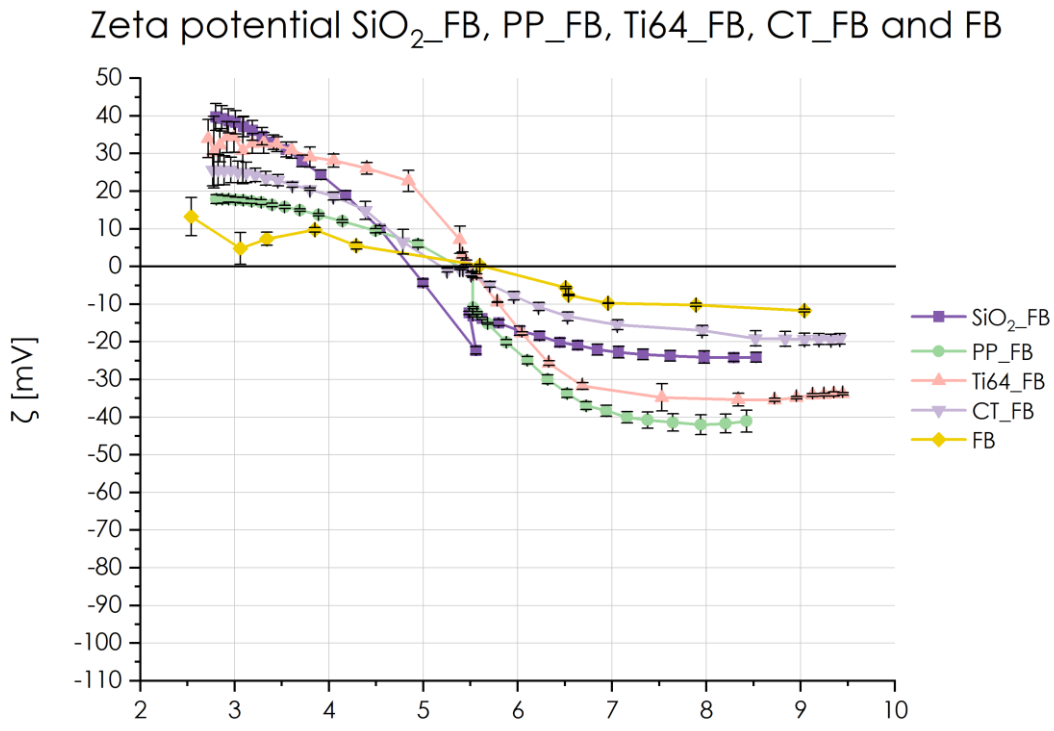

Figure 109: Zeta potential SiO_2_FB, PP_FB, Ti64_FB, CT_FB and FB

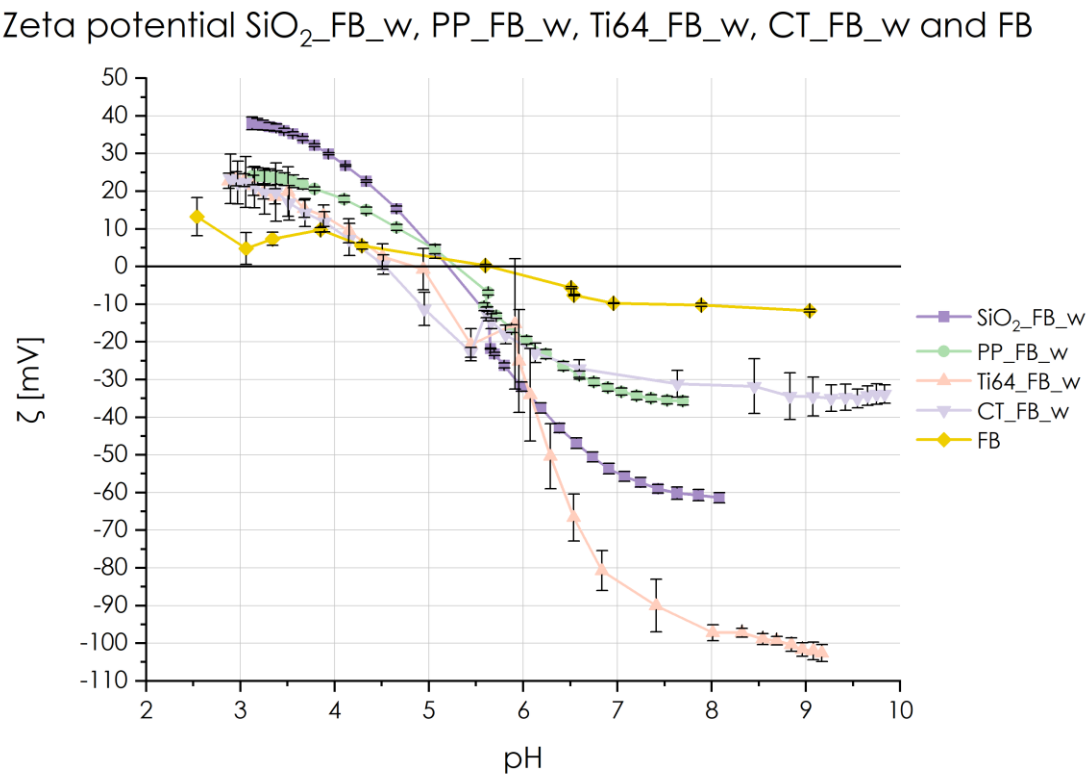

Figure 110: Zeta potential SiO_2_FB_w, PP_FB_w, Ti64_FB_w, CT_FB_w and FB

The zeta potential values related to physiological pH (~7.4) are reported.

Table 24: Zeta potential values for physiological pH

MATERIAL	ZETA POTENTIAL [mV]
SiO_2	-83
PP	-43
Ti64	-60
CT	-31
SiO_2_FB_w	-59
PP_FB_w	-35
Ti64_FB_w	-90
CT_FB_w	-31
FB	-10

Hypotheses about fibrinogen orientation on the surfaces can be done:

- SiO_2_FB_w has probably a side on orientation with the extremities of the fibrinogen that are in contact with the surface: it is reasonable to assume

that there is an attraction between the hydrophilic substrate and the hydrophilic portion of the molecule. At the same time, the hydrophobic portion of the adsorbed fibrinogen must be exposed to the outside in accordance with contact angle and zeta potential values of SiO_2_FB, which revealed a hydrophobic behavior.

Side on conformations can be "αC-hidden" (more probable, with the end portions folded under the central one) or "αC-exposed" (with the fibrinogen molecule stretched on the surface).

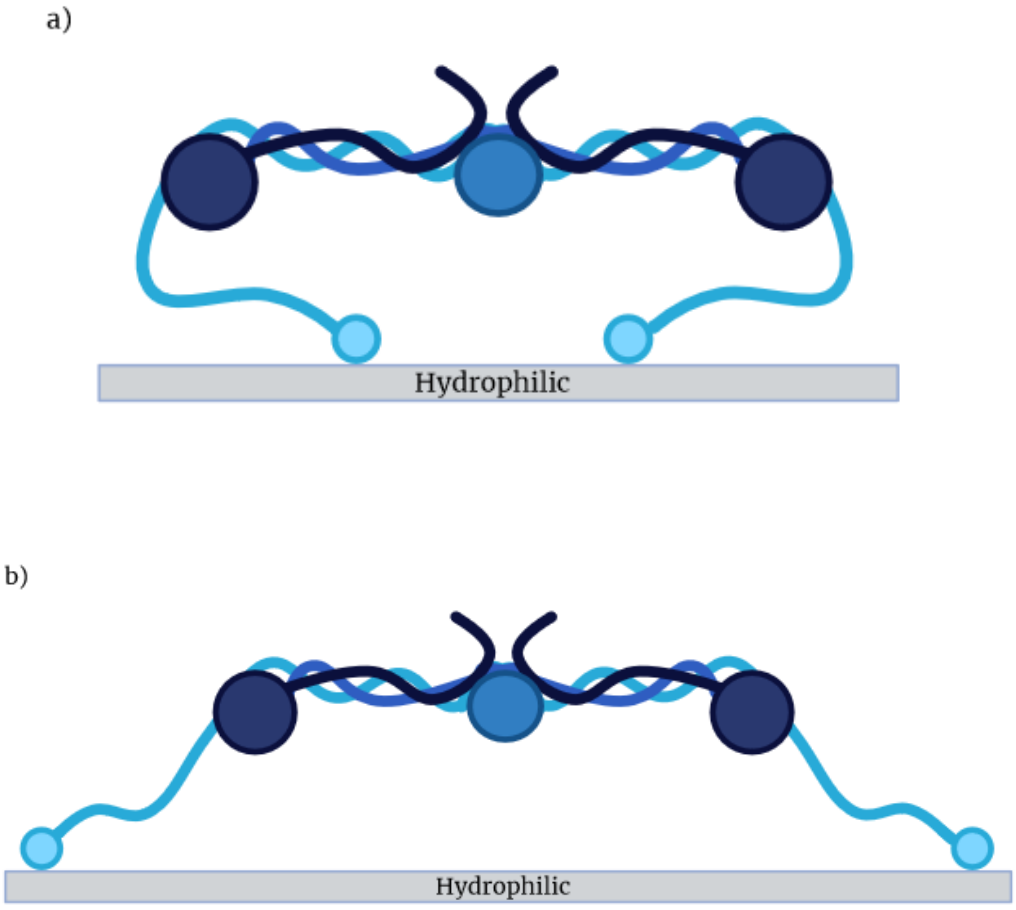

Figure 111: (a) αC- hidden conformation; (b) αC-exposed conformation [created with BioRender]

- PP_FB_w and Ti64_FB_w probably present a side on orientation with the extremities exposed to the outside: this may be due to the attraction between the hydrophobic substrate and the hydrophobic portion of the

molecule. At the same time, the hydrophilic portion of the adsorbed fibrinogen must be exposed to the outside, in that PP_FB_w resulted to be more hydrophilic than SiO_2_FB_w in zeta potential curve.
The conformation is the so-called “extended conformation”.

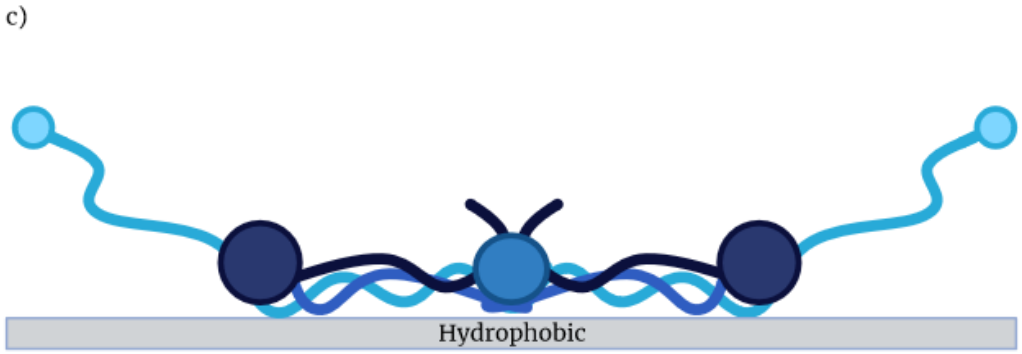

Figure 112: (c) extended conformation [created with BioRender]

- CT_FB_w has probably an end-on configuration with one of the fibrinogen extremities in contact with the surface. It is reasonable to think that there is an attraction between the hydrophilic substrate and the hydrophilic portion of the molecule. At the same time, the hydrophilic portion of the adsorbed fibrinogen must be exposed to the outside in that CT_FB_w resulted to be hydrophilic in zeta potential curve.

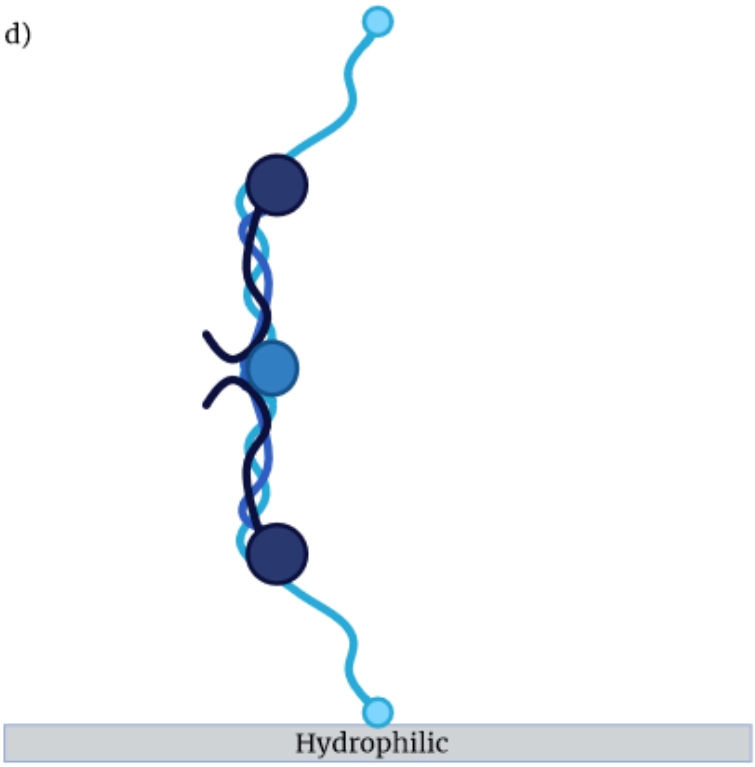

Figure 113: (d) end-on configuration [created with BioRender]

5 CONCLUSION AND FUTURE PERSPECTIVES

The work carried out in this thesis has allowed to study the behavior of different materials which were properly characterized before and after fibrinogen adsorption. The materials, silica and polypropylene, were used as a model of hydrophilic and hydrophobic surfaces respectively and compared to clinical biomaterials such as Ti6Al4V alloy and chemically treated Ti6Al4V alloy, especially when the analyses were more successful.

As a first demonstration of the presence of fibrinogen on the surfaces after the adsorption protocol, PP_FB samples showed some specific circular shapes and radial patterns which were not so evident on SiO_2_FB samples; this was due to the hydrophobic behavior of the first ones which led to a greater amount of adsorbed protein on the surface itself.

The surface characterization gave better results in case of profilometry, confocal microscopy, contact angle and zeta potential compared to SEM/EDS, FESEM and FTIR analyses which were not equally successful.

First of all, compositional analyses on SiO_2 and PP samples showed a variation in atomic percentage of different elements such as Carbon and Oxygen in both cases, Silicon in the first one and Nitrogen in the second one after the adsorption. However, these differences were not significative. In addition, SEM images revealed a smooth surface in SiO_2 samples with an increase of roughness in SiO_2_FB, while PP samples and PP_FB presented a similar roughness. In both cases there was the presence of salt crystals after the fibrinogen adsorption.

As a further evidence, FESEM images gave similar results, majorly highlighting the presence of branched structures in SiO_2_FB case and inhomogeneous surfaces in PP_FB one.

Regarding FTIR analyses, the most successful results were about polypropylene samples: in fact, the presence of fibrinogen in PP_FB determined the formation of a peak in 1651 cm^{-1} that was absent in PP and that was associated to Amide I band, with predominance of α-helix structure. The same results were not obtained for SiO_2 samples, probably because of its hydrophilic behavior which determines generally a lower amount of adsorbed protein on the surface.

The evaluation of roughness parameters, majorly focused on Ra and Sa in case of profilometry and confocal microscopy respectively showed, especially in the second analysis, an increase in surface roughness after the fibrinogen adsorption for SiO_2_FB samples, while PP roughness was not equally affected by the presence of the protein. At the same time, confocal microscopy images and 3D surface reconstructions confirmed the presence of a dendritic structure in SiO_2_FB samples, probably connected to the shrinkage effect of the fibrinogen layer which was adsorbed on the silica's surface. Therefore, it is possible to consider SiO_2 surface as a model for hydrophilic and smooth materials, while PP as a model for hydrophobic and nanostructured ones.

Wettability investigation was more successful on dry samples: in SiO_2 case the presence of fibrinogen led to a decrease of wettability, more evident for the fibrinogen drop; on the other hand, PP samples resulted to maintain a typical hydrophobic behavior, with a slight decrease in the contact angle value for the fibrinogen drop. At the same way Ti64_FB and CT_FB showed a hydrophobic behavior with the fibrinogen drop, but on the contrary, they showed a hydrophilic behavior with the FBS drop. The evaluation of contact angle with the drop of blood showed a hydrophobic behavior after the adsorption for all the samples.

As a conclusion, silica cannot be used as a model material for protein adsorption on CT even though they have a similar behavior in case of water drop: this is due to the high roughness of CT surface which can affect the contact angle value, so that CT wettability by protein solutions, especially in case of a protein mixture such as FBS, was much more similar to Ti64 rather than to SiO_2.

Finally, zeta potential measurement showed a typical hydrophilic and hydrophobic behavior for SiO_2 and PP samples respectively: an increase of the curve slope around the IEP was a demonstration of the decrease of wettability in case of samples which underwent fibrinogen adsorption. In addition, the presence of fibrinogen on the samples' surfaces led to a shift in IEP: in case of SiO_2_FB_w samples, this aspect is more evident in that drying process causes a partial exposure of silica substrate for SiO_2_FB.

Differing from CT, SiO_2 did not present an evident plateau: although in both cases a great number of acidic OH groups was present, in the first one these groups acted as a strong

acid and were completely deprotonated at a specific and low pH value, while in the second one they had a different acidic reactivity, not being completely deprotonated. In addition, the IEPs in Ti64_FB_w and CT_FB_w (with high density of surface polar groups) suggested that the surface coverage was greater in the second case, according to the literature.

Finally, the differences in the slopes of all the samples' curves might be associated to a different orientation in fibrinogen on the surfaces.

Hypotheses about fibrinogen orientation on the surfaces have done too. SiO_2_FB_w samples had probably a side on orientation with the hydrophilic portions interacting with the hydrophilic substrate itself and the hydrophobic ones exposed to the outside: in this case the end portions could be folded under the central one or stretched on the surface. PP_FB_w and Ti64_FB_w had probably a side on orientation with the extremities exposed to the outside and the hydrophobic portion interacting with the substrates which were hydrophobic too. Finally, CT_FB_w had probably an end-on configuration with one of the fibrinogen extremities exposed to the outside and the other one in contact with the surface because of the attraction between the hydrophilic substrate and the hydrophilic portion of the molecule itself.

Considering that the fibrinogen adsorption causes important variations in the surface features and in the tertiary structure of the protein itself, the future perspectives can be summarized into six main points:

- Drying and subsequent shrinkage effects, which have been mainly observed in hydrophilic models, could be further studied in order to investigate the materials behavior and the consequences of the substrate partial exposure.
- Variations in the surface features, especially for what concerns the wettability related to a mixture of proteins such as FBS, need a deepening, in order to identify more appropriate models for clinical surfaces as Ti64 and CT ones.

- Hypotheses about the variation in tertiary structure of the adsorbed fibrinogen and the different orientation of the protein, associated to a variable arrangement of the various domains could be eventually confirmed by further investigations.
- Hemolysis could be evaluated with a view to ulteriorly investigate the blood response to the biomaterial implantation.
- Other protein's adsorption could be evaluated too with the purpose of obtaining a global overview of the formation of the provisional matrix around the implant, to better suppose the body response to the acute inflammatory state.
- Cytocompatibility and cytotoxicity tests could be carried out in order to extend this study to the interaction between the biomaterials and the host organism cells.

REFERENCES

[1] J. W. Weisel and R. I. Litvinov, “Fibrin formation, structure and properties,” *Subcell Biochem*, vol. 82, pp. 405–456, Jan. 2017, doi: 10.1007/978-3-319-49674-0_13.

[2] S. Surma and M. Banach, “Fibrinogen and atherosclerotic cardiovascular diseases—review of the literature and clinical studies,” *International Journal of Molecular Sciences*, vol. 23, no. 1. MDPI, Jan. 01, 2022. doi: 10.3390/ijms23010193.

[3] S. Rossi, “Malattia da accumulo epatico di fibrinogeno: descrizione di due pazienti e identificazione di una nuova mutazione (p.Asp316Asn, Fibrinogeno Pisa) che modifica la struttura della catena gamma del fibrinogeno.”

[4] S. Kattula, J. R. Byrnes, and A. S. Wolberg, “Fibrinogen and Fibrin in Hemostasis and Thrombosis,” *Arteriosclerosis, Thrombosis, and Vascular Biology*, vol. 37, no. 3. Lippincott Williams and Wilkins, pp. e13–e21, Mar. 01, 2017. doi: 10.1161/ATVBAHA.117.308564.

[5] K. Hyltegren, M. Hulander, M. Andersson, and M. Skepö, “Adsorption of fibrinogen on silica surfaces—The effect of attached nanoparticles,” *Biomolecules*, vol. 10, no. 3, Mar. 2020, doi: 10.3390/biom10030413.

[6] P. Zeliszewska, A. Bratek-Skicki, Z. Adamczyk, and M. Cieśla, “Human fibrinogen adsorption on positively charged latex particles,” *Langmuir*, vol. 30, no. 37, pp. 11165–11174, Sep. 2014, doi: 10.1021/la5025668.

[7] Z. Adamczyk, B. Cichocki, M. L. Ekiel-Jezewska, A. Słowicka, E. Wajnryb, and M. Wasilewska, “Fibrinogen conformations and charge in electrolyte solutions derived from DLS and dynamic viscosity measurements,” *J Colloid Interface Sci*, vol. 385, no. 1, pp. 244–257, Nov. 2012, doi: 10.1016/j.jcis.2012.07.010.

[8] J. S. O’Donnell, J. M. O’Sullivan, and R. J. S. Preston, “Advances in understanding the molecular mechanisms that maintain normal haemostasis,” *British Journal of Haematology*, vol. 186, no. 1. Blackwell Publishing Ltd, pp. 24–36, Jul. 01, 2019. doi: 10.1111/bjh.15872.

[9] A. Noori, S. J. Ashrafi, R. Vaez-Ghaemi, A. Hatamian-Zaremi, and T. J. Webster, “A review of fibrin and fibrin composites for bone tissue engineering,”

International Journal of Nanomedicine, vol. 12. Dove Medical Press Ltd., pp. 4937–4961, Jul. 12, 2017. doi: 10.2147/IJN.S124671.

[10] R. I. Litvinov *et al.*, "Polymerization of fibrin: Direct observation and quantification of individual B:b knob-hole interactions," *Blood*, vol. 109, no. 1, pp. 130–138, Jan. 2007, doi: 10.1182/blood-2006-07-033910.

[11] Y. Yang and Y. Xiao, "Biomaterials Regulating Bone Hematoma for Osteogenesis," *Advanced Healthcare Materials*, vol. 9, no. 23. Wiley-VCH Verlag, Dec. 01, 2020. doi: 10.1002/adhm.202000726.

[12] O. V. Kim, R. I. Litvinov, J. W. Weisel, and M. S. Alber, "Structural basis for the nonlinear mechanics of fibrin networks under compression," *Biomaterials*, vol. 35, no. 25, pp. 6739–6749, 2014, doi: 10.1016/j.biomaterials.2014.04.056.

[13] M. Pavlovic, "What are biomaterials?," in *Bioengineering*, Springer, Cham, 2014, pp. 229–244.

[14] U. von Mentzer, C. Corciulo, and A. Stubelius, "Biomaterial Integration in the Joint: Pathological Considerations, Immunomodulation, and the Extracellular Matrix," *Macromolecular Bioscience*, vol. 22, no. 7. John Wiley and Sons Inc, Jul. 01, 2022. doi: 10.1002/mabi.202200037.

[15] N. Huebsch and D. J. Mooney, "Inspiration and application in the evolution of biomaterials," *Nature*, vol. 462, no. 7272. pp. 426–432, Nov. 26, 2009. doi: 10.1038/nature08601.

[16] A. Carnicer-Lombarte, S. T. Chen, G. G. Malliaras, and D. G. Barone, "Foreign Body Reaction to Implanted Biomaterials and Its Impact in Nerve Neuroprosthetics," *Frontiers in Bioengineering and Biotechnology*, vol. 9. Frontiers Media S.A., Apr. 15, 2021. doi: 10.3389/fbioe.2021.622524.

[17] "https://www.docenti.unina.it/webdocenti-be/allegati/materiale-didattico/34131799."

[18] J. M. Anderson, A. Rodriguez, and D. T. Chang, "Foreign body reaction to biomaterials."

[19] T. Albrektsson and C. Johansson, "Osteoinduction, osteoconduction and osseointegration," *European Spine Journal*, vol. 10, pp. S96–S101, 2001, doi: 10.1007/s005860100282.

[20] C. Pandey, D. Rokaya, and B. P. Bhattarai, “Contemporary Concepts in Osseointegration of Dental Implants: A Review,” *BioMed Research International*, vol. 2022. Hindawi Limited, 2022. doi: 10.1155/2022/6170452.

[21] P. Silva-Bermudez, S. Muhl, and S. E. Rodil, “A comparative study of fibrinogen adsorption onto metal oxide thin films,” *Appl Surf Sci*, vol. 282, pp. 351–362, Oct. 2013, doi: 10.1016/j.apsusc.2013.05.133.

[22] I. H. Jaffer and J. I. Weitz, “The blood compatibility challenge. Part 1: Blood-contacting medical devices: The scope of the problem,” *Acta Biomaterialia*, vol. 94. Acta Materialia Inc, pp. 2–10, Aug. 01, 2019. doi: 10.1016/j.actbio.2019.06.021.

[23] H. T. Shiu, B. Goss, C. Lutton, R. Crawford, and Y. Xiao, “Formation of blood clot on biomaterial implants influences bone healing,” *Tissue Engineering - Part B: Reviews*, vol. 20, no. 6. Mary Ann Liebert Inc., pp. 697–712, Dec. 01, 2014. doi: 10.1089/ten.teb.2013.0709.

[24] G. Steiner, S. Tunc, M. Maitz, and R. Salzer, “Conformational changes during protein adsorption. FT-IR spectroscopic imaging of adsorbed fibrinogen layers,” *Anal Chem*, vol. 79, no. 4, pp. 1311–1316, Feb. 2007, doi: 10.1021/ac061341j.

[25] P. Roach, D. Farrar, and C. C. Perry, “Interpretation of protein adsorption: Surface-induced conformational changes,” *J Am Chem Soc*, vol. 127, no. 22, pp. 8168–8173, Jun. 2005, doi: 10.1021/ja042898o.

[26] T. A. Horbett, “Fibrinogen adsorption to biomaterials,” *Journal of Biomedical Materials Research - Part A*, vol. 106, no. 10. John Wiley and Sons Inc., pp. 2777–2788, Oct. 01, 2018. doi: 10.1002/jbm.a.36460.

[27] L. B. Koh, I. Rodriguez, and S. S. Venkatraman, “Conformational behavior of fibrinogen on topographically modified polymer surfaces,” *Physical Chemistry Chemical Physics*, vol. 12, no. 35, pp. 10301–10308, 2010, doi: 10.1039/c001747g.

[28] S. Song, K. Ravensbergen, A. Alabanza, D. Soldin, and J. I. Hahm, “Distinct adsorption configurations and self-Assembly characteristics of fibrinogen on chemically uniform and alternating surfaces including block copolymer nanodomains,” *ACS Nano*, vol. 8, no. 5, pp. 5257–5269, May 2014, doi: 10.1021/nn5013397.

[29] M. Aliofkhazraei and N. Ali, “AFM Applications in Micro/Nanostructured Coatings,” in *Comprehensive Materials Processing*, Elsevier, 2014, pp. 191–241. doi: 10.1016/B978-0-08-096532-1.00712-3.

[30] H. G. Xie *et al.*, “Effect of surface morphology and charge on the amount and conformation of fibrinogen adsorbed onto alginate/chitosan microcapsules,” *Langmuir*, vol. 26, no. 8, pp. 5587–5594, Apr. 2010, doi: 10.1021/la903874g.

[31] Z. Adamczyk, A. Bratek-Skicki, P. Dąbrowska, and M. Nattich-Rak, “Mechanisms of fibrinogen adsorption on latex particles determined by zeta potential and AFM measurements,” *Langmuir*, vol. 28, no. 1, pp. 474–485, Jan. 2012, doi: 10.1021/la2038119.

[32] J. Barberi *et al.*, “Albumin and fibronectin adsorption on treated titanium surfaces for osseointegration: An advanced investigation,” *Appl Surf Sci*, vol. 599, Oct. 2022, doi: 10.1016/j.apsusc.2022.154023.

[33] K. Rechendorff, “The influence of surface roughness on protein adsorption,” 2006.

[34] G. P. Rockwell, L. B. Lohstreter, and J. R. Dahn, “Fibrinogen and albumin adsorption on titanium nanoroughness gradients,” *Colloids Surf B Biointerfaces*, vol. 91, no. 1, pp. 90–96, Mar. 2012, doi: 10.1016/j.colsurfb.2011.10.045.

[35] K. Rechendorff, M. B. Hovgaard, M. Foss, V. P. Zhdanov, and F. Besenbacher, “Enhancement of protein adsorption induced by surface roughness,” *Langmuir*, vol. 22, no. 26, pp. 10885–10888, Dec. 2006, doi: 10.1021/la0621923.

[36] E. Macarena Blanco, M. A. Horton, and P. Mesquida, “Simultaneous investigation of the influence of topography and charge on protein adsorption using artificial nanopatterns,” *Langmuir*, vol. 24, no. 6, pp. 2284–2287, Mar. 2008, doi: 10.1021/la702957f.

[37] M. Wasilewska and Z. Adamczyk, “Fibrinogen adsorption on mica studied by AFM and in situ streaming potential measurements,” *Langmuir*, vol. 27, no. 2, pp. 686–696, Jan. 2011, doi: 10.1021/la102931a.

[38] H. G. Xie *et al.*, “Effect of surface wettability and charge on protein adsorption onto implantable alginate-chitosan-alginate microcapsule surfaces,” *J Biomed Mater Res A*, vol. 92, no. 4, pp. 1357–1365, Mar. 2010, doi: 10.1002/jbm.a.32437.

[39] P. Bernabeu and A. Caprani, “Influence of surface charge on adsorption of fibrinogen and/or albumin on a rotating disc electrode of platinum and carbon,” 1990.

[40] “https://www.jove.com/it/v/5656/scanning-electron-microscopy-sem?language=Italian.”

[41] “https://www.scimed.co.uk/education/sem-scanning-electron-microscopy/.”

[42] “https://serc.carleton.edu/research_education/geochemsheets/techniques/SEM.html.”

[43] A. K. Singh, “Experimental Methodologies for the Characterization of Nanoparticles,” in *Engineered Nanoparticles*, Elsevier, 2016, pp. 125–170. doi: 10.1016/b978-0-12-801406-6.00004-2.

[44] “https://photometrics.net/field-emission-scanning-electron-microscopy-fesem/.”

[45] “https://vaccoat.com/blog/field-emission-scanning-electron-microscopy-fesem/.”

[46] A. Ahmad, I. Ahmad, S. Ramzan, M. Z. Kiyani, D. Dubal, and N. M. Mubarak, “Nanomaterial synthesis protocols,” in *Nanomedicine Manufacturing and Applications*, Elsevier, 2021, pp. 73–85. doi: 10.1016/B978-0-12-820773-4.00010-X.

[47] “https://www.sigmaaldrich.com/IT/it/technical-documents/technical-article/analytical-chemistry/photometry-and-reflectometry/ftir-spectroscopy.”

[48] G. E. Tranter, “FTIR Spectroscopy of Aqueous Solutions,” in *Encyclopedia of Spectroscopy and Spectrometry*, Elsevier, 2017, pp. 762–769. doi: 10.1016/B978-0-12-409547-2.12157-2.

[49] Y. Tkachenko and P. Niedzielski, “FTIR as a Method for Qualitative Assessment of Solid Samples in Geochemical Research: A Review,” *Molecules*, vol. 27, no. 24. MDPI, Dec. 01, 2022. doi: 10.3390/molecules27248846.

[50] “https://www.gdandtbasics.com/what-is-a-profilometer/.”

[51] G. Mabilleau and A. Sabokbar, “In vitro biological test methods to evaluate bioresorbability,” in *Degradation Rate of Bioresorbable Materials: Prediction and Evaluation*, Elsevier Inc., 2008, pp. 145–160. doi: 10.1533/9781845695033.3.145.

[52] “https://astropak.com/surface-roughness-average-ra/.”

[53] A. Nwaneshiudu, C. Kuschal, F. H. Sakamoto, R. Rox Anderson, K. Schwarzenberger, and R. C. Young, “Introduction to confocal microscopy,” *Journal of Investigative Dermatology*, vol. 132, no. 12, pp. 1–5, 2012, doi: 10.1038/jid.2012.429.

[54] P. O. Bayguinov, D. M. Oakley, C. C. Shih, D. J. Geanon, M. S. Joens, and J. A. J. Fitzpatrick, “Modern Laser Scanning Confocal Microscopy,” *Current Protocols in Cytometry*, vol. 85, no. 1. John Wiley and Sons Inc., Jul. 01, 2018. doi: 10.1002/cpcy.39.

[55] “https://ibidi.com/content/216-confocal-microscopy.”

[56] A. D. Elliott, “Confocal Microscopy: Principles and Modern Practices,” *Curr Protoc Cytom*, vol. 92, no. 1, Mar. 2020, doi: 10.1002/cpcy.68.

[57] T. A. Sonia and C. P. Sharma, “Experimental techniques involved in the development of oral insulin carriers,” in *Oral Delivery of Insulin*, Elsevier, 2014, pp. 169–217. doi: 10.1533/9781908818683.169.

[58] “https://www.brighton-science.com/what-is-contact-angle.”

[59] S. Ferraris, M. Cazzola, V. Peretti, B. Stella, and S. Spriano, “Zeta potential measurements on solid surfaces for in Vitro biomaterials testing: Surface charge, reactivity upon contact with fluids and protein absorption,” *Front Bioeng Biotechnol*, vol. 6, no. MAY, May 2018, doi: 10.3389/fbioe.2018.00060.

[60] P. Novák and V. Havlíček, “Protein Extraction and Precipitation,” in *Proteomic Profiling and Analytical Chemistry*, Elsevier, 2016, pp. 51–62. doi: 10.1016/B978-0-444-63688-1.00004-5.

[61] A. Rimola, D. Costa, M. Sodupe, J. F. Lambert, and P. Ugliengo, “Silica surface features and their role in the adsorption of biomolecules: Computational modeling and experiments,” *Chemical Reviews*, vol. 113, no. 6. American Chemical Society, pp. 4216–4313, Jun. 12, 2013. doi: 10.1021/cr3003054.

[62] M. Vallet-Regí and F. Balas, “Silica Materials for Medical Applications,” 2008.

[63] Y. Gao *et al.*, “Multifunctional Role of Silica in Pharmaceutical Formulations,” *AAPS PharmSciTech*, vol. 23, no. 4. Springer Science and Business Media Deutschland GmbH, May 01, 2022. doi: 10.1208/s12249-022-02237-5.

[64] M. Kelly, K. Macdougall, O. Olabisi, and N. McGuire, “In vivo response to polypropylene following implantation in animal models: a review of biocompatibility,” *Int Urogynecol J*, vol. 28, no. 2, pp. 171–180, Feb. 2017, doi: 10.1007/s00192-016-3029-1.

[65] J. Ma, X. Nan, R. M. Larsen, X. Huang, and B. Yu, “Mechanical properties and biocompatibility of functionalized carbon nanotubes/polypropylene composites,” *J Biomater Sci Polym Ed*, vol. 27, no. 10, pp. 1003–1016, Jul. 2016, doi: 10.1080/09205063.2016.1175776.

[66] X. Shi, Y. Sun, P. Wang, Z. Ma, H. Liu, and H. Ning, “Compression properties and optimization design of SLM Ti6Al4V square pore tissue engineering scaffolds,” *Proc Inst Mech Eng H*, vol. 235, no. 11, pp. 1265–1273, Nov. 2021, doi: 10.1177/09544119211028061.

[67] W. Saleem, B. Salah, X. Velay, R. Ahmad, R. Khan, and C. I. Pruncu, “Numerical modeling and analysis of Ti6Al4V alloy chip for biomedical applications,” *Materials*, vol. 13, no. 22, pp. 1–17, Nov. 2020, doi: 10.3390/ma13225236.

[68] S. Spriano, “Materiali per l’ortopedia.”

[69] E. Vernè, “Leghe di titanio.”

[70] Y. F. Zuev *et al.*, “Conformational Flexibility and Self-Association of Fibrinogen in Concentrated Solutions,” *Journal of Physical Chemistry B*, vol. 121, no. 33, pp. 7833–7843, Aug. 2017, doi: 10.1021/acs.jpcb.7b05654.

[71] “https://www.openanesthesia.org/keywords/coagulation-pathway/.”

[72] S. R. Baker and R. A. S. Ariëns, “Fibrin Clot Structure and Function,” in *Cardiovascular Thrombus: From Pathology and Clinical Presentations to Imaging, Pharmacotherapy and Interventions*, Elsevier, 2018, pp. 31–49. doi: 10.1016/B978-0-12-812615-8.00003-X.

[73] “https://www.ahajournals.org/doi/10.1161/ATVBAHA.119.313626.”

[74] “https://www.perfusion.com/coagulation-issues-fibrinolysis-hit-helpful-graphics/.”

[75] M. W. Mosesson, “Fibrinogen γ chain functions,” *Journal of Thrombosis and Haemostasis*, vol. 1, no. 2. pp. 231–238, Feb. 2003. doi: 10.1046/j.1538-7836.2003.00063.x.

[76] J. Barberi and S. Spriano, “Titanium and protein adsorption: An overview of mechanisms and effects of surface features,” *Materials*, vol. 14, no. 7. MDPI AG, Apr. 01, 2021. doi: 10.3390/ma14071590.

[77] “https://www.jeol.com/products/scientific/sem/JCM-6000Plus.php.”

[78] R. Senthil Prabhu, R. Priyanka, M. Vijay, and G. R. Kaviya Vikashini, “Field Emission Scanning Electron Microscopy (Fesem) with A Very Big Future in Pharmaceutical Research,” *Research Article | Pharmaceutical Sciences | OA Journal | MCI Approved | Index Copernicus*, vol. 11, no. 2, pp. 2321–3272, 2021, doi: 10.21276/ijpbs.2021.11.2.21.

[79] “https://www.bridgetronic.com/equipment/62815/.”

[80] B. Campanella, V. Palleschi, and S. Legnaioli, “Introduction to vibrational spectroscopies,” *ChemTexts*, vol. 7, no. 1, p. 5, Mar. 2021, doi: 10.1007/s40828-020-00129-4.

[81] “http://www.ramehart.com/contactangle.htm.”

[82] “https://wiki.anton-paar.com/se-en/zeta-potential/.”